REPORT NO. DOT-TSC-OST-74-6.I

BASIC UNDERSTANDING OF EARTH TUNNELING BY MELTING

Volume I -- Basic Physical Principles

D. L. Black et al

JULY 1974
FINAL REPORT

Prepared for

U.S. DEPARTMENT OF TRANSPORTATION

OFFICE OF THE SECRETARY
Office of the Assistant Secretary for
Systems Development and Technology
Office of Systems Engineering
Washington DC 20590

The contents of this report reflect the views of the Westinghouse Astronuclear Laboratory which is responsible for the facts and the accuracy of the data presented herein. The contents do not necessarily reflect the official views or policy of the Department of Transportation. This report does not constitute a standard, specification or regulation.

Technical Report Documentation Page

1. Report No.	2. Government Accession No.	3. Recipient's Catalog No.
OT-TSC-OST-74-6.I		

4. Title and Subtitle	5. Report Date
ASIC UNDERSTANDING OF EARTH TUNNELING BY MELTING olume I -- Basic Physical Principles	July 1974
	6. Performing Organization Code
7. Author(s)	8. Performing Organization Report No.
D. L. Black et al *	DOT-TSC-OST-74-6.I
9. Performing Organization Name and Address	10. Work Unit No. (TRAIS)
Westinghouse Electric Corporation Astronuclear Laboratory Post Office Box 10864 Pittsburgh PA 15236	OS-433/R4502
	11. Contract or Grant No.
	DOT-TSC-591
12. Sponsoring Agency Name and Address	13. Type of Report and Period Covered
.S. Department of Transportation ffice of the Secretary ffice of the Assistant Secretary for Systems Develop- ent and Technology; Office of Systems Engineering ashington DC 20590	Final Report April - September 1973
	14. Sponsoring Agency Code

15. Supplementary Notes *Under contract to: U.S. Department of Transportation
Transportation Systems Center
Kendall Square
Cambridge MA 02142

16. Abstract A novel technique, which employs the melting of rocks and soils as a means excavating or tunneling while simultaneously generating a glass tunnel lining and/ primary support, was studied. The object of the study was to produce a good basic derstanding of the fundamental process, its limits and capabilities, as applied to rge scale (∿ 10 m diameter) transportation tunnels.

A description of process is developed through the use of functional flow dia-ams, from which five modes of thermal tunneling are defined, ranging from complete bris consolidation into the liner to complete extrusion and removal of the debris.

For calculation purposes, five geologic modes of the near-surface continental ust are presented representative of approximately 95% of the total land area, from consolidated sediments to igneous rocks. Thermophysical properties are synthesized om the composition of the components.

Basic physical principles are used to derive functional equations governing the imary process variables in five separate areas: thermal power and penetrator tem-rature (end of Volume I), thrusting force earth structural, glass liner structural, d melt cooldown. These were related to independent variables of penetration vel-ity and tunnel geometry and to the geologic model properties.

Some potential design solutions are proposed to obviate some problems and mitations. A comparison with small scale test data indicates that the process is edictable but that thermal stress cracking of the glass liner would minimize its nsideration for the primary tunnel support.

17. Key Words		18. Distribution Statement
bterrene ermal Tunneling ckmelt ass	Hydrofacture Tunnel Lining	DOCUMENT IS AVAILABLE TO THE PUBLIC THROUGH THE NATIONAL TECHNICAL INFORMATION SERVICE, SPRINGFIELD, VIRGINIA 22151.

19. Security Classif. (of this report)	20. Security Classif. (of this page)	21. No. of Pages	22. Price
Unclassified	Unclassified	188	

orm DOT F 1700.7 (8-72) Reproduction of completed page authorized

PREFACE

This report on a "Basic Understanding of Earth Tunneling by Melting" was prepared for the Transportation Systems Center of the Department of Transportation, Cambridge, Massachusetts. All the requirements of Contract DOT-TSC-591 are fulfilled by this report which contains the details of the technical work performed from April 2, 1973 to October 2, 1973. The contract was performed under the technical direction of the Power and Propulsion Branch of TSC/DOT, Mr. John Putukian, Technical Monitor.

This study was conducted by the Westinghouse Astronuclear Laboratory, Pittsburgh, Pennsylvania. The project Manager was Dr. D. L. Black; principal investigators were Dr. J. W. H. Chi, Dr. R. A. Smith, and Mr. D. B. Roberts of Westinghouse Georesearch Laboratory; technical advisors were Mr. R. R. Holman and Mr. R. Flaherty.

The guidance, reviews and comments of Dr. E. Foster and Mr. R. McFarland at DOT are most gratefully appareciated.

TABLE OF CONTENTS

VOLUME I

TABLE OF CONTENTS
(Continued)

TABLE OF CONTENTS
(Continued)

TABLE OF CONTENTS
(Continued)

TABLE OF CONTENTS
(Continued)

TABLE OF CONTENTS
(Continued)

TABLE OF CONTENTS
(Continued)

LIST OF ILLUSTRATIONS

VOLUME I

LIST OF ILLUSTRATIONS
(Continued)

LIST OF ILLUSTRATIONS
(Continued)

LIST OF ILLUSTRATIONS

VOLUME II

LIST OF ILLUSTRATIONS
(Continued)

LIST OF ILLUSTRATIONS
(Continued)

LIST OF ILLUSTRATIONS

(Continued)

LIST OF ILLUSTRATIONS
(Continued)

LIST OF TABLES

VOLUME I

VOLUME II

LIST OF ABBREVIATIONS AND SYMBOLS

A	Characteristic area
A_m	Melt to earth/rock interfacial area
A_p	Heated portion of penetrator surface area
cm	Centimeter
C	Effective mean circumference of heated portion of penetrator plus liner; Distance from hole center to surface of earth
C_p	Specific heat
D	Characteristic diameter
D_B	Bore Diameter, $D_p + 2\delta$
D_p	Penetrator diameter
E	Modulus of elasticity or Young's Modulus
f	Coefficient of sliding friction
$f_{e,s}$	Area extruded of U_∞ divided by area of penetrator, S_p
f_{ex}	Area of solid are divided by area of penetrator, S_p
F	Thrusting force
F_a	"Adhesion" force or force to overcome frictional drag
F_f	Frictional drag forces
F_N	Thrust force normal to the surface of the glass liner
F_p	Pressure or form drag

F_s	Stem drag
F_T	Total applied thrust load
g_c	Conversion constant
h	Heat transfer coefficient
hr	Hour
H	Tunnel and surface lift height
k	Thermal conductivity
k_{eff}	Effective thermal conductivity
k_m	Thermal conductivity of the melt at the melting point
K	Degrees Kelvin
L_c	Cooled afterbody length, controlled cooldown section
L_H	Length of heated portion of penetrator
m	Meter
mm	Millimeter
M_1	Mass of processed debris
M_2	Mass of unprocessed debris
M_d	Mass of debris (melt and cored materials)
M_{up}	Unprocessed muck
M_E	Melt extruded as debris
M_L	Melt in liner
M_T	Total melt

N	Newton
p	Local pressure
p_∞	Ambient or lithostatic pressure
P_T	Total power required
q_a	Axial or stem losses
q_f	Fusion power
q_l	Heat loss
$q_{l,s}$	Heat loss to earth/rock
q_m	Melt power
q_s	Sensible heat
q_{su}	Melt superheat
Q_c	Total rate of heat removal from glass liner
Q_D	Heat removed from debris
Q_T	Total thermal power
r	Radial position
r_B	Bore radius = $r_p + \delta$
r_c	Core radius
r_i	Inner radius of penetrator
r_p	Radius of penetrator
R	Hole radius

s	Second
S	Surface for heat or load transfer
S_m	Cross-sectional area of earth/rock melted
S_p	Cross-sectional area of penetrator
t	Time
t_c	Controlled liner cooldown time
t_r	Residue time
T_{eu}	Maximum end use temperature
T_L	Liner solidus temperature
T_m	Soil/rock melting temperature
T_{max}	Maximum penetrator surface temperature
T_o, T_i	Initial temperature
T_s	Penetrator surface temperature or glass liner inside surface temperature
T_{sp}	Strain point, corresponds to $10^{13.5}$ poises
T_∞	Ambient undisturbed rock temperature (soil temperature)
T_δ	Glass liner outside surface temperature
u	Velocity component in the x direction
U	Temperature excess
U_e	Extrusion velocity
U_{min}	Minimum velocity associated with a given thermal power
U_∞	Velocity of penetration

v	Velocity component in the y direction
W	Watt
x	Cartesian coordinate
y	Cartesian coordinate
z	Cartesian coordinate

GREEK LETTERS

α	Coefficient of thermal expansion or thermal diffusivity
β	Empirical constant
γ	Empirical constant
δ	Glass liner thickness
δ_e	Effective depth of heat penetration in earth/rock by passing penetrator
ΔE	Activation energy
ΔP	Pressure drop
Δt	Dwell time or time increment
ΔT	Temperature difference
ΔT_a	Maximum allowed temperature difference
ΔT_m	Melt superheat difference
θ	Angle of conical penetrator
λ	Latent heat of fusion
μ	Viscosity
ν	Poisson's ratio
ξ	Moving coordinate $= x - U_\infty t$
ρ	Density
σ	Stress
σ_a	Allowed thermal stress
σ_s	Structural stress limit

ϕ	Temperature excess
ϕ_o	Heat flux for liner cooldown
ψ	Empirical geometrical shape factor or temperature excess

SUBSCRIPTS

a	Axial
B	Bore
d	Debris
e	Earth/rock
g	Glass
l	Loss
L	Liner
m	Melt
o	Initial
P	Penetrator

1.0 INTRODUCTION

This final technical report encompasses the work performed from April 2 to October 2, 1973, under Contract DOT-TSC-591 entitled "Basic Understanding of Earth Tunneling Through Melting."

1.1 BACKGROUND

The Los Alamos Scientific Laboratory (LASL) initially explored the feasibility of rock melting as an alternate drilling method in the 1960-1962 period resulting in a U. S. Patent (3, 357, 505). Feasibility was indicated by relatively simple devices which were built and tested at the Laboratory. These tests included boring holes at steady rates (~1 m/h) in samples of local material such as basalt and igneous rock without any problems in deformation or tip corrosion. Except for the interest that was generated, no activity resulted from this work until the 1970's.

In early 1971 LASL extended the analyses and proposed continuation of the development of a rock melting Subterrene. The concept was judged to be feasible and within the grasp of present technology. LASL has supported the Subterrene project since about April 1971, and has subsequently successfully melted holes in a variety of different rock types including 55 mm (2 inch) penetrations to depths of nearly 25 meters (80 feet) and corings up to 114 mm (4-1/2 inch) in diameter. Also, laboratory testing has demonstrated a capability to penetrate water-saturated rock, a variety of low density soils, water-saturated alluvium, and high density rock such as basalt. In each case a reasonably good, stable glass-lined hole was achieved.

Data obtained in these laboratory tests and in the field tests (vertical boring and horizontal boring) have yielded a simplified linear relationship regarding power and the rate of advance. Simultaneously, the development of thermal analysis techniques and approaches to guide and optimize the penetrator geometry, heater requirements, and insulation systems have been initiated by LASL. Computer programs which provide for describing the melting of rock and viscous flow field have been developed. However, a thorough review and determination of the physical processes by which the rock melting penetrator operates had not been accomplished at LASL in these early phases of the program.

The process being developed at LASL is based on the concept of progressive local melting of

rocks and earth. This process results in a molten glass lined hole with no debris; or, removal of cores, as provided in controllable extrusions where full consolidation is not desired or possible. The basic rock heat transfer/melting processes are relatively well defined and are considered amenable to theoretical analysis and predictions. Also, this rock melt can be formed into a glass lining with some controllability with respect to conventional methods of glass forming.

Thus, LASL has demonstrated the ability to not only successfully melt rock and penetrate the earth leaving glass lined holes, but also has provided a reasonable foundation of analytical models for prediction; but the simplified models available were insufficient for predicting or extrapolating to other conditions at the start of this study.

1.2 STUDY OBJECTIVES

Since rocks and earth are usually mixtures of minerals and generally have relatively low melting points (1200 - 1500°K), this process appears to have a wide-spread application with a number of potential advantages over conventional "drilling" methods.

1. Higher rates of penetration are potentially possible.
2. The capability of forming a liner has the potential of obviating the need for a support structure.
3. The potential for the reduction of or the elimination of mucking requirements.

If such a technique can be applied to large scale tunneling operations such as those required for the formation of transportation tunnels, it would then represent a significant technological breakthrough. The feasibility of the technique has been demonstrated only under limited conditions. The experimental data obtained apply also to limited conditions. Moreover, functional relations of some of the physical processes involved were not available. Because of these facts, adequate evaluation of the capabilities and limitations of the technique for large scale tunneling applications are required for this study.

For an evaluation of this type, it is essential to predict the performance of the given tunneling operation in terms of the power requirements, liner thickness and the rates of penetration as releated to the tunnel diameter, depth of tunneling, quality of glass liner formed, etc.

The following study objectives were outlined in the proposal, WANL-BP-3001, and were addressed throughout the program.

1. To describe the fundamental physical processes involved in this technique.

2. To determine the key parameters.

3. To provide functional relations among these key parameters enabling the evaluation of process feasibility and limits of large scale application. These relations include

   Geometry variables

   Power requirements

   Thrust loads

   Rates of penetration

   Earth structural behavior

   Liner structural behavior

   Material constraints

4. To define additional critical data requirements at the end of the program.

1.3 STUDY APPROACH

Toward fulfilling the preceeding study objectives, the following study approach was selected and carried throughout the program.

1. Provide detailed descriptions of the basic processes involved in 5 potential modes of tunneling from the basic concept of melting rock/earth. Functionally analyze these processes using systems engineering techniques to determine the parameters and controlling variables affecting the capabilities and limitations of these modes of operation.

2. Identify and define the major parameters affecting the performance, capabilties and limitations of each mode of tunneling from the functional analysis and fundamental equations.

3. Conduct basic theoretical analyses (as opposed to a computerized numerical solution) of the governing physical processes involved, develop analytical models and derive functional relations of the controlling variables.

4. Verify the functional relations derived by correlation with existing experimental data.

5. Generalize the functions to apply to all modes of tunneling, all scales of tunneling, and all types of rock and soil materials that may be encountered under normal tunneling conditions.

The above five statements formed the basis for the program work statements. Tasks 1 through 5 in Figure 1-1 correspond directly with them.

The performance of each task requires several disciplines; e.g., analysis of the physical process variables requires structural mechanics, fluid mechanics, and thermal analysis as a minimum. The compilation of this report for this reason is not formulated into chapters defined by a task, but rather by a discipline related to one part of the process. This is consistent with a fundamental assumption of the study; i.e., a valid theoretical description of these events can be obtained by mathematically decoupling the phenomenological equations for them.

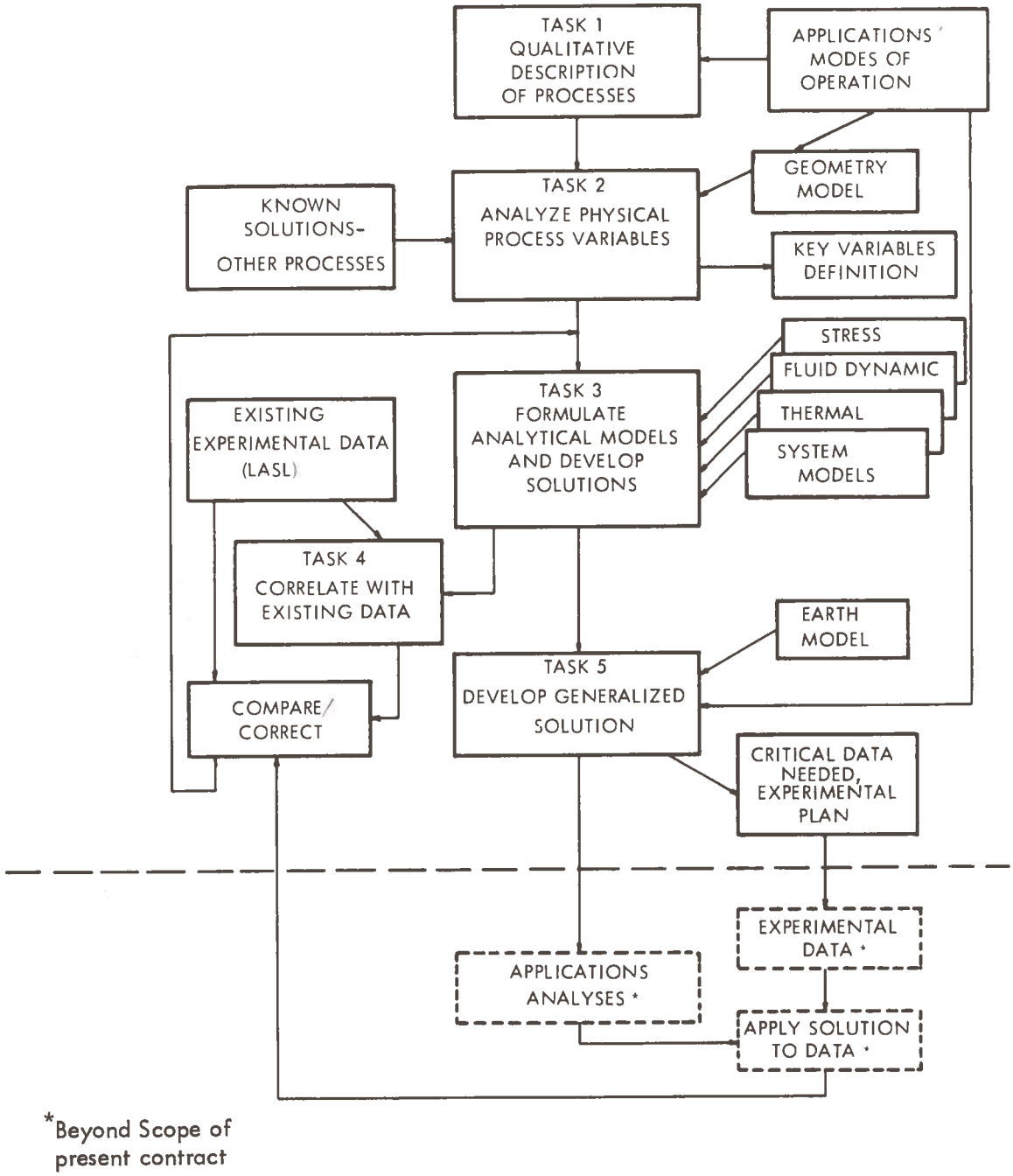

*Beyond Scope of present contract

Figure 1-1. Program Logic Flow Diagram

2.0 SUMMARY

2.1 DESCRIPTION OF APPROACH AND WORK ACCOMPLISHED

Based on early work and those carried out concurrently with this study at the Los Alamos Scientific Laboratory (LASL), five "modes" of tunneling were identified. These were associated with the following three distinctive types of penetrator design concepts:

1. Conical consolidator
2. Extruder
3. Coring penetrator with or without extrusion

The conical penetrator was designed specifically for making holes through unconsolidated earth/rock whose density is appreciably less than that of the glass made from this material. Extrusion of a part or all of the melt becomes necessary when the density of the glass is equal to or less than that of its parent earth/rock material. A coring penetrator was considered for large scale tunnel excavations.

The physical processes involved in the hole boring/tunnel excavation technique were identified and studied. Five typical earth geological models were formulated. Each model has its unique physical characteristics and specified composition and physical properties. Physical models of typical penetrator designs were also assumed. Functional relations of controlling variables were then derived for the following:

1. Heat transfer processes
2. Melt flow process
3. Earth structure
4. Liner structure
5. Liner cooldown

2.2 HEAT TRANSFER AND MELT FLOW ANALYSES

The mathematical models and functional relations for heat transfer and melt flow were derived from closed form analytic solutions of the basic equations of energy, motion, and continuity. The heat transfer models permit the evaluation of the total thermal power required and the maximum local heat flux.

The calculation of these parameters require the specification of the rate of penetration, penetrator geometry, penetrator dimensions, glass liner thickness, and earth/rock and melt physical properties.

The functional relations derived for the melt flow process permit the calculation of the following:

- Total applied thrust load
- Melt pressure and stress on the penetrator, and
- Forces on the glass liner required for thrusting

The information needed to determine the above parameters are identical to those needed for the thermal calculations.

The functional relations for glass liner cooldown permit estimates of the controlled liner cooldown time and the length of controlled cooldown sections required.

The calculation of these parameters from the functional relations require the specification of the thickness of the melt layer and glass liner, earth/rock as well as melt and glass physical properties, and cooldown heat flux.

Attempts were made to verify the functional relations derived by correlation with the limited experimental data. Excellent correlations were obtained for the following areas when adequate experimental data were available:

1. Thermal power requirement for all five modes of tunneling and all three penetrator designs/concepts.

2. Total applied thrust loads for conical consolidating penetrators only.

3. Transient cooldown temperatures of the inner surface of the glass liner only.

Because of the experimental verifications, high degrees of confidence can be placed on the predictions of the following:

- Thermal power requirement, maximum penetrator surface temperature, maximum heat flux, maximum rates of penetration, liner thicknesses allowed, etc., for all five modes of tunneling, all three penetrator designs/concepts and all types of earth/rock materials.
- Total thrust load, melt pressure, stress on the penetrator, and forces on the glass liner wall to effect thrusting for conical consolidating penetrators only.
- Temperatures of the inner surface only of any glass liner during cooldown.

Where the functional relations had not been verified experimentally, assumptions were made to permit estimates of the design parameters of interest. These include the following:

- Thrust loads for coring, extruding penetrations, melt pressure, stress on heated penetrator surface, and pressure on glass liner wall.
- Glass liner thicknesses required to overcome primary and secondary loads.
- Glass liner cooldown requirements to prevent thermal stress cracking.
- Controlled liner cooldown time and lengths of cooldown section required.

Although many of the functional relations developed have not been verified experimentally, it was felt that they are adequate for scoping calculations and preliminary conceptual design

calculations. Scoping calculations were carried out covering ranges of parameters of interest to transportion tunnel excavations. These include the following:

- Depth of tunneling operation
- Tunnel diameter up to 10 meters,
- Rates of penetration of ~100 meters/day (or better),
- Loose, unconsolidated, alluvial type earth/rock material.

The results of these analyses show that penetrator surface temperatures severely limit the rate of penetration or the geometry of the penetrator that can be considered for all modes of tunneling.

For example, with a plain conical, LASL experimental type consolidating penetrator, the maximum penetrator diameter that can be considered when using tungsten as the material of construction is only 45 mm at 0.1 mm/sec rate of penetration and only 90 mm at 0.05 mm/sec rate of penetration. These limitations are only slightly improved when extrusion of a portion of the melt is included.

Although appreciable improvements are made when coring is added to extrusion, the operating limits are still far short of the goals set for practical tunneling applications. As typical illustrations with tungsten as penetrator material of construction and tunneling through unconsolidated alluvial type materials, a 10 meter diameter tunnel can advance at a rate of approximately 2 meters/day. At 50 meters/day, the maximum tunnel diameter is on the order of 1 meter. This is due to the excessive temperature drops across the melt for reasonable melt thicknesses.

The problem is completely eliminated if a glass liner is not required. This may be the case when tunneling through highly consolidated rock such as basalt, granite or competent rocks.

These identified limitations are design-oriented. Penetrator design changes were proposed to overcome the limitations. These include the following features: (1) the use of segmented and extended surface areas to reduce the heat flux, (2) extruding the melt into a liner of the

desired thickness. This minimizes the melt thickness over the heated portions of the penetrator to minimize the penetrator surface temperatures.

Preliminary calculations showed that with these design features, a coring penetrator that can form a 10 meter tunnel diameter has the potential for advancing through alluvial-tyoe materials at > 100 meters/day.

2.3 EARTH AND GLASS LINER STRUCTURAL ANALYSES

The development of functional relations for the stress fields evolved with concern for those variables which could control or limit the earth tunneling process; and these were related to the earth's structural behavior and the glass liner's structural integrity. The descriptions for earth structural behavior included the environmental boundary conditions imposed by the earth's own weight, tectonic residual stress, imposed temperature changes, melt pressure and earth moisture. The structural integrity evaluation for the glass liner included the effects of earth loads, penetrator thrusting loads, and the thermal cooldown loads.

The criteria imposed upon the earth to arrive at tunneling limitations consistent with the earth stress analysis were that of no surface fissures, no significant surface upheaval, and no earth collapse into the melt zone which would be evidenced by an earth surface collapse. With these criteria a minimum allowable tunneling depth was established, and the limitations for melt pressure were established for any tunnel depth greater than the minimum allowable. The conclusions derived from the idealizations of elasticity, isotropy, homogeneity and plain-strain are:

- If the earth's surface is free of dead weight, the crown of the tunnel bore should be at least a tunnel bore diameter below the earth's surface.
- Under adverse operating conditions such as a water saturated highly porous medium, the direction of earth fissures and therefore the likelihood of surface upheaval or surface fissures can be estimated only after first conducting field experiments to determine the tectonic residuals, the percent water saturation and porosity, the extent of medium non-uniformity, and the direction of any earth medium anisotropies.

For example, in an isotropic media without a tectonic residual stress, the preferred fracture direction is vertical. With a horizontal tectonic stress ($P_T > \rho_e C$) in excess of the tunnel centerline depth component of vertical overburden, the fractur tendency would be horizontal. In a non-uniform medium with an overlying hard sed metary rock strata a vertical fracture is likely to be arrested and diverted to a horiz plane.

- When crack propagation is undesirable, it can be precluded with operational melt pressures of values less than the local vertical overburden in zones of moderate ($P_T \geq \rho_e C$) tectonic compression or with operational melt pressures of values less than the local horizontal overburden in zones of no tectonic compression. Without prior determinations of residual tectonic compressive stresses, a conservative melt pressure for the avoidance of crack propagation would be:

  $$p \leq \frac{\nu}{1 - \nu} \rho_e C$$

- The propagation of a fissure will depend upon the melt pressure and the volume avail ability of a substance which can fill and occupy the created crack void volume. To this end, methods were provided to evaluate melt and water volume availability.

- When a fissure is desirable, such as may be required for the disposal of excess water, melt pressures must exceed the local overburden stress component. This eventuality has been considered here by providing relationships which define the allowable and required penetrator melt pressure consistent with both surface upheaval and surface fissure.

- The alternative approach to minimizing any water disposal problems is by penetrator design. The design configuration must tend toward a very thin liner and a large percentage of mucking.

A structural integrity evaluation of the glass liner was provided to describe the state of stress and stability under primary loading and to define cooling rate requirements consistent with thermoeleastic stress limitations. The primary loads were separated into externally applied earth loads and internally applied thrust loads. The secondary loads were defined as those resulting from transient and residual thermal stress.

Three separate earth load models on the liner were considered. They were: (1) A condition of hydrostatic pressure characterized the liner loads from an idealized earth model composed of a plastically behaving medium, possibly best characterized by quicksand. This is an unlikely earth medium in which design considerations would have to resolve the initial liner support problem during cooldown in parallel with a penetrator "sinking" problem. Nevertheless, this idealized earth model was included as a limiting case of a more general earth model, because it provided a valid liner stability criterion against buckling which was extrapolateable to other earth model liner loading conditions. (2) The condition of no lateral restraint characterized the liner loads from an earth settling directly above the tunnel liner. This model was conceived by envisioning vertical but no lateral earth settlement about the liner, and it was inspired by recognizing two unique features associated with tunneling by heated penetrators. These are the volumetric contraction tendency of the solidifying liner and the potential for both planned and unplanned earth fracture and upheaval. The sequence of events in arriving at this earth model liner loading condition is a horizontal fissure with upheaval followed by liner radial contractions and then a vertical earth settlement. (3) The condition of restrained lateral deformation characterized the liner integrity by an earth load model with structural consequences lying between those of the hydrostatic pressure model and the model of no lateral restraint. It assumed that earth settlement about the glass liner is such that it returns to the overburden condition which existed prior to the tunnel formation. This model is best envisioned as appropriate in unfractured earth media characterized by the Poission ratio values above 0.3, and these are the sands, clays, and shales.

The allowable tunneling depth for each of these models was established as a function of glass strength, earth density, liner thickness and other related material properties.

Two penetrator primary load models on the liner were considered. They were a thrust producing model and a penetrator weight model. The choice for a thrust model was a conservative radial ring pressure load with a coefficient of friction for the transmittal of this radial load to axial thrust. The major conclusions, about the thrust model, derived from the integration of Figures 9-7, 9-5, 7-11, and 7-12 are:

- With minimal design effort, the primary stresses induced by a thrusting mechanism are not limiting when compared to the stresses from the earth primary loads.

- The design effort here would deal with providing an adequate friction coefficient at the thruster/liner interface. Based on a glass liner tensile strength of 1.48×10^7 N/m^2 (2150 psi) and tunnel diameters not to exceed 10 meters, it was determined that if the thrusting coefficient of friction is less than about 0.2, that the thrust required to advance the penetrator may always exceed the allowable thrust. If the thrusting coefficient of friction is about 0.5, the required liner thickness is about 6 to 9% of the penetrator radius for tunnel diameters in the range of 10 to 6 meters. If the thrusting coefficient of friction is about 1.0, the required liner thickness is about 4 to 7% of the penetrator radius in the range of 10 to 6 meter tunnel diameters.

The penetrator weight primary load model considered the glass liner as a beam on an elastic foundation with the penetrator weight evenly distributed over a length which was studied as a variable defined by multiples of the penetrator diameter. The primary conclusions from the penetrator weight model were:

- Penetrator allowable densities increase as the earth elastic foundation stiffness increases.
- A sample problem with conservative assumptions indicated the penetrator weight should not limit the tunneling feasibility provided its average density over its liner-supported length does not exceed 460 gm/cm^3. This compares to an earth density of about 2.4 gm/cm^3 and a structural steel density of about 7.8 gm/cm^3.

The recommendation for any future efforts in the area of primary load analysis should logically be deferred until sufficient liners have been produced to experimentally generate good estimates for the liner material properties, especially its strength. If a cracked liner is the only alternative, it is recommended that tests be conducted on experimental liners under simulated earth loading conditions to evaluate the arching stability of scale models which may or may not be free of thermal stress cracks. The major uncertainity in scale model testing with a brittle material is that associated with Weibull's theory which would indicate the larger the sample size, the weaker the material.

The glass liner secondary load analysis provided the thermal stress equations which can be used to evaluate the inner tunnel wall deformations, transient cooldown stress levels and residual stress levels which in turn have defined the allowable cooling temperature gradients. Three models describing the thermoviscoelastic behaviorial characteristics of the solidifying glass liner were analyzed, and these are:

1) Plane strain with no axial deformation and with no radial deformation at the outer surface: The earth media in which this model could most likely represent the solidification process is dense rock formations which would be capable of arching in hoop compression as the liner unsuccessfully tends to contract at its outer surface. The conclusion reached here was that if the earth/glass interface remains stationary during the cooling process, the glass will experience both radial and longitudinal cracking irrespective of the cooling temperature profile. The stress/strength ratio for the best possible profile, that of uniform cooling, was approximately 20 to 1.

2) Plane strain with unconstrained axial contraction and with unconstrained radial contraction of the outer surface: In this model the liner must be capable of separating itself from the earth at the glass/earth interface and the liner must be free to "slide" (contract) in the axial direction. For horizontal tunneling in any media, this is a very unlikely model, because even with separation at the interface, the weight of the liner and the weight of the penetrator/equipment will result in a large normal contact force along the bottom exterior side of the tunnel in contact with the earth. Possibly, the water saturated clays and sand would permit liner axial contraction by slipping conditions. Another possible earth media which may allow a liner axial contraction is dry, low density earth which would crush and densify in the process. The conclusion arrived at for this unlikely structural model was that glass liner cracking could be avoided by controlling the transient temperature gradients. A computed value of about $25^{\circ}C$ identified the maximum allowable difference between a surface and the average liner at a given axial location.

3) Plane strain with no axial deformation and with unconstrained radial contraction at the outer surface: With this model the earth offers virtually no tensile normal traction at the glass/earth interface, but rather than separating at that interface, the earth maintains sufficient contact to provide the friction that would prevent a glass liner axial contraction. This model is best visualized as being representative in the not so crushable materials, especially in zones where tunnel collapse is to be expected without a liner. The conclusion reached for this model was that irrespective of the cooling technique; transverse glass liner cracking should be expected.

There does exist the possibility of encountering earth media in a long tunnel wherein any or all three of these models would best represent the glass solidification stresses at different regions of penetration. Realistically, combinations of these models will prevail in unknown proportions. At the extreme of freedom, the transient thermal gradients were characterized by limiting values that would prevent glass cracking, but from the viewpoint that "fixity" cannot be overlooked as an approachable boundary condition, glass liner cracking should be expected as a worst case design condition.

2.4 CONCLUSIONS

Based on the results of the study and parametric analyses, major conclusions have been drawn for the various areas studied. These are summarized in this section.

2.4.1 Limits of Operating Capabilities

1. Based on the specific penetrator designs designated in the 5 modes of tunneling, it is concluded that large tunnels can be created at reasonable penetration rates only with very thin glass liners, i.e., of $\leq$ 1 cm.

2. For reasonable glass liner thicknesses, i.e., $>5\%$ of radius, these basic penetrator designs are only suitable for relatively small scale penetrators. For these designs, operating capabilities are severely constrained by penetrator surface temperature limitations.

3. These limitations can be removed by the use of an extended surface, segmented heater penetrator concept proposed in this study for large scale tunneling applications. Preliminary scoping calculations have shown that tunnel diameters up to 10 meters and tunneling rates of $\sim$ 100 meters/day are potentially attainable with this concept. However, conceptual design studies are needed to establish this as a practical approach.

4. Thermal power requirements for the proposed penetrator design are relatively low. They are on the order of 20 megawatts for 6 meter tunnels tunneling through unconsolidated earth/rock and 40 to 50 megawatts for tunneling through consolidated material at a rate of 100 meters/day.

2.4.2 Applied Thrust Loads

1. For small scale penetrators, pressure drag (or form drag) is the dominant contribution to total thrust load requirements. Minimum thrust load is simply the ambient pressure times the penetrator cross-sectional area.

2. Frictional drag forces due to flow of molten earth/rock over heated portions of the penetrator are negligible when compared to other forces.

3. Frictional drag forces over melt cooldown section (adhesion forces) can be important for relatively long cooldown sections. For penetrators where the length of the cooldown section is on the order of the penetrator diameter, the contribution to applied thrust loads from pressure drag and adhesion forces are of the same order of magnitude.

4. The minimum stresses on the penetrator for large scale Mode 5 tunneling as a result of applied thrust loads are small (less than 7×10^6 N/m^2 or 1000 psi) for tunneling at depths up to 40 meters.

5. The limited thrust load data from extruders have not been correlated successfully with functional relations. Calculated thrust loads are much smaller than experimental values.

6. Typical thrust loads are 9×10^5 kg ($\sim 10^3$ tons) for a 6 meter tunneler at reasonable advance rates.

2.4.3 Earth and Glass Liner Structural Phenomena

Based on earth primary load analyses, the following conclusions can be drawn:

1. The model for the condition of restrained lateral deformation indicates the required liner thickness to be about 23% of the penetrator radius for a tunnel centerline depth of 70 meters. This corresponds to a zero margin of safety against a longitudinal tensile crack under the following conditions: earth density = 0.0025 kg/cm^3, earth Poisson ratio = 0.35, glass tensile strength = 1.48×10^7 N/m^2 ($\sim$2150 psi) Under these same conditions, the required thickness is about 8% of the penetrator radius for a tunnel centerline depth of 10 meters.

2. The model for the condition of no lateral restraint indicates the required liner thickness to be about 75% of the penetrator radius for a tunnel at 70 meters of centerline depth and about 21% for the 10 meter deep tunnel. This is based upon the same conditions given above.

3. The liner thicknesses required to prevent liner cracking under external earth loading indicate that liner buckling is not a problem.

The glass liner secondary load analyses yield the following conclusions:

1. If the earth/glass interface remains stationary during the cooling process, the glass will experience both radial and longitudinal cracking irrespective of the cooling temperature profile. The stress/strength ratio for the best possible profile, that of uniform cooling, was approximately 20 to 1.

2. The conclusion arrived at for the model where the liner is capable of separating from the earth at the glass/earth interface is that glass liner cracking could be avoided by controlling the transient temperature gradients. A computed ΔT_a of about 25°C is identified to be the maximum allowable difference between a surface and the average liner temperature at a given axial location.

3. Based on the model of plane strain with no axial deformation and with unconstrained radial contraction at the outer surface where the earth maintains sufficient contact to provide the friction that would prevent a glass liner axial contraction, it is concluded that irrespective of the cooling technique, transverse glass liner cracking may be expected.

2.4.4 Melt Cooldown Requirements

Cooldown times and lengths of controlled cooldown sections predicted based on using extended afterbodies and LASL small penetrator design practice and for tunneling conditions of interest have been shown to be excessive and impractical for large tunnels.

Two methods to solve this problem have been proposed. These methods require study and further conceptual design and analyses as well as experimental research in order to determine practical limits of capabilities and real large tunnel limitations. The most probable solution may well be designs permitting thermal stress cracking as verified in cracked liner insitu experiments.

2.5 RECOMMENDED FUTURE WORK

The limitations of the tunneling technique that have been identified and the proposed solutions are summarized in Table 2-1. The types of solutions proposed were developed only to a level which indicated the following potential capabilities:

- Large tunnel diameters (up to 10 meters)
- Thick glass liners (of any necessary thickness)
- High rates of penetration (of > 100 meters/day)
- Reasonable length of the controlled cooldown section

It is evident that all of the attractive features possessed by the basic technique of rock/earth melting for tunnel excavation have been considered desirable to retain and design approaches have been conceived which permit this. These are discussed in Chapter 11.

TABLE 2-1

LIMITATIONS AND DESIGN SOLUTIONS FOR SUBTERRENE TUNNELING

Limitation Identified	Design Solution
Penetrator surface temperature limits the rate of penetration for given glass liner thickness required.	Extended heated surface area to reduce surface heat flux.
Glass melt thickness determined by penetrator surface temperature limits the liner thickness.	Extrude molten melt into the liner thickness desired in the unheated section, maintaining a thin melt thickness over the heated surface area.
Non-homogeneous earth/rock materials causes hot spots and reduces the rate of penetration.	Use segmented heaters in conjunction with a new type of thermal control heat pipe.
Effect of gravity will cause "slumping" of the melt.	Control melt pressure distribution by controlling and varying the rate of extrusion through multiple extrusion ports.
Leading edge heat flux for high rates of penetration and large penetrators is excessive for conventional heat transport mechanisms.	Use heat pipes to transport thermal power from the heat source to the penetrator.
Excessive cooldown time and length of controlled cooldown section.	Implant coolant tubes in the molten glass to reduce conduction path length and increase the heat flux.
Frictional drag over melt cooldown section increases the applied thrust load.	Implant coolant tubes into the molten glass to reduce the length of cooldown required.
Glass liners of reasonable thicknesses will most likely crack during cooldown.	Compressive strength of crack glass liner should remain high and adequate for the support of earth primary loads. Seal the liner with a sealant or second liner that does not require structural strength. Implant reinforcing/structural material in glass.

The design solutions proposed appear to be technically feasible. However, experimental testing and further analyses of conceptual design efforts will be needed to verify this. In particular, experimental data are presently needed in the critical area of potential glass liner structural capability with cracking under controlled cooldown conditions. The following future studies are therefore proposed:

1. Evaluate and analyze the capability of extended surface, segmented heater designs as proposed here for practical tunnel excavations. An integrated conceptual penetrator design study is necessary to properly evaluate all the features proposed, because of the close interactions of the important design parameters involved. All of the solutions proposed in Table 2-1 shall be considered and integrated into the conceptual design study.

2. Experimental and analytical study of thrust load requirements for extruders and corers, the two modes of operation that were found necessary for large scale tunnel excavations. Evaluate melt pressure effects.

3. Experimental study of controlled glass liner cooldown to evaluate the effect of liner thickness and glass and earth/rock physical properties on the properties of the glass liner following cooldown. Of particular interest is the quality and the state of the glass liner under different cooldown conditions.

4. Since the glass liners tend to crack, determine the compressive strength of glass liners of different thicknesses, made from various earth/rock materials and different radii of curvature with cracks.

Brief statements of these problems, proposed approaches to solution and suggested tasks are outlined in the form of individual programs in Appendix A.

3.0 FUNCTIONAL DIAGRAMS

A functional logic diagram was developed as a means of identifying all the principle functions involved and the mechanisms required to carry out the tunneling objectives. A simple logic was used in developing the functional diagrams that began with the end effect desired; i.e., a tunnel. These functional diagrams were established to provide a disciplined method to more easily evaluate separate, particular requirements and also maintain their relationship so that evaluation and integration of these requirements would be possible. The four levels of logic (steps) were defined as follows:

1. Effects desired (end product)
2. Functions performed (to obtain effect)
3. Changes required for function completion (define start to finish)
4. Mechanisms required to accomplish changes

The principle benefits derived from the functional diagram include not only systematic definition of each pertinent function but also systematic development of requirements, identity of interrelationships, and visualization of relative significance of the particular mechanisms.

The effect of a particular application (i.e., mode of tunneling, operating conditions, and specific tunnel requirements) can be evaluated for each third level "change required" situation. Integration of the subsequent specific requirements and identification with necessary mechanisms provide the definition needed for design and operating analyses.

The first two levels of the functional logic diagrams are indicated in Figure 3-1. The third and fourth levels are indicated in Figures 3-2 and 3-5. Details of the third and fourth levels, where pertinent, are indicated in Figures 3-6 through 3-14.

The zero level of this system is the specific operation objective -- to make a tunnel. The first level effects desired would, therefore, include three distinct items, (1) the physical advancing of the tunneler or penetrator, (2) the forming of a competent liner, and (3) the removal of excess rock/earth not consolidated or utilized within the tunnel.

The specific functions providing these effects are simply defined at the second level for the earth melting hot penetrator approach. This level is still quite general, however, without definition of the quantitative changes desired from the function.

From this second level, the required changes involved and the affected parameters can be defined. This provides the third level. The third and fourth levels have been developed to the extent of identifying the blocks in which the process requirements needed in this study are defined. Needed inputs, assumptions, and quantified constraints have been identified at these levels as shown in the figures. Where the function does not involve a basic process requiring development in this study, it is not carried to any further detail.

As noted in the following, a significant number of identified functions do not relate to the development of basic process understanding which is the objective of this study. These functional requirements are called out as they are identified, however, and their significance noted for consideration in other needed efforts.

Almost invariably, the outputs of the evaluations indicated in the third level (changes required in performing functions) provide design inputs and permit identifying design requirements for given performance requirements. For this reason, these blocks are detailed in the areas in which the significant rock melting and liner forming functions are carried out. Third levels in the area of control and debris removal have not been detailed beyond identity of the functions and changes required.

This study does not go into any of the design/performance associated areas except to point where incompatibilities exist and suggest possible design approaches that might resolve them. The following is concluded from the functional logic.

1. Although control of the penetrator does not fall under the direct functions relating to the basic rock/earth melt process, it nevertheless is a crucial part of making a tunnel. Design requirements and control concepts must be developed and carried along with the penetrator design at the second, or "function" level, to assure a viable and feasible system concept.

2. Constraints on displacing the melt and forming the liner interface with earth boundary conditions and need to be defined. For the purpose of this study, the assumptions shown in the third level blocks have been made. Also, earth/rock melt functions, although not directly concerned with the boundary interface conditions as are the melt displacing and liner formations, do require definition of interface constraints at some early time regarding acceptable local and distant temperature, heat dissipation levels, and ground displacement.

3. Although not directly related to the basic process of rock/earth melting, the design capabilities regarding source of power, cooling system, means of heat transfer, and other design considerations need to be defined in evaluating the feasibility of a practical concept. These areas are also identified at the fourth levels of the diagram. Several of these key areas are discussed in Chapter 11.

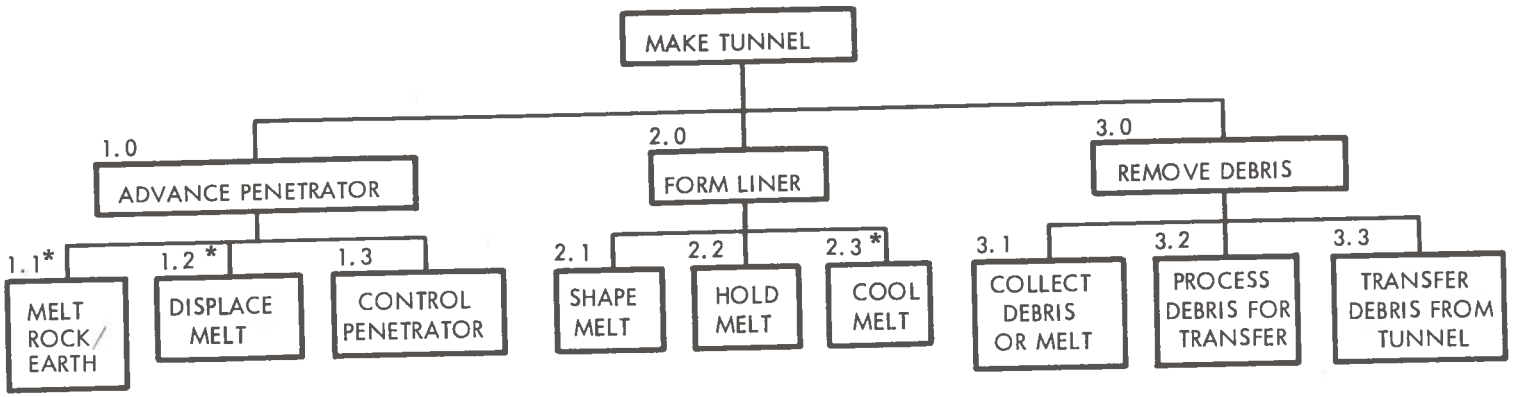

Level 1 Logic: Effects Desired (End Product)

Level 2 Logic: Functions Performed (to obtain effects)

*Principal process related functions

Figure 3-1. First and Second Level System Functional Diagram

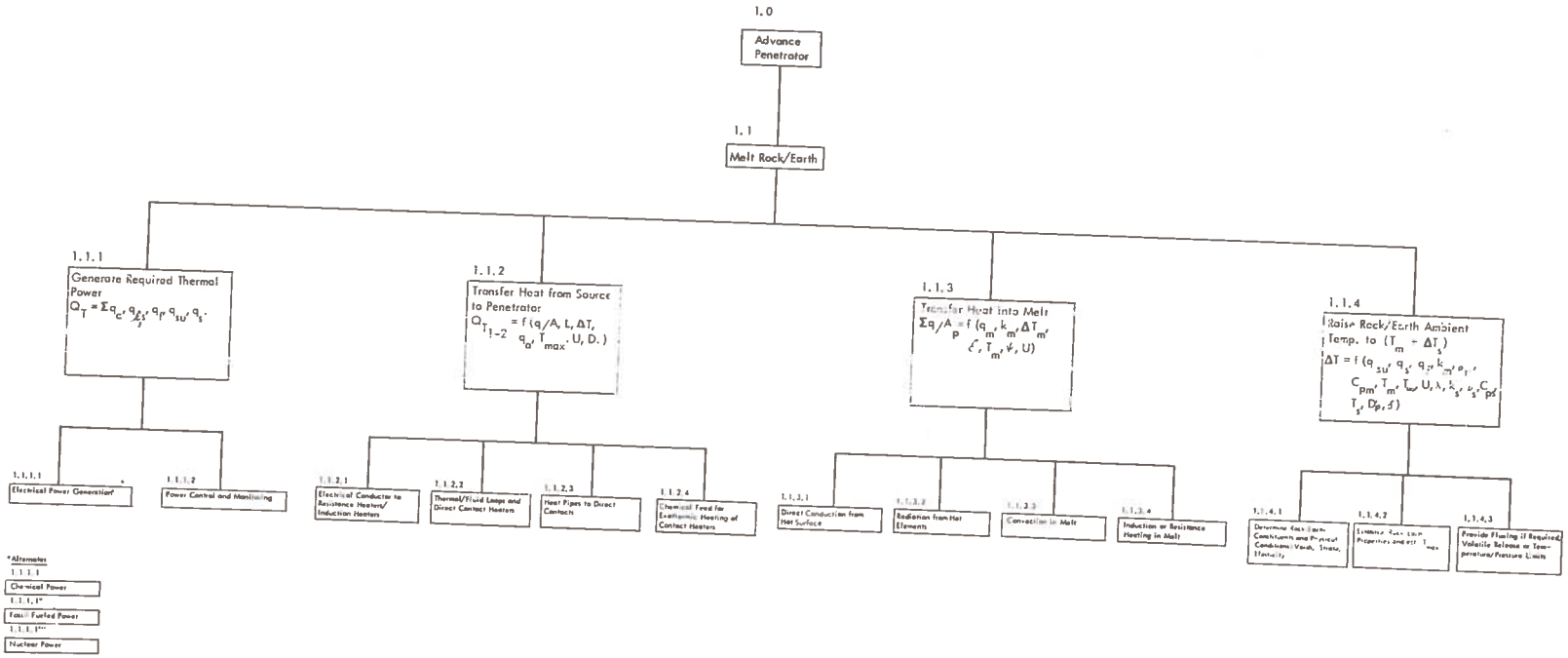

Level 3 Logic: Changes required for function completion (define start to finish)

Level 4 Logic: Mechanisms required to accomplish changes

Figure 3-2. Expansion of Second Level Block 1.1 Function (Melt Rock/Earth)

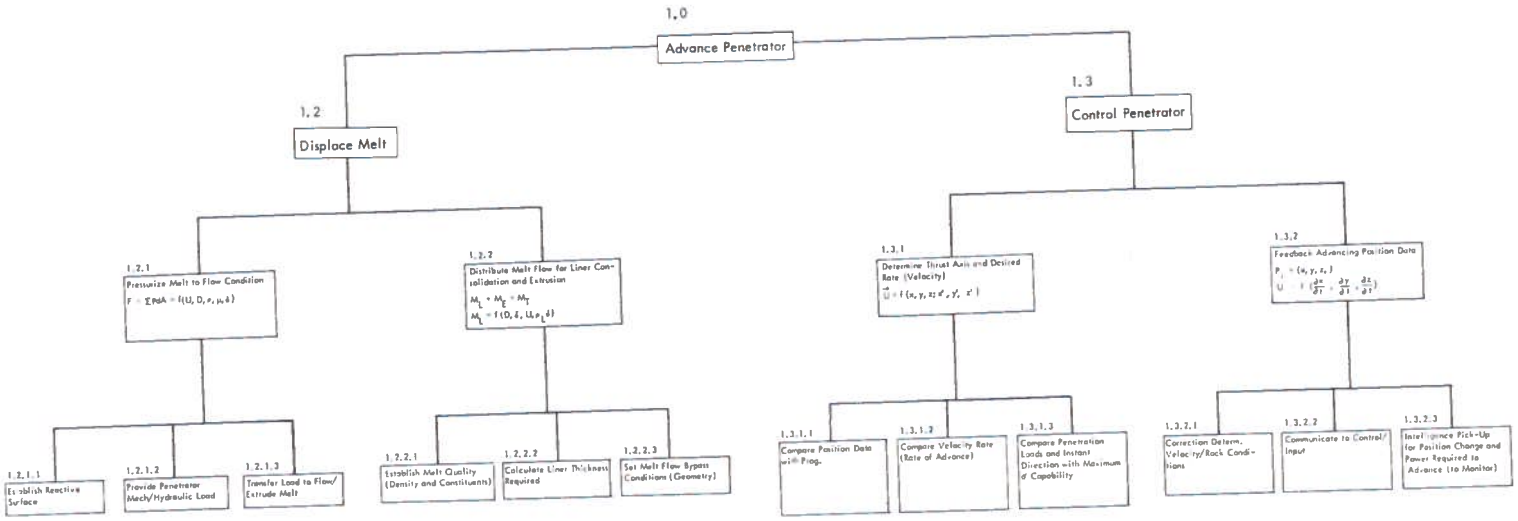

Figure 3-3. Functional Diagram (Continued)

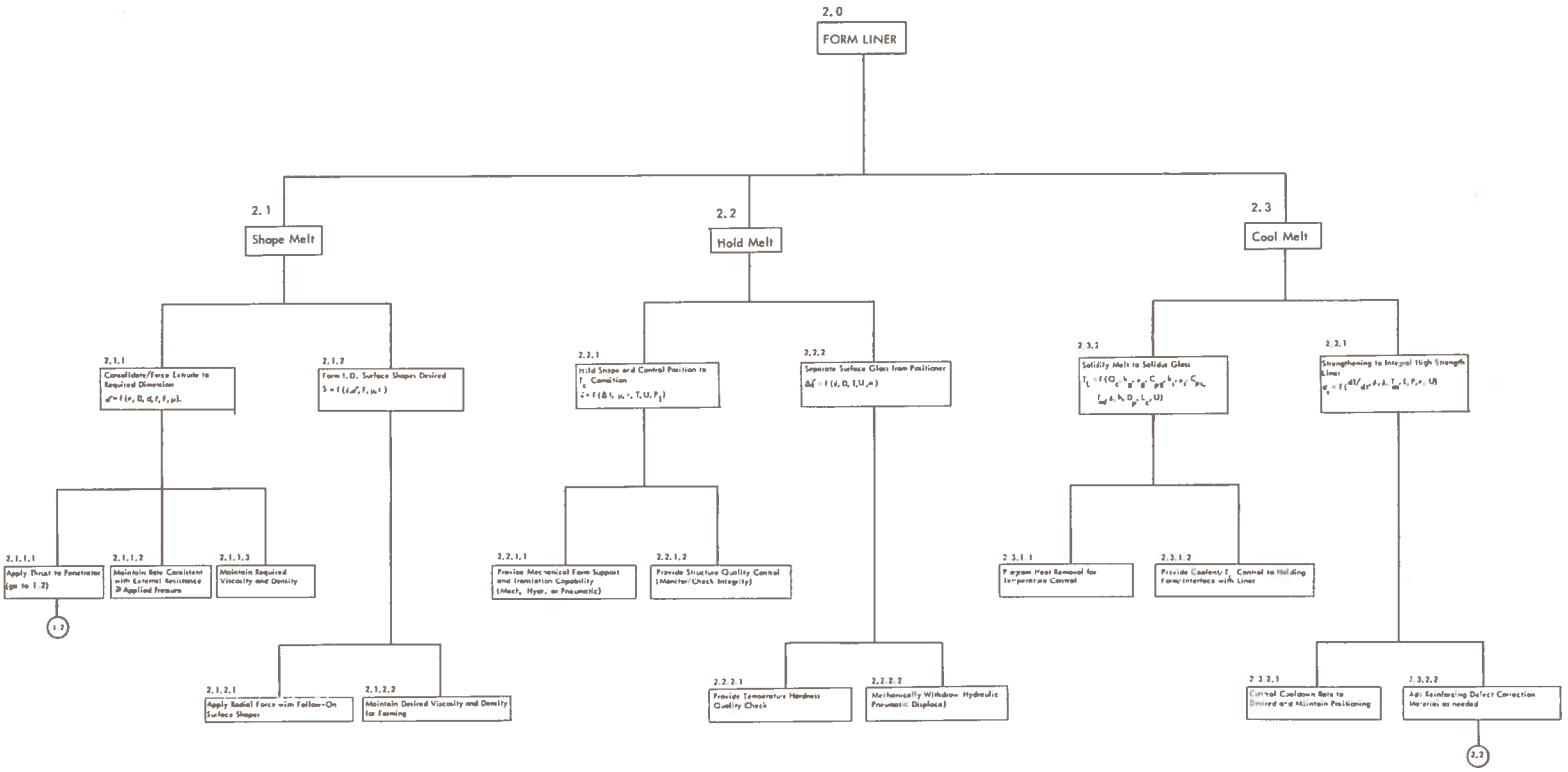

Figure 3-4. Functional Diagram (Continued)

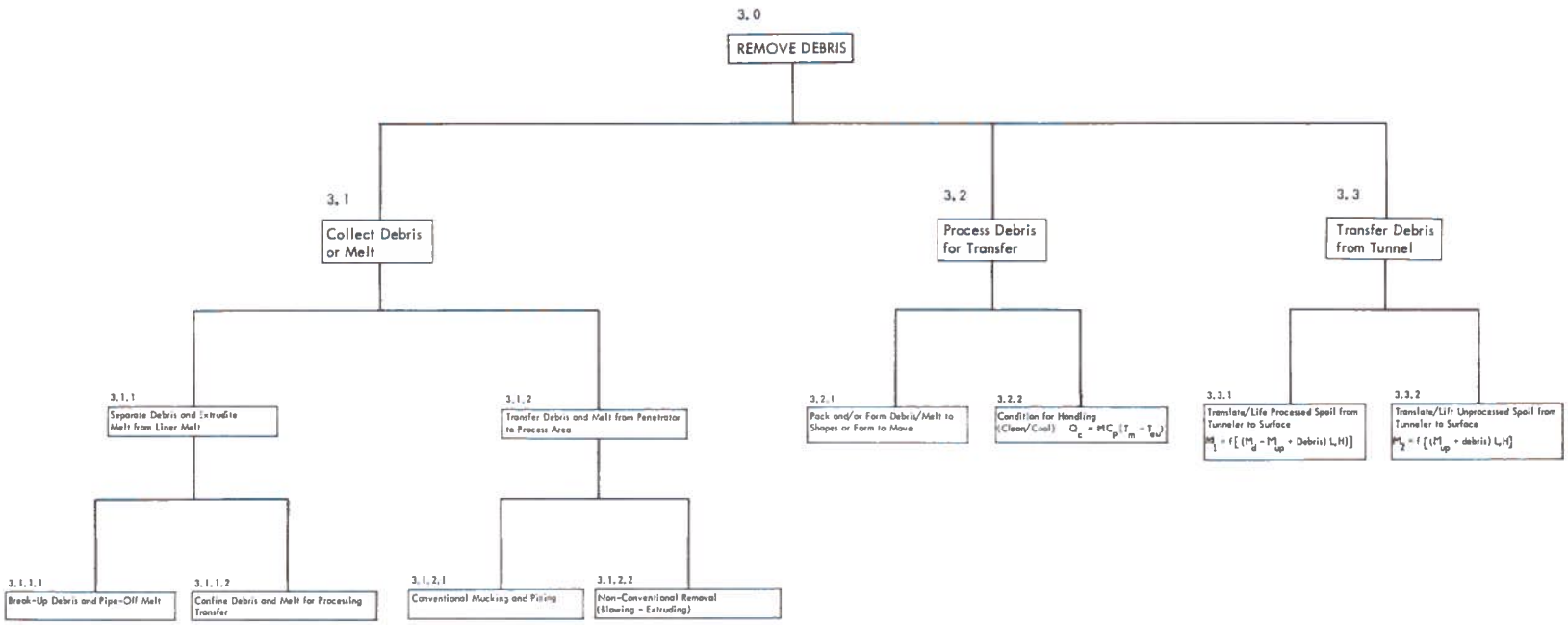

Figure 3-5. Functional Diagram (Continued)

1.1 Melt Rock/Earth

1.1.1

Generate Required Thermal Power

$Q_T = \Sigma q_a, q_{\ell,s}, q_f, q_{su}, q_s$.

Quantity Inputs:

- Velocity Advance
- Tunnel Dimensions
- Rock/Earth Properties
- Mode of Penetration (% Melt & Solids)
- System Efficiencies

Quantity Outputs:

- Heat Required by Melt and Losses = $Q_{thermal}$

Assumptions:

- Modes of Heat Loss
- Homogeneity
- Effective Heat Capacities
- Effective Latent Heat
- Constituents by %

1.1.2

Transfer Heat from Source to Penetrator

$Q_{T_{1-2}} = f(q/A, L, \Delta T, q_a, T_{max}, U, D.)$

Quantity Inputs:

- Thermal Power Req'd
- Distance from Source
- Temperature (max)
- Heat Flux (max)
- Velocity

Quantity Outputs:

- Q_T Constraints

Assumptions:

- System (Heat Pipes, Electrical/Drum Conductors, Fluid Loop)

1.1.3

Transfer Heat into Melt

$\Sigma q/A_p = f(q_m, k_m, \Delta T_m, \delta, T_m, \psi, U)$

Quantity Inputs:

- Penetrator Geometry
- $q_a + q_f + q_{\ell,s}$
- Velocity
- Materials Properties
- Initial Temperature

Quantity Outputs:

- Max. Heat Flux
- Max. Velocity Capabilities = $f(T_{max}, Q_T)$

Assumptions:

- Homogeneity
- Effective Surface Contact = % Available local S.
- Uniform Heat Flux
- $(T = f(\psi))$

1.1.4

Raise Rock/Earth Ambient Temp. to $(T_m + \Delta T_s)$

$\Delta T = f(q_{su}, q_s, q_f, k_m, \rho_m, C_{pm}, T_m, T_\infty, U, \lambda, k_s, \rho_s, C_{ps}, T_s, D\rho, \delta)$

Quantity Inputs:

- Initial Temperatures
- Rock/Earth Properties
- Rock/Earth Mass Distributions
- Volatiles/Voids
- T Melt Desired (+ Fluxing & Super Heat?)

Quantity Outputs:

- T_{max} - Melt Temperature
- Volatiles Dispersed
- Max. Temperature Limit

Assumptions:

- Homogeneity
- Limiting Temperatures
- Effective Heat Capacities & λ s
- Constituents & Voids
- Flux Effects & Effective λ s

Figure 3-6. 3rd Level - Changes Required

1.1.1 Generate Thermal Power

1.1.1.1*

Electrical Power Generation*

Quantity Inputs:

- Power Requirements
- Volume/Geom. Limits
- System Constraints
- Mode of Drilling (Manned?)
- Safety/Operational & Life Requirements-Power Profiles
- Operational/Environmental Constraints

Quantity Outputs:

- Power Plant/System Specified

Assumptions:

- Max. Rates
- Variation Constraint

1.1.1.2

Power Control and Monitoring

Quantity Inputs:

- Variation Limits
- Reaction Envelope
- Operating Envelope
- Fail Safe Requirements
- Etc.

Quantity Outputs:

- Maximum Rates
- Deviation Factors

Assumptions:

- Existing Control Systems

*Alternates

1.1.1.1

Chemical Power

1.1.1.1"

Fossil Fueled Power

1.1.1.1'''

Nuclear Power

Figure 3-7. 4th Level - Mechanism to Accomplish Changes

1.1.2 Transfer Heat From Source

1.1.2.1	1.1.2.2	1.1.2.3	1.1.2.4
Electrical Conductor to Resistance Heaters/ Induction Heaters	Thermal/Fluid Loops and Direct Contact Heaters	Heat Pipes to Direct Contacts	Chemical Feed for Exothermic Heating of Contact Heaters

1.1.3 Transfer Heat To Melt

1.1.3.1	1.1.3.2	1.1.3.3	1.1.3.4
Direct Conduction from Hot Surface	Radiation from Hot Elements	Convection in Melt	Induction or Resistance Heating in Melt

1.1.4 Raise Rock/Earth Temperature

1.1.4.1	1.1.4.2	1.1.4.3
Determine Rock/Earth Constituents and Physical Conditions (Voids, Strata, Elasticity)	Establish Rock/Earth Properties and est. T_{max}	Provide Fluxing if Required, Volatile Release or Temperature/Pressure Limits

Figure 3-8. 4th Level - Mechanism to Accomplish Changes

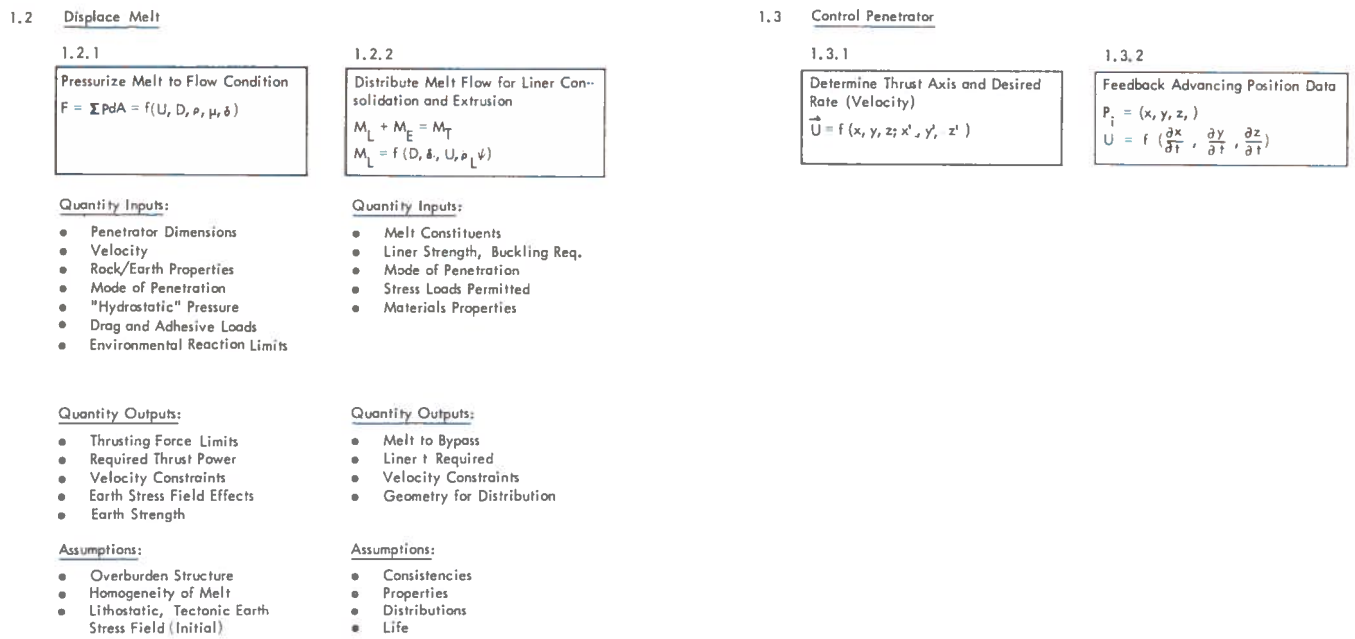

Figure 3-9. 3rd Level - Changes Required

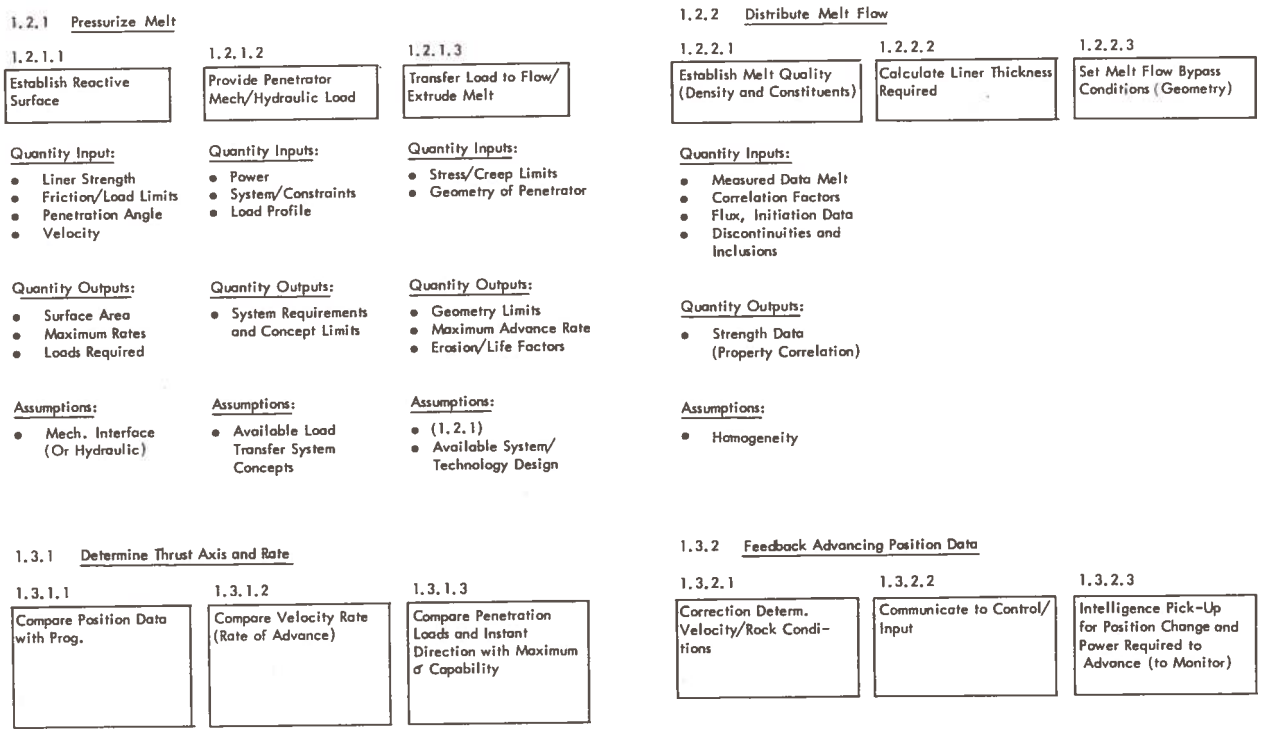

Figure 3-10. 4th Level - Mechanism to Accomplish Changes

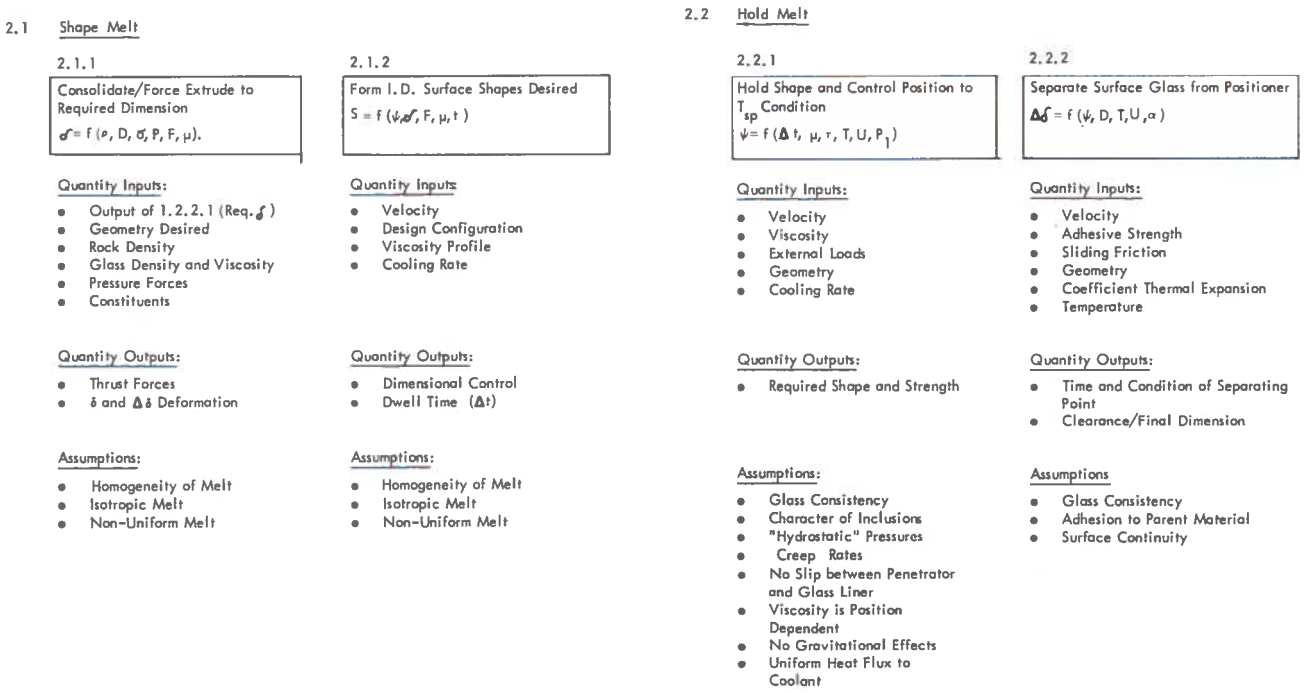

Figure 3-11. 3rd Level - Changes Required

2.3 Cool Melt

2.3.1

Solidify Melt to Solidus Glass

$T_L = f(Q_c, k_g, \rho_g, C_{pg}, k_e, \rho_e, C_{p,e}, T_\infty, \delta, h, D_p, L_c, U)$

Quantity Inputs:

- Rock/Earth Properties
- Glass Melt/Solid Properties
- Velocity of Penetration
- Penetrator Dimension
- Coolant Temperature
- Film Coefficient
- Cooling Rate

Quantity Outputs:

- Liner Temperature at End of Penetrator Afterbody

Assumptions:

- Uniform Velocity Gradient
- Variable Viscosity
- Effective Rock/Soil Properties
- Effective Glass Properties
- Uniform Heat Flux
- Constant Coolant Temperature

2.3.2

Strengthening to Integral High Strength Liner

$\sigma_s = f(dT/dt, \psi, \delta, T_\infty, E, P, \rho, U)$

Quantity Inputs:

- Strength
- Velocity
- Rock/ Earth Properties
- Glass Constituents
- Geometry (ψ, δ, D)
- External Loads
- Glass Properties
  - Coefficient of Thermal Expansion
  - Upper and Lower Annealing Temp.
  - Youngs' Modulus
  - Poissons' Ratio

Quantity Outputs:

- Required Cooling Rate
- Glass Surface Compression

Assumptions:

- Tempering Increases Glass Strength
- Homogeneous Glass
- Isotropic Glass
- Non-Uniformity of Glass Properties

Figure 3-12. 3rd Level - Changes Required

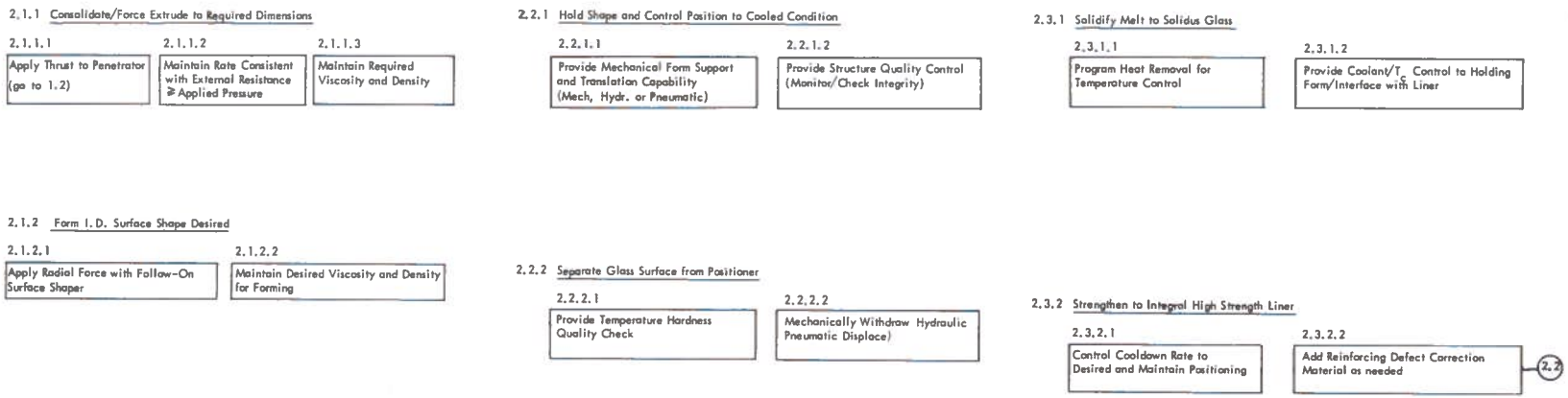

Figure 3-13. 4th Level - Mechanism to Accomplish Changes

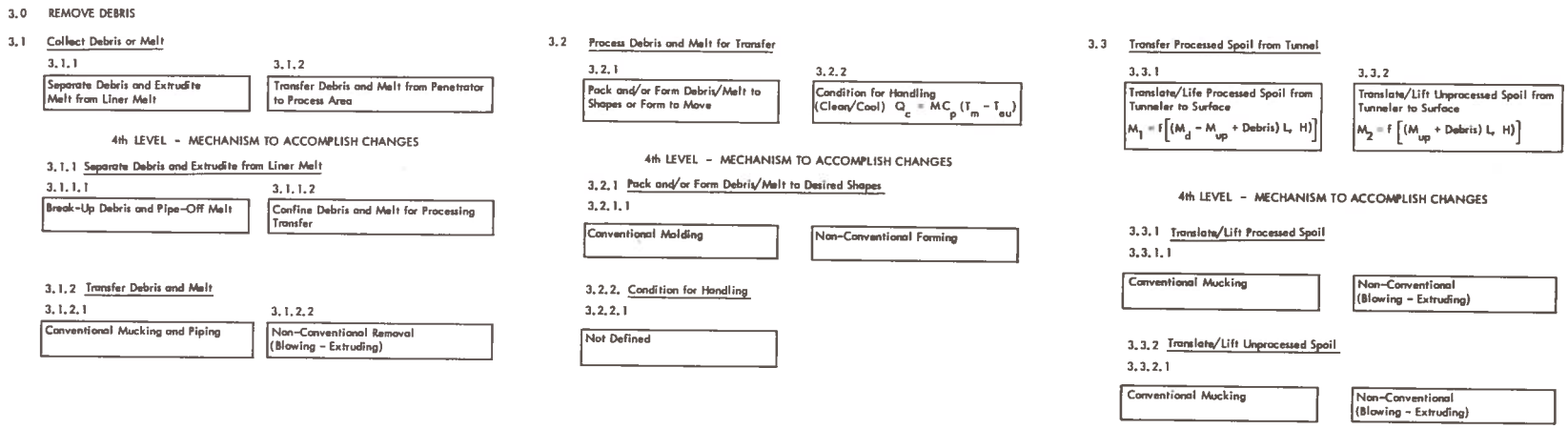

Figure 3-14. 3rd Level - Changes Required

4.0 TUNNELING MODE DESCRIPTIONS

Tunneling by earth melting has been categorized into five different modes, which are all described in this section. The modes are compared on a qualitative basis. A generalized mass balance is then given, and is applied to each mode.

4.1 MODE DEFINITION

Five modes of tunneling which were identified in the previous section and which are continuously referenced in the succeeding sections are defined below

1. Complete meltdown of tunnel cross section and complete consolidation of melt into glass liner.

2. Complete meltdown of tunnel cross section and partial consolidation of melt into glass liner, the remainder being back-extruded.

3. Complete meltdown of tunnel cross section and total back-extrusion of melt. (No glass liner is formed.)

4. Partial meltdown of tunnel cross section with complete consolidation of melt into glass liner (no excess melt) and excavation of the solid core.

5. Partial meltdown of tunnel cross section with partial consolidation of melt into glass liner, and excavation of solid glass lined core or removal of excess melt with solid core.

The first three modes require complete meltdown of the tunnel cross section while the last two require excavation. Although Modes 3 and 4 are classified separately, they are special cases of the more general modes defined by 2 and 5, respectively. In a real physical process they would be difficult to achieve; i.e., the design of a Mode 3 penetrator would require an approach which eliminated <u>all</u> radially outward heat losses while a Mode 4 penetrator would require an approach which eliminates <u>all</u> radially inward heat losses. If any

melt is formed in Modes 3 and 4 other than in the region for which they are defined, Mode 3 becomes Mode 2 and Mode 4 becomes Mode 5.

Lithofracture (creation of radial cracks in parent earth material into which melt can flow as an independent means of melt disposal) is not included in the mode definitions as a separate category but it can be superimposed as a single additional process to any mode. The word "lithofracture" classically refers to the fracture of hard rock. In this report the word is used generally to include any induced separation in the parent earth material whether it be hard rock or unconsolidated material.

4.2 COMPARISON OF TUNNELING MODES

Before introducing the quantitative analytical expressions describing the various functions and interactions from a penetrator, a qualitative comparison among the five modes was made, based primarily on definitions and judgment and not on quantitative evaluation. A summary of the results is given in Table 4-1. This table is headed by a schematic of a penetrator for each of the modes, as applied to a circular tunnel cross section, only. The results, however, apply to any cross section.

4.3 MASS CONTINUITY RELATIONS

The liner thickness can be controlled by the mode of penetation. The maximum thickness is obtained in Mode 1 with complete meltdown of the tunnel cross section and of the parent earth material consolidated or densified into the liner. Figure 4-1 shows a schematic of a generalized cross section of a tunnel and some nomenclature definitions to be used in the following equation development. A gross balance over the fully developed cross section yields

Original Earth Mass	=	Lithofracture Storage	+	Outer Liner
$\rho_e A_p U_\infty$	=	$\rho_g A_L U_L$	+	$\rho_g (A_g - A_p) U_\infty$
	+	Inner Liner	+	Solid Core
	+	$\rho_g (A_i - A_c) U_{ex}$	+	$\rho_e A_c U_\infty$ (4-1)

TABLE 4-1

QUALITATIVE COMPARISON OF VARIOUS MODES OF TUNNELING

TUNNELING MODES	1		2		3		4		5	
DESCRIPTION OF TUNNELING MODES	Complete Meltdown and Complete Consolidation into a Glass Liner		Complete Meltdown and Partial Consolidation Plus Back Extrusion		Complete Meltdown and Total Back Extrusion		Meltdown of Annular Region and Complete Consolidation into a Glass Liner, Core Excavation		Meltdown of Annular Region and Partial Consolidation with Excess Melt Removal	
	w/o Litho.	Lithofracture	w/o Litho	Lithofracture	w/o Litho	Lithofracture	w/o Litho	Lithofracture	w/o Litho.	Lithofracture
Characteristics of Modes of Tunneling										
Excavation Requirement	No	No	No	No	No	No	Yes	Yes	Yes	Yes
Debris Removal Requirement	No	No	Yes	Yes	Yes	Yes	Yes	Yes	Yes	Yes
Tunnel Support Requirement	No	No	No	No	Yes	Yes	No	No	No	No
Type of Soil/Rock for which It is Most Suitable	Low Density	Low Density	Any	Any	Any	Any	Any	Any	Any	Any
Size of Hole/Tunnel for which It is Most Suitable	Small	Medium	Small	Medium	Small	Small	Any	Any	Any	Any
Relative Thickness of Liner	Large	Medium	Small	Small	None	None	Small	Small	Small	Small
Control of Liner Properties	Controllable	Difficult	Controllable	Difficult	Controllable	Difficult	Controllable	Difficult	Controllable	Difficult
Power Requirements:										
Melting Power	High	High	High	High	Medium	High	Low	High	Low	High
Heat Losses	High	Higher	High	Higher	Medium	Medium	High	Higher	High	Higher
Frictional Drag	Low	High	High	High	High	High	Low	High	Medium	High
Adhesion Forces	Low	Low	Low	Low	Higher	Higher	High	High	Low	Low
Excavation	Zero	Zero	Zero	Zero	Zero	Zero	Higher	Higher	High	High
Debris Removal	Zero	Zero	Low	Lower	Medium	Low	High	High	High	Medium
Pressure Drag	High	High	High	High	High	High	High	High	High	High
Melt Removal	Zero	Zero	Low	Low	High	Medium	Zero	Zero	Low	Zero

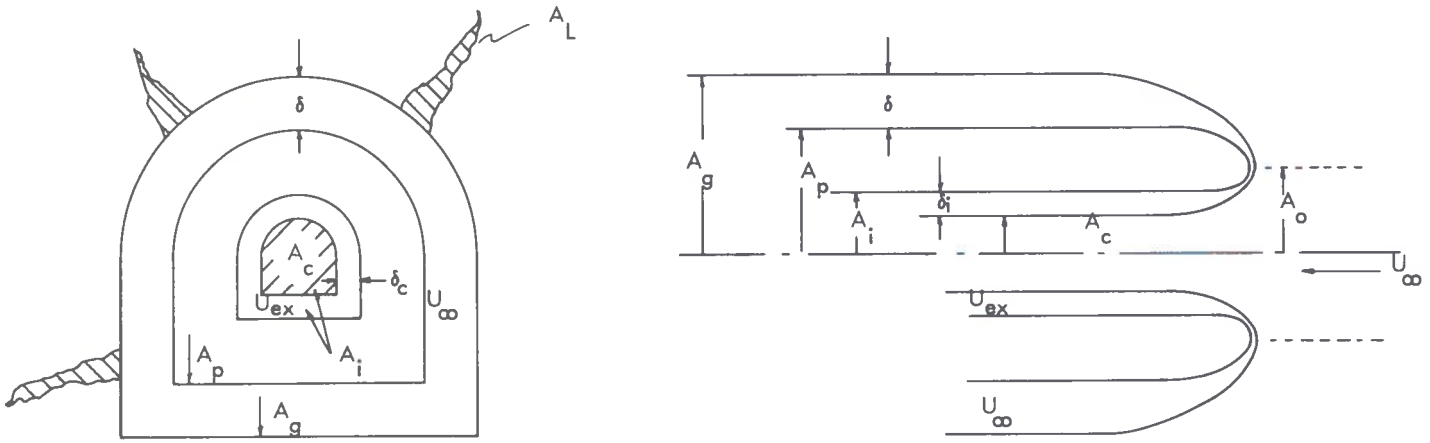

Figure 4-1. Generalized Mass Balance with Nomenclature

The stagnation point is then defined by the area A_o. All mass inside A_o passes through the interior of the penetrator and all mass between A_p and A_o passes to the outside of the penetrator. The mass balances in terms of the stagnation area are

$$\rho_e (A_p - A_o) U_\infty = \rho_g A_L U_L + \rho_g (A_g - A_p) U_\infty \quad (4\text{-}2)$$

$$\rho_e A_o U_\infty = \rho_g (A_i - A_c) U_{ex} + \rho_e A_c U_\infty \quad (4\text{-}3)$$

The sum of these two equations is Equation (4-1). The identified modes of tunneling are here discussed in relation to the results of the generalized mass balance and geometric variables, but for equal penetration and extrusion velocities and in terms of the stagnation area.

1. Complete meltdown and consolidation into a glass liner: For this mode of tunneling A_o is zero, and without lithfracture, A_L would be zero.

2. Complete meltdown and partial consolidation into the liner plus back extrusion of excess melt: In this mode: if $\rho_e A_o = \rho_g A_i$, then $2\delta_c = D_i$ and the velocity of glass or melt extrusion at the location of D_i is equal to the penetrator velocity, U. If $\rho_e A_o > \rho_g A_i$, then the velocity of extrusion at the location of D_i must exceed the penetrator velocity, U. If $\rho_e A_o < \rho_g A_i$, then the velocity of extrusion at the location of D_i must be less than the penetrator velocity which means that the flow has become discontinuous or in other words the cross section, A_i, is not completely occupied by glass or melt. Again without lithofracture A_L would be zero.

3. Complete meltdown and total back extrusion of melt with no liner formation: In this mode $A_o = A_p$, and A_L must be zero, because if cracks do form there is no mechanism to drive melt beyond the stagnation circumference defined by $D_o = D_p$. The same discussion on the relationships between velocity, $\rho_e A_o$ and $\rho_g A_i$ presented for Mode 2 also apply.

4. Partial meltdown of tunnel cross section with the formation of a tunnel liner only and with excavation of an earth core: In this mode $A_i = A_o$ and δ_c is equal to zero. Without lithofracture A_L would be zero.

5. Partial meltdown of tunnel cross section with the formation of a tunnel liner and core liner with excavation of the core liner and core earth: For clarification this is the mode tunneling shown on the schematic in Figure 3-1. In this mode of operation A_i must be less than A_o, and $\rho_e A_o$ must be less than $\rho_g A_i$. For the special cases of $\rho_e A_o \geq \rho_g A_i$ this becomes Mode 2 without an earth core where the melted core at the D_i location either exceeds or equals the penetrator velocity. Again, without lithofracture A_L would be zero.

A very useful relationship which "falls-out" of the mass balance equation is the generalized relationship between penetrator velocity (U_∞) and the mass rate of earth which must be melted, ($\dot{m}_e$).

$$\dot{m}_e = U_\infty \left(\frac{\rho_e \rho_g}{\rho_g - \rho_e} \right) \quad (A_p - A_L - A_i) \tag{4-4}$$

For Mode 1, A_i is zero and for Mode 3 A_L is zero as previously discussed. When the geometric requirements imposed by the mass balance are combined with this equation a relative ranking of required heat of fusion rates, $\dot{Q}_\lambda = \dot{m}_e \lambda_s$, can be made if one assumes that U_∞, ρ_e, ρ_g, and A_p are fixed in the absence of lithofracture.

$\dot{Q}_{\lambda 1} > \dot{Q}_{\lambda 2}$, because $> \delta_1 > \delta_2$

$\dot{Q}_{\lambda 2} > \dot{Q}_{\lambda 3}$, because $> \delta_2 > \delta_3$

$\dot{Q}_{\lambda 3} > \dot{Q}_{\lambda 5}$, because $> A_{i3} < A_{i5}$

$\dot{Q}_{\lambda 5} > \dot{Q}_{\lambda 4}$, because $> A_{i5} < A_{i4}$

Lithofracture can lower the required heat of fusion rate in all of these modes except for Mode 3 in which it does not apply.

Equation (4-1) is a generalized mass balance relationship and can be particularized to any geometry. For the sake of numerical example, a circular or annular geometry applied to Figure 4-1 is selected to demonstrate the utility of these relationships in terms of the radii of the circle rather than a general area. In all cases lithofracture is not considered ($A_L = 0$).

Mode 1 simplifies to

$$\delta = \frac{D_p}{2}\left[\sqrt{\frac{1}{1-\rho_e/\rho_g}} - 1\right] \qquad (4\text{-}5)$$

Figure 4-2 shows the glass liner thickness for 3 and 9 meter diameter tunnels as a function of the density ratio. From Equation (4-5) and from the figure, it is seen that the liner thickness asymptotically approaches infinity as the density ratio approaches 1.0. Thus, Mode 1 is only feasible if the glass is more dense than the parent material.

If the glass liner thickness generated is excessive when compared with that required based on glass liner strength requirements, part of the melt can be back extruded as in Mode 2 tunneling. In this mode, the glass liner thickness generated is a function of the rate of extrusion (U_{ex}) and the rate of penetration (U_∞) in addition to the variables given above. For Mode 2 tunneling, a mass balance yields the following functional relation for the glass liner thickness

$$\delta = \frac{D_p}{2}\left[\sqrt{\frac{1-\left(\frac{r_i}{r_p}\right)^2 \frac{U_{ex}}{U_\infty}}{1-\frac{\rho_e}{\rho_g}}} - 1\right] \qquad (4\text{-}6)$$

where r_i is the radius of the throat of the penetrator. This equation merely gives the outside melt (or glass liner) thickness. At the throat of the extrusion tube, there is a melt

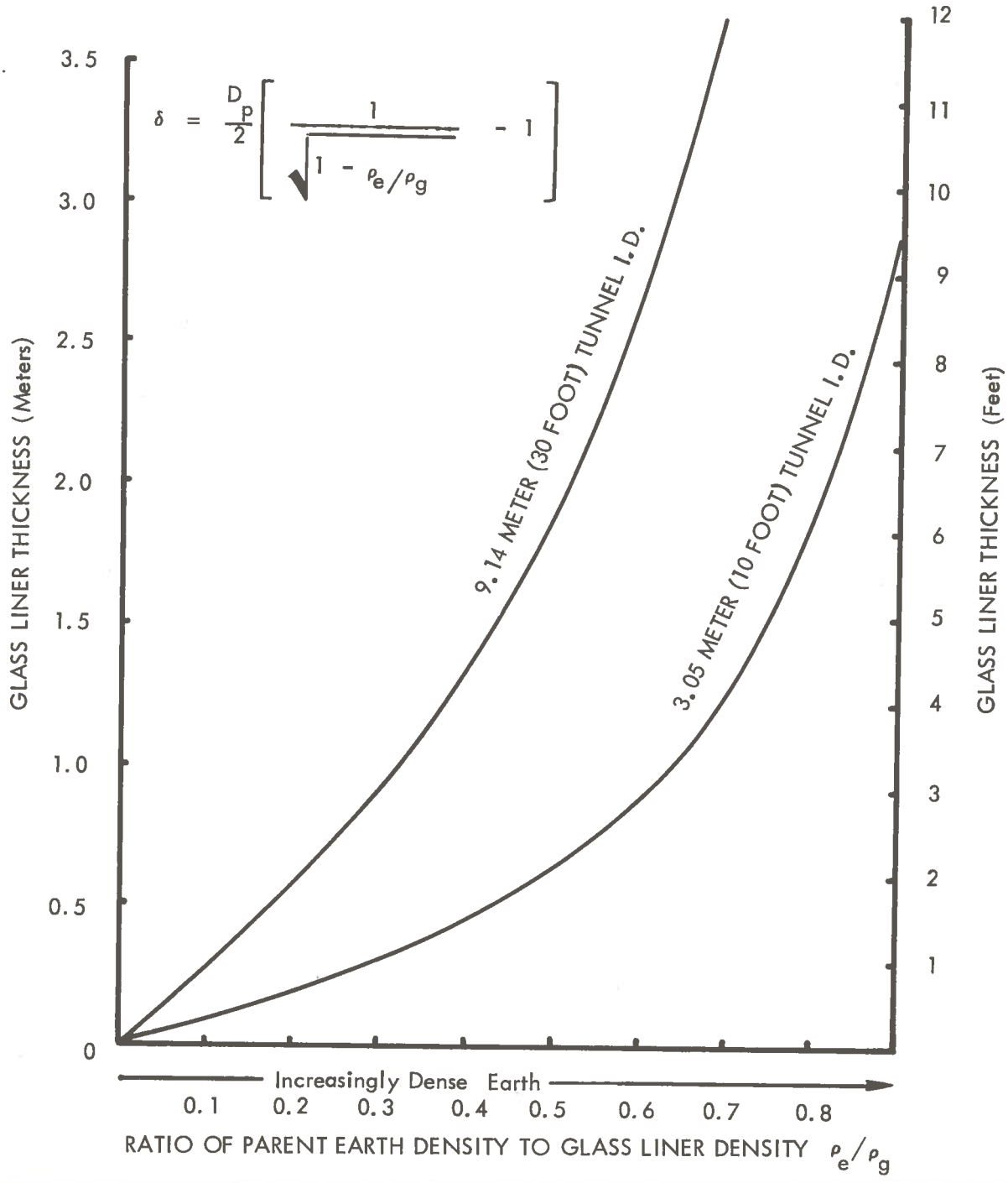

Figure 4-2. Effect of Earth to Glass Liner Density Ratio and Tunnel Diameter on Glass Liner Thickness Mode 1 Operation

thickness associated with a given rate of extrusion. In general, this thickness should not exceed the maximum glass liner thickness in an optimum penetrator design. Figure 4-3 demonstrates Equation (4-6) for a 9 meter tunnel in terms of f_{ex}, the ratio of the area extruded at the penetrator velocity to the area of the penetrator, i.e.,

$$f_{ex} = \left(\frac{r_i}{r_p}\right)^2 \frac{U_{ex}}{U_\infty} \qquad (4\text{-}7)$$

For certain types of glass, where its density is on the same order of magnitude as that of the parent earth/rock material, it may be necessary to extrude most if not all of the molten material as in Mode 3 tunneling. In this mode, a thin layer of melt outside the penetrator is necessary to reduce frictional drag. However, this thickness can be negligible; for all practical purposes, it can be regarded as non-existent except from the frictional drag standpoint. In this case, the melt thickness at the throat of the extrusion tube is given by the equation

$$\delta = \frac{D_p}{2} \sqrt{\frac{\rho_e}{\rho_g} \left(\frac{U_\infty}{U_e}\right)} \qquad (4\text{-}8)$$

The first three modes of tunneling are expected to be practical for relatively small penetrators, because the melt thickness is directly affected by the penetrator size. As the melt thickness increases, the melt superheat increases, thus increasing the penetrator surface temperature. Consequently, for these modes of tunneling, the maximum practical penetrator size is determined by material temperature limitations. This penetrator size limitation can be partially avoided by melting an annular region only, while the central core is removed by conventional means as in Modes 4 and 5.

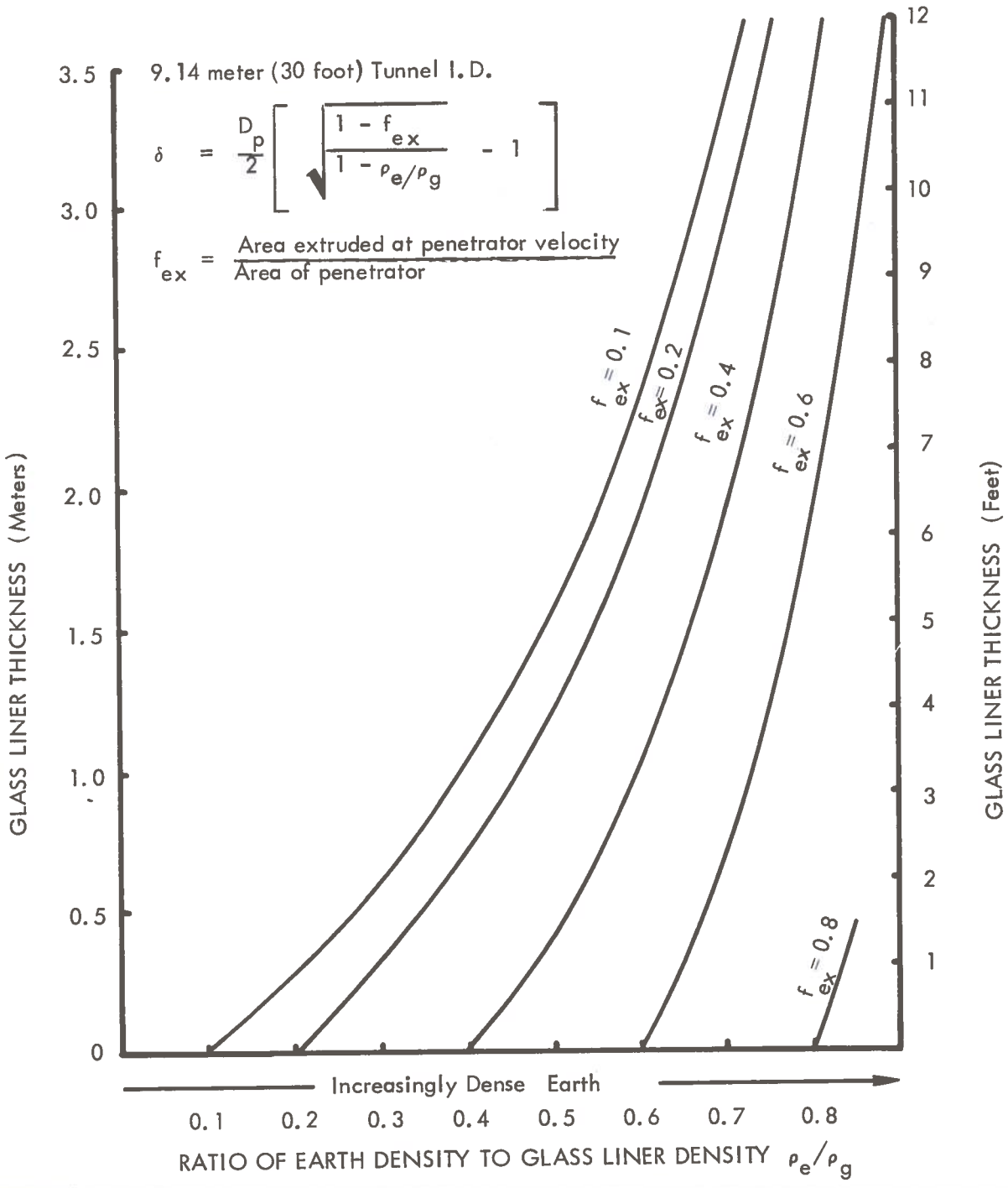

Figure 4-3. Effect of Earth to Glass Liner Density Ratio and Fraction of Melt Back-Extruded on Glass Liner Thickness Mode 2 Operation

The melting of an annular region can be accomplished with or without extrusion. Mode 4 gives this type of operation without extrusion. Mode 4 gives this type of operation without extrusion. This is similar to the full consolidation mode of operation, and is limited in its application to tunneling through unconsolidated earth/rock materials. In this mode of operation, a thin layer of melt on the inner surface of the penetrator must be created to minimize frictional drag. However, for purposes of estimating the thermal power requirements, this melt thickness can be neglected. The glass liner thickness generated in Mode 4 tunneling is given by the equation

$$\delta = \frac{D_p}{2}\left[\sqrt{\frac{1-\left(\frac{r_c}{r_p}\right)^2\left(\frac{\rho_e}{\rho_g}\right)}{\left(1-\frac{\rho_e}{\rho_g}\right)}} - 1\right] \qquad (4\text{-}9)$$

where r_i is the penetrator inside radius. Figure 4-4 shows a numerical example of Mode 4 operations for a 9 meter tunnel in terms of solid core to penetrator area ratio, $(r / r_p)^2$.

In Mode 5 tunneling, part of the melt is back extruded along the inner surface of the penetrator. The outer glass liner thickness is then dependent on the rate of extrusion (U_{ex}) as well as the rate of penetration (U_∞). Equation (4-1) reduces to

$$\delta = \frac{D_p}{2}\left[\sqrt{\frac{1-\left(\frac{r_i}{r_p}\right)^2\frac{U_{ex}}{U_\infty}+\left(\frac{r_c}{r_p}\right)^2\left(\frac{U_{ex}}{U_\infty}-\frac{\rho_e}{\rho_g}\right)}{\left(1-\frac{\rho_e}{\rho_g}\right)}} - 1\right] \qquad (4\text{-}10)$$

The five modes of tunneling and their corresponding liner thickness equations are summarized in Figure 4-5.

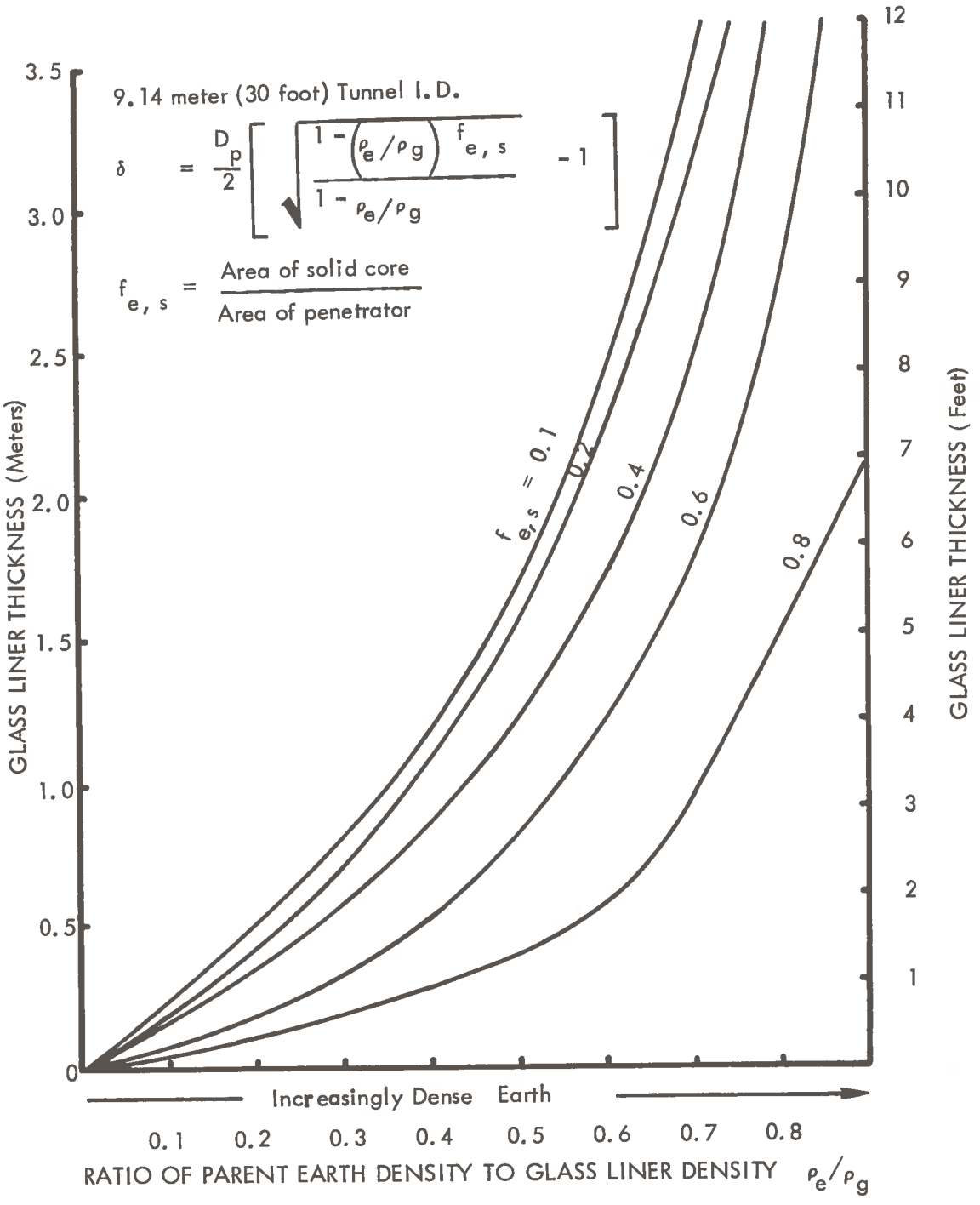

Figure 4-4. Effect of Earth to Glass Liner Density Ratio and Ratio of Solid Core to Bore Area Ratio on Glass Liner Thickness Mode 4 Operation

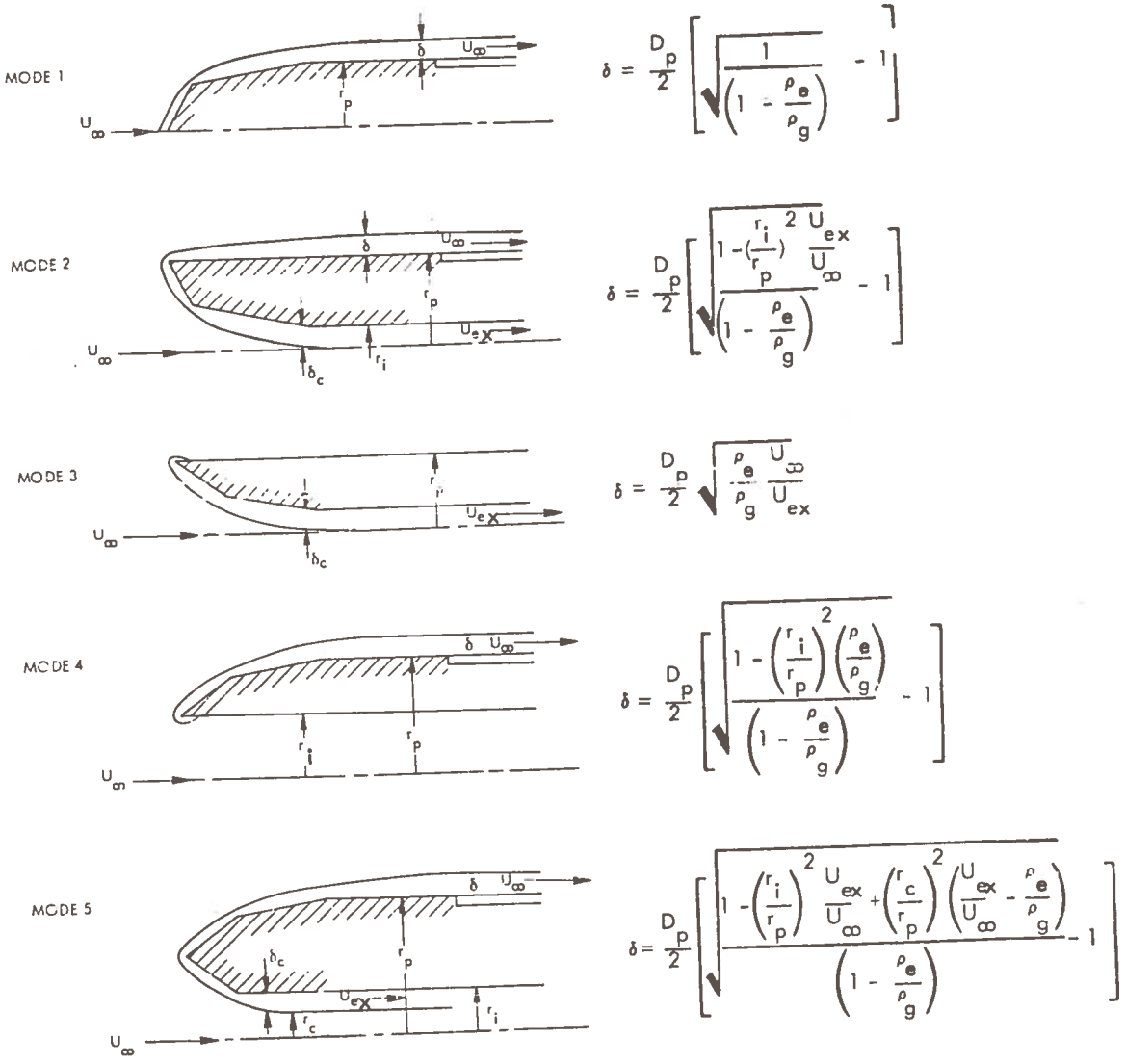

Figure 4-5. Functional Relations for Liner Thicknesses δ for Various Modes of Circular Tunneling

5.0 GEOLOGIC MODELS

The physical processes identified in the earth/rock melt technique required definition of earth/rock conditions. Five typical earth geological models have been formulated. These models have been developed to cover the majority of cases of near surface continental crust. They represent about 95% of these materials. Typical conditions to be usually experienced are defined by two of these models, UNCON and SOSED, that predominate in most urban areas.

5.1 INTRODUCTION

The geologic data and physical changes in rocks or soils that can be expected with the operation of a subterrene melting device have been derived. Most of the needed information on rock melting can be obtained from previous research on the generation of magmas (naturally occuring molten rock) by heat and pressure within the crust and upper mantle of the earth. This information can also provide insight into the composition and characteristics of the resulting glasses after the melts have solidified. A limitation of the available data is that the objective of most of the existing studies has been an understanding of processes occurring at depths of 10 to 100 km where the pressures are from 3 to 30 kilobars.

To obtain information useful to the present study, the extreme low end of the pressure range previously investigated must be used. The temperatures involved in magma generation, however, are from 700°C to 1500°C and in fact seldom exceed 1000°C within the crust - well within the range of interest. Further, many of the laboratory experiments intended to study the crustal and upper mantle processes have been limited by the temperature and pressure capability of available laboratory equipment, so that many experiments have been conducted at temperatures and pressures comparable to those of interest in the subterrene study. Some information is also available on rock melting at or near atmospheric pressure. The literature of ceramics provides an important source of information, especially on the characteristics of the resulting glasses.

The distribution of various types of rocks in the near-surface continental crust is tabulated, and five earth models are defined, representing about 95% of the near-surface materials. The applicability of the geologic models is specified in Section 5.4 of this report. These are based on the area distribution of continental rock types as tabulated in Section 5.2.

5.2 DISTRIBUTION OF ROCK TYPES IN NEAR-SURFACE (10 to 100 m Depth) CONTINENTAL CRUST

The near-surface crustal materials in which the subterrene tunneling device will operate can be approximated by considering the geographic distribution of typical materials. The three major divisions of continental rocks normally tabulated are the Precambrian shields, the sedimentary platforms, and the folded geosynclinal belts. The distribution of these units is given by Ronov and Yaroshevsky (5-1) and by others (5-2, 5-3), as follows:

	Total Continental Area ($km^2 \times 10^6$)	Percent of Continental Area
Precambrian shields	29.4	19.7%
Platforms	66.9	44.9%
Folded belts	52.7	35.4%
	149.0	100.0%

The distribution of the various rock types in the near surface material (10 - 100 m) is essentially the same as the distribution of surface areas, which are available in the literature cited above. In a geologic sense, the term rock includes the soft unconsolidated materials, such as alluvium, as well as the hard material referred to as rock in civil engineering. Therefore, the soft materials ("soils in civil engineering) are included in the rock types tabulated below, from the authors previously cited.

The sedimentary platforms (44.9% of continental area) are composed of:

Sands	23.6%
Clays, shales, etc.	49.5%
Carbonates	21.0%
Evaporites	2.0%
Volcanics	3.9%
	100.0%

The shields (19.7% of continental area) are composed of:

Granite	18.1%
Granodiorite, diorite	19.9%
Syenite, nepheline syenite	0.3%
Gabbro	3.7%
Peridotite	0.1%
Gneiss	37.6%
Schist	9.0%
Marble	1.5%
Amphibolite	9.8%
	100.0%

The folded belts (35.4% of continental area) are composed of:

Sands	18.7%	
Clays, shales, etc.	39.4%	
Carbonates	16.3%	
Evaporites	0.3%	
Basalt	12.6%	25.3%
Andesite	10.2%	
Rhyolite	2.5%	
	100.0%	

Summary of Distribution by Area

The area distribution of the various rock types can therefore be summarized as follows:

			Total % of continental area
Sands	=	23.6% of 44.9% = 10.6% 18.7% of 35.4% = 6.6%	17.2%
Clays, shales, etc.	=	49.5% of 44.9% = 22.2% 39.4% of 35.4% = 13.9%	36.1%
Carbonates	=	21.0% of 44.9% = 9.4% 16.3% of 35.4% = 5.8% 1.5% of 19.7% = 0.3%	15.5%
Evaporites	=	2.0% of 44.9% = 0.9% 0.3% of 35.4% = 0.1%	1.0%
Granites	=	18.1% of 19.7% =	3.6%
Granodiorite, diorite	=	19.9% of 19.7% =	3.9%
Syenite, nepheline syenite	=	0.3% of 19.7% =	0.06%
Gabbro	=	3.7% of 19.7% =	0.7%
Peridotite	=	0.1% of 19.7% =	0.02%
Gneiss	=	37.6% of 19.7% =	7.4%
Schist	=	9.0% of 19.7% =	1.8%
Amphibolite	=	9.8% of 19.7% =	1.9%
Basalt, diabase	=	12.6% of 35.4% =	4.5 *
Andesite	=	10.2% of 35.4% =	3.6%
Rhyolite	=	2.5% of 35.4% =	0.9%
Misc. Volcanics, (mostly basalt & diabase not included in 4.5% above)	=	3.9% of 44.9% =	1.8 *
			99.98%

*Some of the volcanics were specified as basalt, andesite, or rhyolite, and some were indicated only as "miscellaneous volcanics." For this study, estimate that basalt + diabase total = 5.5% and miscellaneous total = 0.8%.

5.3 CHANGES IN ROCK OR SOIL ASSOCIATED WITH A SUBTERRENE HEATING DEVICE

The changes in rocks or soils of importance to the subterrene study have been categorized (for another purpose) by S. P. Clark, Jr. (5-4) and P. J. Wyllie (5-3) as follows:

1. Polymorphic transitions (solid-solid reactions)

2. Dissociation reactions:
   - Dehydration
   - Decarbonation
   - Desulfurization

3. Melting reactions:
   - Anhydrous melting
   - Melting under water pressure

In the following discussion, each of these factors will be considered, with specific reference to the case of rock/earth melting device operating near the surface of the earth. The confining pressure at the contact between the melt and the penetrator is taken to be in the range of 2 to 100 bars (approximately 2 to 100 atmospheres). (1 bar = 0.9869 atm. = 1.0197 kg/cm^2).

Most of the phase transitions on heating are endothermic, as are dehydration, decarbonation, and decomposition reactions. Crystallization, oxidation, and some other chemical reactions are exothermic (5-5). However, the net change in heat content (enthalpy) from all these processes is reflected in the final figures for heat required for each of the models in Section 5.4.

5.3.1 Polymorphic Transitions (Solid-Solid Reactions)

Many minerals, when subjected to heat and pressure, undergo phase transitions from one crystallographic form to another before they ultimately melt or decompose. For example, one of the most common groups of mineral phases, or polymorphs, has the composition SiO_2.

The principal crystallographic forms of SiO_2 are quartz (the lowest temperature form) tridymite, and cristobalite. In addition, each of the three has a low temperature form and a high temperature form. These various polymorphs are summarized below. The density figures are from Robie (5-6, 5-7, 5-8).

	Density (g/cm	Crystal system
Low quartz (α)	2.64 at 25°C	hexagonal
High quartz (β)	2.53 at 575°C	hexagonal
Low tridymite	2.26 at $\cong$ 25°C	orthorhombic
High tridymite	2.19 at 405°C	hexagonal
Low cristobalite	2.33 at 25°C	tetragonal
High cristobalite	2.19 at 405°C	isometric

Additional high temperature/pressure forms, coesite and stishovite, the hydrous form opal ($SiO_2 \cdot n H_2O$), and other rate forms, are less important in the present study. The transition from α-quartz to coesite is pressure sensitive, coesite being the more dense form (2.91 g/cm. The transitions from low to high temperature forms are rapid and easily reversible. The phase transitions, however, are slow. The higher temperature forms can exist metastably at lower temperatures. Some of the phase relationships in SiO_2 are shown in Figure 5-1. As noted previously, only the low end of the pressure range is relevant to the present investigation. In general higher pressure favors the more dense forms. Other solid-solid transitions of importance include:

Aragonite - calcite

$$CaCO_3 \longrightarrow CaCO_3$$

(orthorhombic) (hexagonal)

Kyanite - sillimanite

$$Al_2SiO_5 \longrightarrow Al_2SiO_5$$

(triclinic) (orthorhombic)

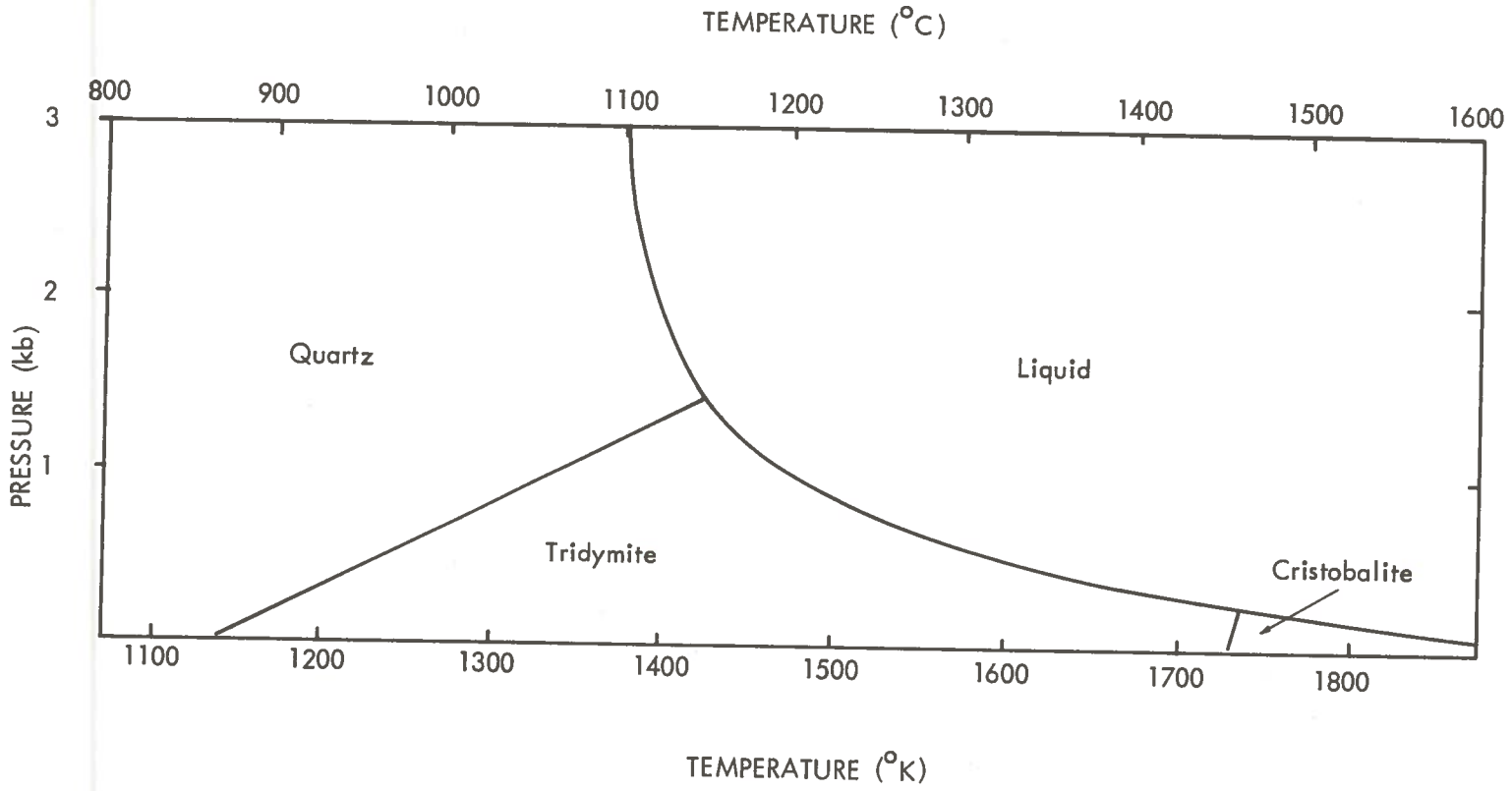

Figure 5-1. Phase Relations in SiO_2 Under Water Pressure (Clark, 5-4)

5.3.2 Dissociation Reactions

Dehydration

The principal reactions involving dehydration that will be important in this application are as follows:

Reaction	Temperature in °C at 0.5 kb
goethite to hematite $2FeOOH \rightarrow Fe_2O_3 + H_2O$	150*
gypsum to anhydrite $CaSO_4 \cdot 2H_2O \rightarrow CaSO_4 + 2H_2O$	< 100
muscovite to sanidine + corundum $KAl_2(AlSi_3O_{10})(OH)_2 \rightarrow KAlSi_3O_8 + Al_2O_3 + H_2O$	635
gibbsite to boehmite $Al(OH)_3 \rightarrow AlOOH + H_2O$	100
dehydration of clays	~ 100-200** 400-800***

* 130°C at atmospheric pressure

** loosely held, adsorbed, and interlayer water

*** dehydroxylation of the clay lattice

These reactions are illustrated by dehydration of the common hydrous iron oxide goethite ("limonite"), shown in Figure 5-2. This reaction is only slightly pressure sensitive, and the phase boundary occurs at 130°C at low pressures. The iron oxides are present in almost all near-surface rocks. This dehydration reaction and similar ones, especially in clays, will provide a source of water even in essentially dry rocks, with the result that the melting can occur under hydrous conditions. This depresses the melting points, as will be discussed in Section 5.3.3.

Decarbonation

Carbonate minerals are common constituents of most rocks and soils, so the reactions involving evolution of carbon dioxide (CO_2) will be especially important. These reaction temperatures vary from 500 to 1000°C, as shown in the following table:

	Temperatures in °C at 0.25 kb	at 0.002 kb
Calcite to lime $CaCO_3 \longrightarrow CaO + CO_2$	1000° *	900°
dolomite to calcite + periclase $CaMg(CO_3)_2 \longrightarrow CaCO_3 + MgO + CO_2$	710°	600°
Magnesite to periclase $MgCO_3 \longrightarrow MgO + CO_2$	650°	550°
rhodochrosite to manganosite $MnCO_3 \longrightarrow MnO + CO_2$	615°	500°

* at 7 atmospheres

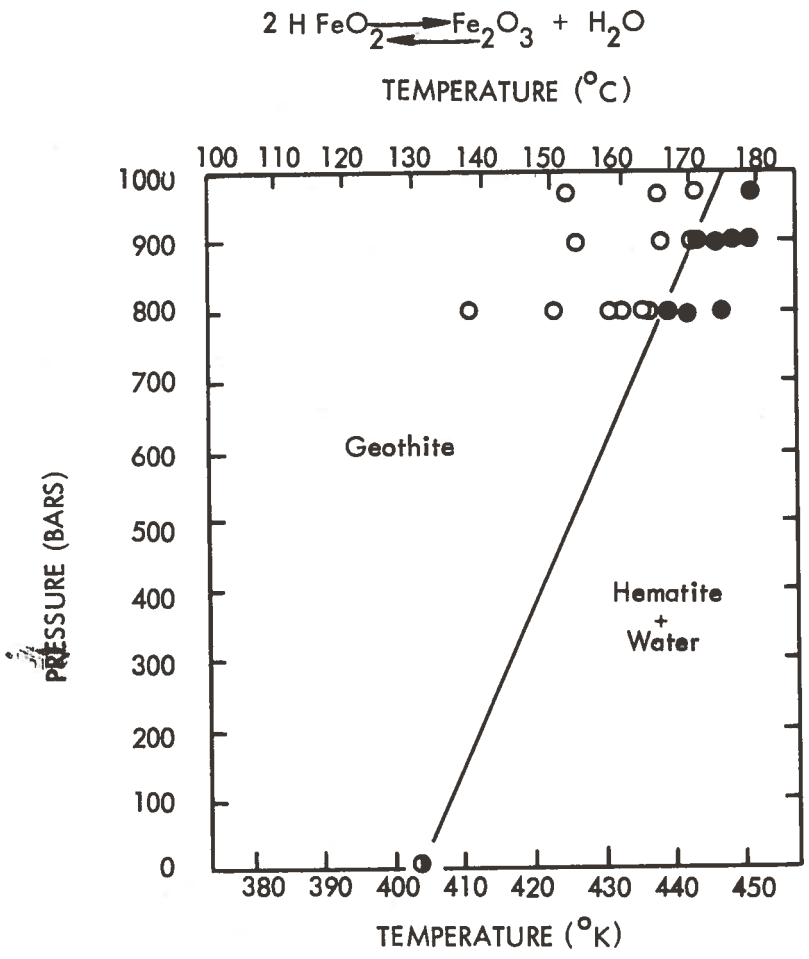

Figure 5-2. Geothite-Hematite Phase Boundary (Garrels & Christ, 5-9)

The solubility of the resulting CO_2 in the melt, or in the aqueous interstitial fluid, is strongly pressure dependent. It seems likely that the CO_2, steam, and other volatile products will have to be vented from the system. This may be an advantage since venting the steam around the penetrator could provide hydrous conditions at the penetrator surface, thereby lowering the melting temperatures.

Figure 5-3 shows the pressure-temperature relationships in the decomposition of calcite, probably the most common carbonate mineral. The difference between the two curves is attributed by Harker and Tuttle (5-10) to the fact that Smyth and Adams (5-11) used heating experiments only. Harker and Tuttle used heating and cooling. The difference is apparently due to a superheating phenomenon and illustrates the importance of metastable phases. The curve of Smyth and Adams is more pertinent to the present study.

In the evolution of CO_2 from calcite, each 100 gm of $CaCO_3$ yields 43.4×10^3 calories (182×10^3 joules). The resulting 56 gm of CaO must then be taken into solution in the melt, or incorporated unmelted into the glass liner. (The melting point of CaO is 2580°C.) This would be a serious problem in a pure limestone, but in the impure materials normally encountered, the CaO could probably be taken into solution in the melt. This will be discussed in Section 5.5 (the CALCI model).

Desulfurization

The most common sulfide minerals are pyrite (isometric) and its polymorph marcasite (orthorhombic). Both have the composition FeS_2. Another common group of minerals has the approximate composition FeS (pyrrhotite). All these minerals liberate SO_2 when heated under oxidizing conditions, and other oxides of sulfur or sulfuric acid under hydrous conditions. These sulfur compounds can be powerful agents for taking the other rock materials into solution. Under near-surface conditions some of the sulfide minerals will normally have been weathered to hydrous iron sulfates or oxides.

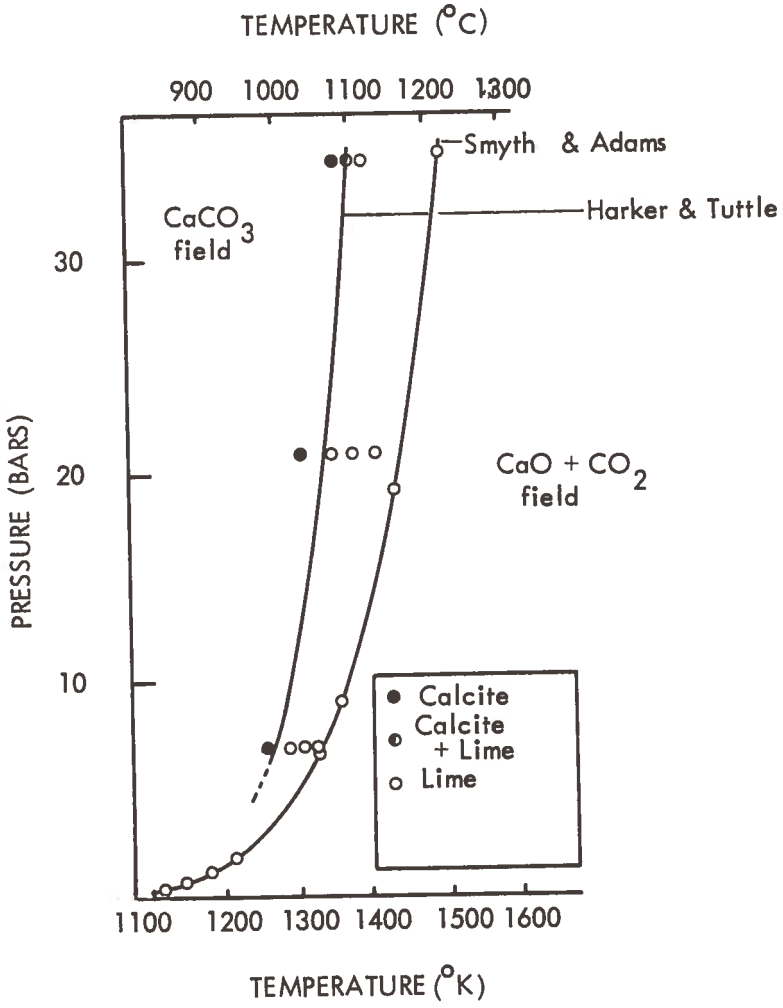

Figure 5-3. The Reaction $CaCO_3 \longrightarrow CaO + CO_2$

5.3.3 Melting Reactions

The effect of pressure in an anhydrous system is to increase the melting points by about 50-100°C, for a pressure increase from atmospheric to 10 kb. However, in a hydrous system the effect of pressure is to decrease the melting points by about 50-200°C, for a pressure increase from atmospheric to 1 kb. This is illustrated by the following table, abstracted from Clark (5-4), showing the relationships for some common minerals.

Anhydrous Melting	pressure kb	Melting point °C 0	10
Albite (Na-felspar)		1120	1240
Enstatite (Mg-pyroxene)			1670
Diopside (Ca, Mg-pyroxene)		1390	1520
Halite (NaCl)		800	1000

The anhydrous melting points of many common minerals are above 1500°C, for example quartz (1610°C), corundum (2000°C), olivine (1500-1900°C depending on iron content), and the various garnets. However, these materials can be taken into solution in the melts of the minerals with lower melting points.

Melting Under Water Pressure

The pressure dependent melting curve of the common soda feldspar, albite, is shown in Figure 5-4. Albite melts at about 1120°C at low pressure. However, the common potash feldspar (shown in Figure 5-5) melts incongruently. That is, as the temperature and pressure are increased, an intermediate liquid phase develops which reacts with the remaining solid - to produce a new solid and a new liquid, both different in composition from the original solid. At even higher temperature and pressure, the melting is incomplete. The melting of many silicate systems is incongruent; as in this example. As the temperature of the rock is increased, the solid decomposes to form one or more new crystalline phases and a liquid, neither of which has the composition of the orginal rock. The intermediate liquid typically is richer in silica than the original rock.

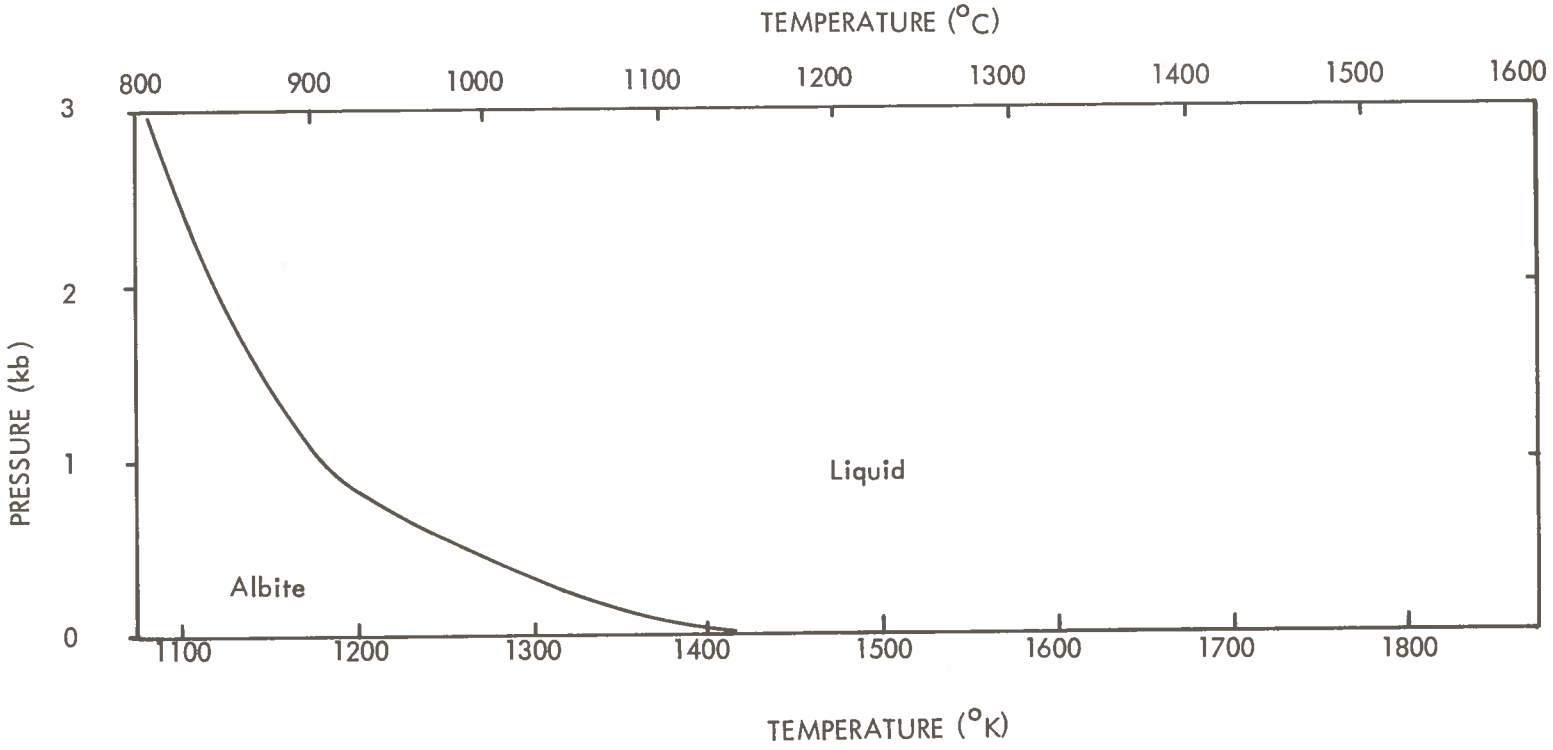

Figure 5-4. Melting Curve of Soda Feldspar ($NaAlSi_3O_8$) Under Water Pressure

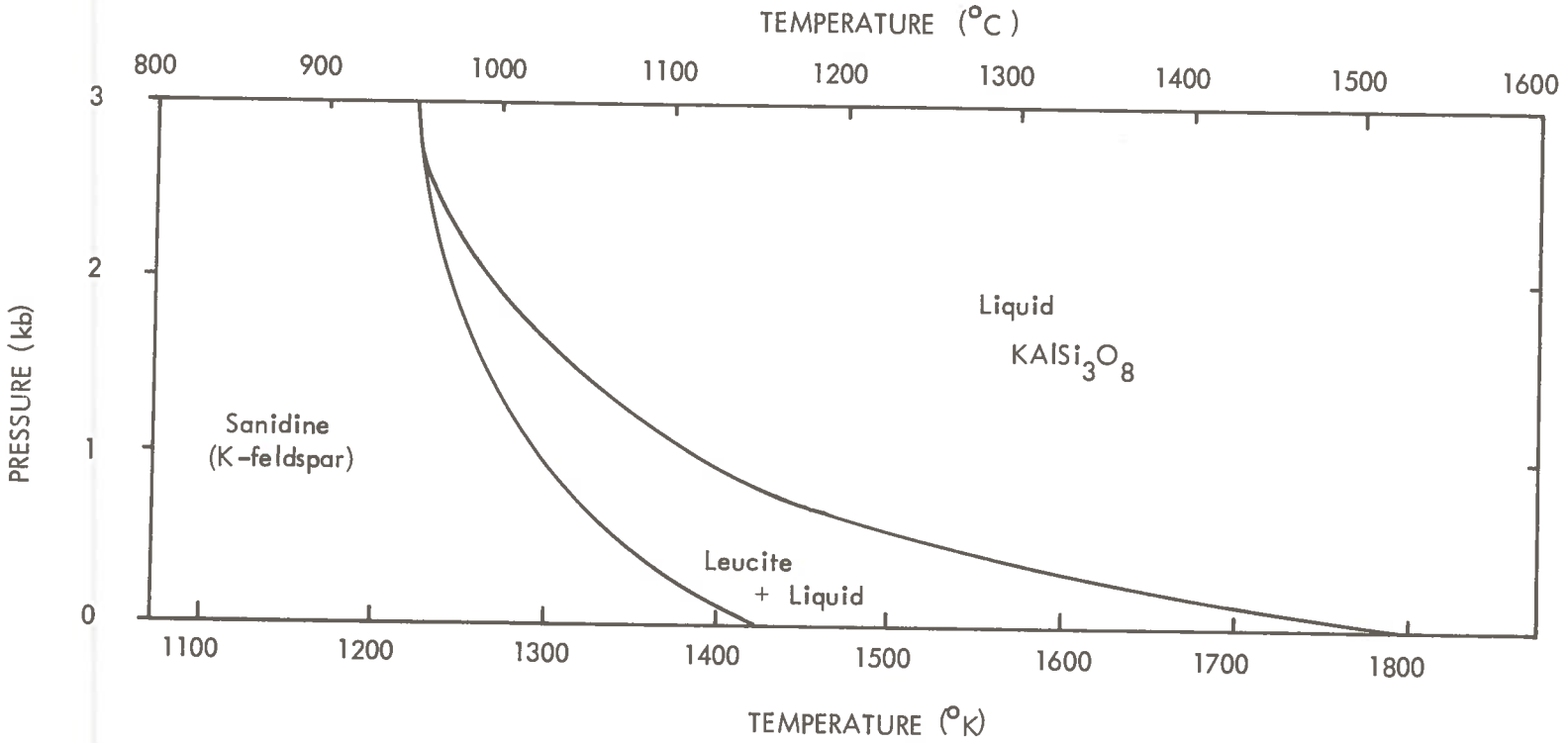

Figure 5-5. Phase Relations of Potash Feldspar ($KAlSi_3O_8$) Under Water Pressure

The following table, also from Clark (5-4) shows some examples of melting points under hydrous conditions.

	Pressure (kb)		
	0	1	2
Albite	1120°C	905°C	845°C
Diopside	1390	1330	1315
Anorthite (Ca-feldspar)	1550	1405	1340
Sanidine (K-feldspar)	1150-1520	1000-1120	980-1020
Quartz	1610	1230	1130
Tridymite	1700	--	--

A more complex set of melting curves is shown in Figure 5-6. Most natural systems will be still more complex, but these curves can serve as an example of expected conditions. Under anhydrous conditions, the soda-rich feldspar melts at a lower temperature than the potash-rich feldspar. Under hydrous conditions, all the melting points are depressed and the difference between the two types is less pronounced. Most natural silicate systems will have melting curves of this type.

From the above it can be seen that the temperature required for a complete or nearly complete fusion of most rocks will be determined by the hydrous melting curves and by the presence of fluxing materials, either naturally occurring or added. The temperatures may be as low as 800-1000°C if fluxing materials are present.

The effect of water pressure on geochemical reactions can be illustrated by two other examples.

The temperature of the transition of the hydrous iron oxide, goethite, into hematite is given by Garrels and Christ (5-9) as 130°C at atmospheric pressure and increasing slightly with pressure to 140°C at about 200 atmospheres (Figure 5-2). However the dehydration temperature of goethite under anhydrous conditions is about 350 to 400°C.

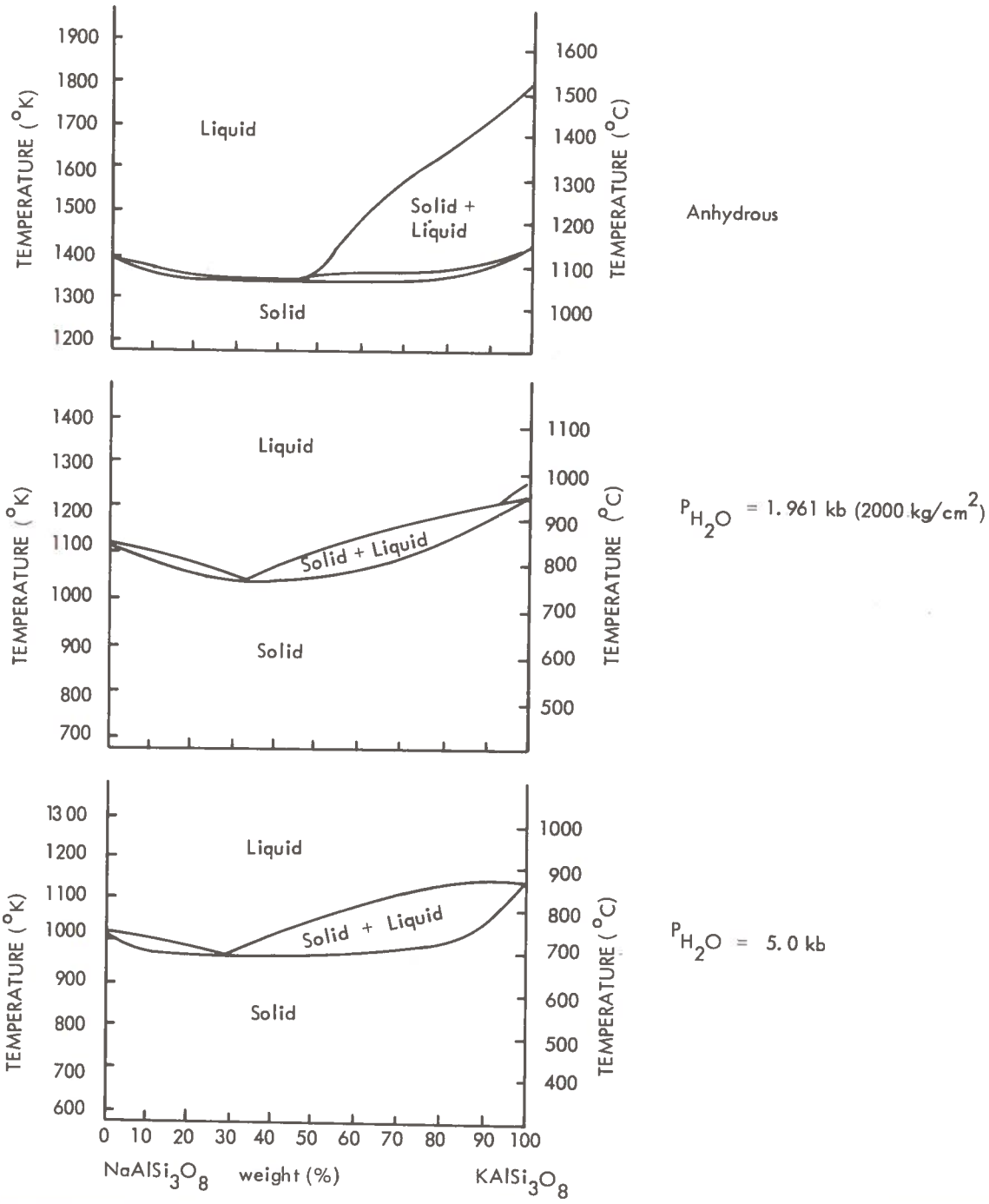

Figure 5-6. Melting Relationships in Sodium-Potassium Feldspar Systems (Clark, 5-4)

In a study of the effect of water on the compressive strength of diabase, Simpson and Fergus (5-13) found that diabase saturated with water had only about 60% of the compressive strength of the dried material. Other solvents did not have the same effect, illustrating the fact that the reaction was not simply a capillary action. Simpson and Fergus found the compressive strength of diabase saturated with water to be about 2700 kg/cm^2. This value is more relevant to the subterrene investigation than their values for dry material.

5.4 GEOLOGIC MODELS

5.4.1 Description of Five Models

The physical, chemical and mineralogical properties of the rock/earth to be encountered by the subterrene will be specified in terms of the following five geologic models.

1. UNCON - Unconsolidated sediments such as alluvial silt, and/or fine gravel; water saturated; with minimal anisotropy from stratification or jointing.

2. SOSED - Relatively soft sedimentary rock such as a calcareous shale or impure shaly sandstone, water saturated, with anisotropy introduced by stratification (grain orientation and interbedding) and jointing.

3. MASIG - Massive igneous rock of intermediate composition (granodiorite), without significant rock anisotropy introduced by joint systems, flow structure, or shear zones.

4. FOLIA - Igneous or metamorphic rocks with significant structural complexity in the form of foliation, jointing, flow structure, or shear zones; having an intermediate composition, equivalent to granodiorite.

5. CALCI - Dolomitic shaly limestone, with minor amounts of quartz, feldspar, and mafic minerals; with significant anisotropy introduced by jointing and interbedding.

5.4.2 Tabulation of Model Characteristics

In Table 5-1 the five geologic models are first specified in terms of the nominal mineralogic composition. Next the corresponding grain size, bulk density and porosity are specified, consistent with the stated descriptions of each model, and the chemical and physical properties needed for prediction of subterrene performance are listed for each model.

Since the figures for heat content are on a dry weight basis, they can be converted to joules/cm^3 of dry material by multiplying by the dry density values from Table 5-1. To convert to a water-saturated basis, which is the normal field condition, it is then necessary to add the quantity of heat needed to account for the interstitial water. The uncertainty here is in estimating the temperature to which the water must be raised before it is extruded around the penetrator, and estimating the portion of the water that must be vaporized. For the following it is assumed that all the interstitial water must be converted to steam, and its temperature increased by 100°C (i.e., from 25°C to 125°C). Each gram of water will therefore require 540 + 100 cal = 640 cal = 2678 joules. For each model the additional heat requirement is related to the porosity, as follows:

Heat Required (298°K to 90% Fusion)	UNCON	SOSED	MASIG	FOLIA	CALCI
Dry weight basis	2822	4370	5197	5049	7576
Pore water	(0.40 x 2678)	(0.17 x 2678)	(0.01 x 2678)	(0.03 x 2678)	(0.05 x 2678)
	1071	455	27	80	134
Total joules/cc	3893	4825	5224	5129	7710

TABLE 5-1a

GEOLOGIC MODELS

		Nominal Composition (dry weight % basis)					
		Quartz	Feldspars K	Feldspars Na-Ca	Ferromagnesian Minerals	Carbonate Minerals	Clay Minerals
1.	UNCON Unconsolidated sediments such as alluvial silt, sand, and/or fine gravel; water saturated; with minimal anisotropy from stratification or jointing.	45	15	15	10	5	10
2.	SOSED Relatively soft sedimentary rock such as calcareous shale or impure shaly sandstone, water saturated, with anisotropy introduced by stratification (grain orientation and interbedding), and jointing.	30	15	15	15	10	15
3.	MASIG Massive igneous rock of intermediate composition (granodiorite), without significant rock anisotropy introduced by joint systems, flow structure, or shear zones.	20	15	45	20	-	-
4.	FOLIA Igneous or metamorphic rocks with significant structural complexity in the form of foliation, jointing, flow structure, or shear zones; having an intermediate composition, similar to granodiorite.	15	15	40	20	5	5
5.	CALCI Dolomitic shaly limestone, with minor amounts of quartz, feldspars, and mafic minerals; with significant anisotropy introduced by jointing and interbedding.	8	5	2	5	70*	10

*Calcite 50%
Dolomite 20%

TABLE 5-1b

GEOLOGIC MODEL DATA

	Grain Size (mean dia.)	Bulk Density[1] Dry	Bulk Density[1] Saturated	Rock Porosity	Joint[2] Porosity	Total Porosity	Total Permeability[3] Parallel	Total Permeability[4] Transverse
UNCON	1 mm	1.5 g/cm^3	1.9 g/cm^3	40 %	0 %	40 %	5×10^{0}[5]	3×10^{0}[5]
SOSED	0.1 mm	2.3	2.5	15	2	17	1×10^{-1}	1×10^{-2}
MASIG	2 mm	2.8	2.8	0.7	0.3	1.	3×10^{-3}	1×10^{-3}
FOLIA	2 mm	2.7	2.7	1.	2.	3.	5×10^{-3}	1×10^{-3}
CALCI	0.01 mm	2.6	2.6	2..	3.	5.	3×10^{-2}	1×10^{-3}

(1) Density of total mass, including joints, etc. Data from George (5-14), Manger (5-15) and Daly, et al., (5-16)

(2) Including all secondary porosity, such as joints, shear zones, vugs, etc.

(3) Parallel to the principal bedding, foliation, or joint/shear planes.

(4) Normal to the principal bedding, foliation, or joint/shear planes.

(5) This figure is intrinsic permeability, which is a property of the medium and independent of the nature of the fluid. The units are $(\mu m)^2 = 10^{-12}\ m^2 = 10^{-8}\ cm^2 = 1.013$ darcy. Data from Davis and DeWiest (5-17) and Krumbein and Sloss (5-18).

TABLE 5-1b
(Continued)

GEOLOGIC MODEL DATA

Model	Rock Physical Properties (1)				Melting Range		Melt Viscosity at 90% fusion temp. (poises)	Density of Glass Produced
	Poisson's Ratio (σ)	Young's Modulus (E) kg/cm^2	Compressive Strength kg/cm^2	Thermal (2) Expansion (Volume %)	First Melting (3)	90% Fusion (4)		
UNCON	0.45	1.0×10^4	280	-30	1300°K	1500°K	3×10^4	2.3 g/cm
SOSED	0.38	1.0×10^5	560	-12	1300	1400	6×10^3	2.3
MASIG	0.18	1.0×10^6	2500	12	1400	1500	1.5×10^4	2.5
FOLIA	0.24	1.0×10^6	1400	9	1300	1450	9×10^3	2.4
CALCI	0.35	1.0×10^5	900	-36	1600(5)	1740(5)	5×10^1	2.4

(1) Properties of the total rock mass, including joints, shear zones, and stratification.

(2) Thermal expansion of rock, from ambient to melting temperature, plus expansion on melting. The figures are negative for the first two models, because of their porosity, and for the CALCI model because of loss of CO_2.

(3) Melting point of the lowest melting major component. Reactions taking place below this temperature include dehydration, polymorphic transitions, possible decarbonation and/or desulfurization. Melting of minor constituents (chlorides, sulfates, etc.) will occur at lower temperatures and is disregarded. It is assumed that no fluxing material is added, and that the natural fluxing materials are least important in Model No. 3.

(4) It is assumed that minor refractory minerals such as garnet and zircon, and some of the SiO_2, remain in the solid phase and are extruded with the glass without having been melted.

(5) Strongly pressure dependent. If a pressure of ~1000 psia (70 kg/cm^2) can be maintained, a liquid melt may be achieved at ~1500°K.

TABLE 5-1b
(Continued)

GEOLOGIC MODEL DATA

		Thermal Conductivity[1]	
		Parallel	Transverse
1.	UNCON	4	4
2.	SOSED	11	8
3.	MASIG	21	21
4.	FOLIA	22	20
5.	CALCI	22	20

[1] $W/cm \cdot {}^{\circ}K \times 10^{-3}$ at $600^{\circ}K$; figures are for dry rock; models 1 and 2 will be strongly affected by interstitial water and/or steam which will increase the conductivity to values nearly as high as models 3 and 4. Convection is not included. (For references see Section 5.5.1; the accuracy of these estimates is about $\pm$ 50%.)

TABLE 5-1c

HEAT CONTENT OF EARTH MODELS,
25°C (298°K) to 90% Fusion
(References 5-19, 5-20)
Dry Weight Basis

	joules/gram			
	UNCON	SOSED	MASIG	FOLIA
25°C to 1000°C (1273°K)	1150	1150	1140	1140
1273°K to 90% fusion	261	145	256	200
Heat of fusion	320	350	370	370
Volatilization of minor CO_2, etc.	100	180	50	100
Volatilization of bound water*	50	75	40	60
Total joules/gm	1881	1900	1856	1870
joules/cm	2822	4370	5197	5049

*Based on percentage of clay minerals and ferromagnesian minerals in comparison with CALCI model, for which percent bound water was calculated (1.65% H_2O = 37 joules/gm).

TABLE 5-1d

HEAT CONTENT OF CALCI MODEL,
25°C (298°K) to 90% Fusion
(References 5-19, 5-20)
Dry Weight Basis

		cal/gm	joules/gm
25° C to 870°C (1)	=	230	962
CO_2 evolution (2)	=	303	1270
870°C to 1000°C (3)	=	20	84
1000°C (1273°K) to 1740°K (3)	=	72	301
Heat of fusion	=	62	260
Vaporization of bound water (1.65% by wt)	=	9	37
	Total joules/gm		2914
	joules/cm		7576

(1) Estimated from Bedford limestone and Tennessee marble (Ref. 5-19) = 237 cal/gm
Rockville quartz monzonite = 216 cal/gm

(2) 43.4×10^3 cal/100 gm = 434 cal/gm (+56 gm of CaO/mol of $CaCO_3$)
at 70% purity = 304 cal/gm
= 1270 joules/gm

(3) Specific heat estimated at 0.22 cal/gm °K for the 0.7 gm remaining for each 1.0 gm of rock.

5.4.3 Applicability of Geologic Models to Continental Near-Surface Rocks and Soils

The five models are representative of the following proportions of the total of continental near-surface materials.

UNCON	21%
SOSED	33%
MASIG	16%
FOLIA	10%
CALCI	15%
	95%

On this basis the five models will cover about 90-95% of the near-surface continental crustal materials. It is estimated that almost all sands, clays, and shales will fit into either the UNCON or SOSED models, depending on their degree of induration and stratification. Similarly, most of the igneous rocks will fit into the MASIG model, most of the schist, gneiss and slate will fit into the FOLIA model, and most carbonate rocks will fit reasonably well into the CALCI model. The very pure end-members such as 100% quartz sandstone or 100% limestone are so unusual that they do not need to be considered as models. In nature, the interbedded rocks and impure mixtures of various rocks and minerals are much more common, especially when considered on the scale of a tunnel of 5-10 meter diameter. Most areas that are settled and built-up to urban conditions where significant tunneling may be expected, will have a predominance of UNCON and SOSED.

It is obvious that a very pure quartz sandstone (melting point = 1610°C = 1883°K) or a pure limestone (melting point of CaO = 2850°C = 3123°K) could not be melted without the addition of fluxes. In the following calculations, the totals applicable to each model are derived.

UNCON:		1/2 of sands (17.2%/2), 1/3 of clays & shales (36.1%/3)	=	20.6 %
SOSED:		1/2 of sands (17.2%/2), 2/3 of clays & shales (36.1%/ 2/3)	=	32.7 %
MASIG:	(a)	granite (3.6%), granodiorite (3.9%), syenite (0.06%), nepheline syenite (0.06%), 1/2 of gneiss (7.4%/2), 1/2 basalt (5.5%/2), 1/2 of andesite (3.6%/2), 1/2 rhyolite (0.9%/2)	=	16.3 %
FOLIA:	(b)	schist (1.8%), 1/2 of gneiss (7.4%/2), 1/2 basalt (5.5%/2), 1/2 of andesite (3.6%/2), 1/2 of rhyolite (0.9%/2)	=	10.5 %
CALCI:		carbonates	=	15.5 %
			Subtotal	95.6 %
	(c)	Evaporites		1.0 %
		Gabbro		0.7 %
		Peridotite		0.02%
		Amphibolite		1.9 %
		Miscellaneous volcanics		0.8 %
		Other, including coal, sulfide rocks, iron ores (Fe_2O_3 or Fe_3O_4), phosphate rock, peat, etc.		1.0 %
			Total	100.0%

(a) The gneisses are included 1/2 in MASIG and 1/2 in FOLIA. It is estimated that 1/2 the gneisses show significant anisotropy from flow structure and/or foliation, and so are included in FOLIA; while the remaining 1/2 are nearly isotropic, and so are included in MASIG even though gneisses are metamorphic rocks by definition.

(b) The extrusive igneous rocks (basalt, andesite, and rhyolite) are included 1/2 in MASIG and 1/2 in FOLIA because the ones with significant anisotopy from flow structure and/or interbedding are better represented by FOLIA, even though they are not metamorphic.

(c) Gypsum, anhydrite, rock salt, sylvite (KCl), etc. Chemically precipitated limestone and dolomite are specifically excluded, having been included in the 15.5% above.

5.5 DISCUSSION OF SELECTED PHYSICAL AND CHEMICAL PROPERTIES

5.5.1 Thermal Conductivity

In minerals of the cubic system, the conduction of heat is isotropic and can be described by a single constant. In other minerals, either two or three principal conductivities must be defined. In rocks the thermal conductivity is determined by the orientation and packing of the mineral grains, and by the interstitial fluid. A significant amount of anisotropy can be caused by the bedding, foliation, fracturing, veining, or jointing. Some representative values are as follows, from Clark (5-21):

	Temp. °C	No. of Samples	Conductivity (10^{-3} cal/cm sec° C) Mean	Range
Shale	~ 20	14	3.55	2.8-4.2
	~ 20	6	5.7	4.7-5.9
	~ 20	5	4.9	
Slate	0		5.2	
	100		4.7	
Quartzite	0		14.9	
	100		12.5	

	Temp. °C		No. of Samples	Conductivity (10^{-3} cal/cm sec °C) Mean	Range
Quartzitic sandstone	0	Parallel		13.6	
	100	to		10.6	
	200	bedding		9.0	
	0	Normal		13.1	
	100	to		10.3	
	200	bedding		8.7	
Limestone	20			5.7	
	350			3.2	
Carbonaceous limestone	0	Parallel		8.2	
	100	to		7.0	
	200	bedding		6.5	
	0	Normal		6.1	
	100	to bedding		5.4	
Dunite	0		3	12.4	
	50		3	10.5	
	100		3	9.4	
	200		3	8.1	
Granite (3 localities)	0			6.66	
	50			6.25	
	100			5.90	
	200			5.50	

	Temp. °C	No. of Samples	Conductivity (10^{-3} cal/cm sec °C)* Mean	Range
	0		5.80	
	50		5.60	
	100		5.42	
	200		5.12	
	0		8.4	
	50		7.8	
	100		7.2	
	200		6.5	
	300		5.9	
Hudson River Sand ~	20°C		0.65 at 0.2% moisture 3.94 at 30% moisture	

*(To convert to W/cm · K x 10^{-3} multiply by 4.184)

The apparent systematic decrease in thermal conductivity with heating, from 0°C to 300°C, is probably due to moisture loss. A better indication of the change of conductivity with temperature is given by Murase and McBirney (5-22). They show that the conductivity of andesite is about constant (at 2.6 x 10^{-3} cal/cm · sec °C) from 0°C to 600°C, and increases to 4.5 x 10^{-3} between 600°C and 1500°C. They show the conductivity of basalt decreasing slightly from 0°C to 1100°C, and then increasing between 1100°C and 1500°C. The range of values for basalt is from 2.3 x 10^{-3} to 5.4 x 10^{-3} (all units are cal/cm · sec °C). The values for the five models given in Table 5-1 are derived from the data of Murase and McBirney (5-22) and from those of Clark (5-21). The values given by Clark are in general

somewhat higher than those of Murase and McBirney, probably because Clark's data are field measurements in which interstitial water is a factor. Another source of data on thermal conductivity of fluid-saturated rock is Somerton (5-23). In general, the variation within rock types is greater than any systematic variation between rock types. For stratified rocks the conductivity normal to the bedding is 5-20% less than parallel to the bedding. In sedimentary rocks (with normal porosity) the convection cells in the pore fluids will also be important and will be anisotropic in accordance with the ratio of fluid permeabilities normal and parallel to the bedding. The thermal conductivity is strongly dependent on porosity and fluid saturation. The values for water and air at 30°C are 1.5×10^{-3} and 0.063×10^{-3} cal/cm · sec · °C (Clark 5-21).

5.5.2 Average Densitities of Rocks and Corresponding Glasses

The average densities of near-surface geological materials are shown in the following table. For solid rocks the corresponding glasses are ~ 10% less dense than the rock. This is also shown by the natural SiO_2 glass, lechatelierite, which has a density of 2.2 g/cm^3 (Ref. 5-8), somewhat less than the common crystalline forms of SiO_2 (2.26 to 2.65). For sediments with significant porosity, the glass should be 10-20% more dense than the rock. For most igneous and metamorphic rocks, the difference in density between dry and saturated conditions is insignificant (< 0.02 g/cm. However, for sediments with significant porosity, the density differences can be considerable, as shown by the table.

	Number of Samples	Density (g/cm^3) Mean	Range
Granite	155	2.67	2.52-2.80
glass	15	2.37	2.33-2.41
Syenite	24	2.76	2.63-2.90
glass	3	2.45	2.44-2.47
Diorite	13	2.84	2.72-2.96
glass	3	2.47	2.40-2.57
Gabbro	27	2.98	2.85-3.12
glass	11	2.77	2.70-2.85

	Number of Samples	Porosity*	Density (g/cm^3) Mean	Density (g/cm^3) Range
Sandstones	637	0.7-33.7		2.17-2.70**
Carbonate Rocks	353	2.9-28.8		2.23-2.66
Shales	> 38	4.0-33.5		2.06-2.66
Sand, clay, gravel, soil	87	38.9-74.7		1.44-1.93
Gneiss	7		2.69	2.66-2.73
	19		2.61	2.59-2.63
	25		2.84	2.70-3.06
Schist	76		2.82	2.70-2.96
	50		2.82	2.73-3.03
Slate	17		2.81	2.72-2.84

*Range of means (%)

**Saturated bulk densities

References:

George (5-14)

Daly, et al (5-16)

Bean (5-24)

Clark (5-25)

Eaton & Rosenfeld (5-26)

5.5.3 Viscosity and Melting Characteristics

The viscosity of melted rock or earth varies widely with temperature and with chemical composition. Most silicate rocks do not have a fixed melting temperature but instead melt incongruently - that is, they melt over a temperature range of as much as 300°C (as discussed in Section 5.3.3). The viscosities of the five models are shown on the following figures (Figures 5-7a through g) for the range from 1100°C (1373°K) to 1700°C (1973°K). This covers the temperature interval from first melting to 90% fusion for all the models. The curves are estimates derived mainly from the data of Bacon et al (5-27), with cross-checking of earlier results given by Birch & Dane (5-28) and Clark (5-29). Bacon's results (5-27) show measured viscosity values for ten rock samples between 1084°C and 2200°C (1357°K to 2473°K). The samples tested are 2 granites, 2 basalts, 1 gabbro, 1 rhyolite, 1 quartzite, and 1 sandstone.

The curve for the CALCI model is based on older data given by Birch & Dane (5-28) for the minerals wollastonite (48% CaO, 52% SiO_2) and diopside (26% CaO, 18% MgO, 56% SiO_2), and by Clark (5-29) for various mixtures of CaO, MgO, Al_2O_3 and SiO_2. It is estimated that the CALCI melt will be the least viscous of the five models. From the curves for the various rock types, it can be seen that the range of viscosity for a given temperature and rock type can be as much as two orders of magnitude. For each model and temperature, an order of magnitude estimate is about all that is possible with available data.

Since the melting of most silicate rocks will occur over a range of temperature, the values given in Table 5-1 (Section 5.4.2) are for the first melting temperature and for the temperature at which 90% of the material (dry weight basis) will be molten. The remaining 10% of unmelted crystals can be incorporated into the glass liner. The melting ranges are derived mainly from data in Clark (5-4), Roedder (5-30) and Wyllie (5-3).

The melting characteristics of carbonate rocks are treated separately because of the special problems associated with the evolution of CO_2. These rocks are represented by the CALCI

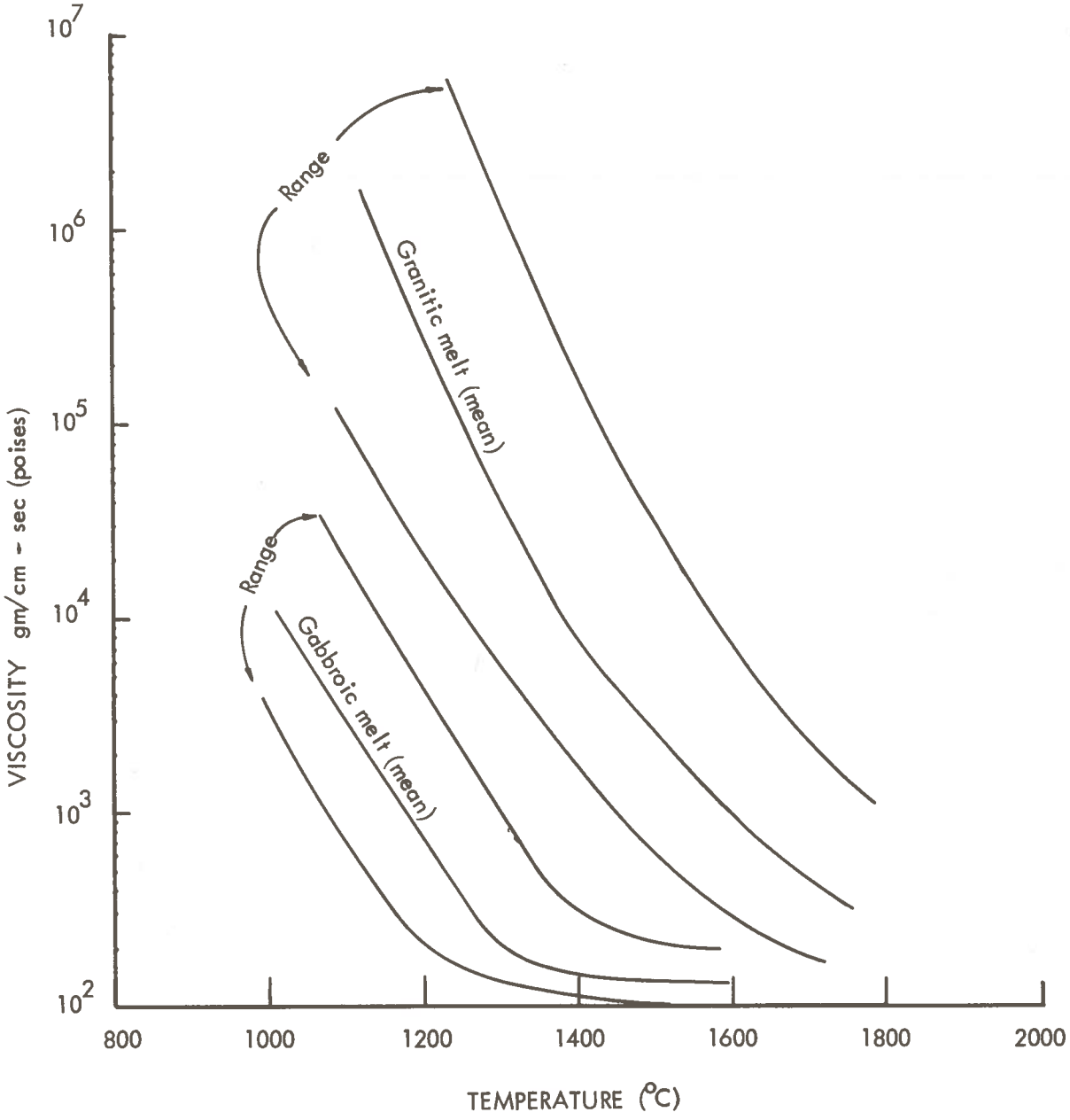

Figure 5-7a. Mean Value and Ranges, Viscosity VS. Temperature Granitic Melts and Gabbroic Melts

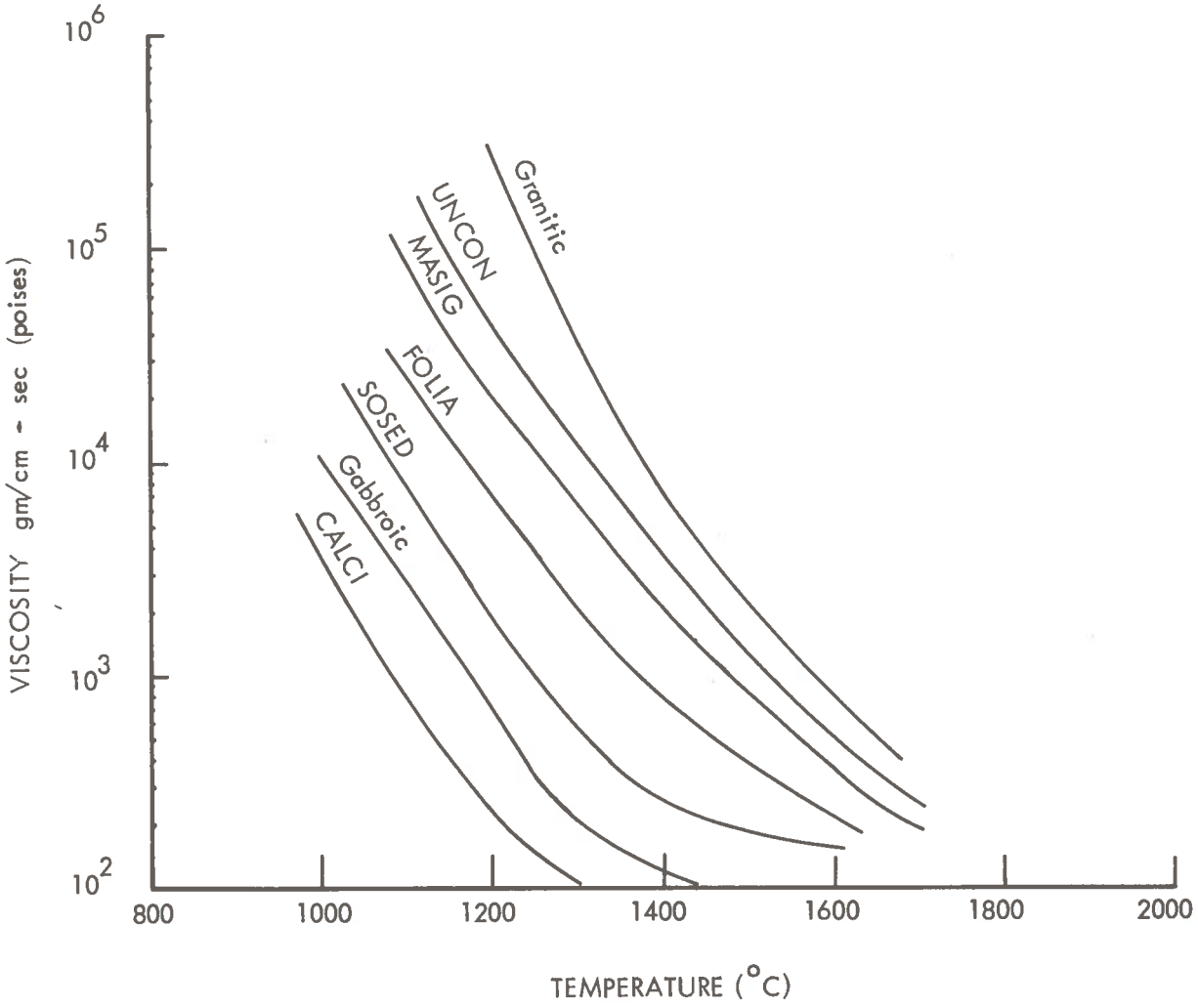

Figure 5-7b. Mean Values, Viscosity VS. Temperature

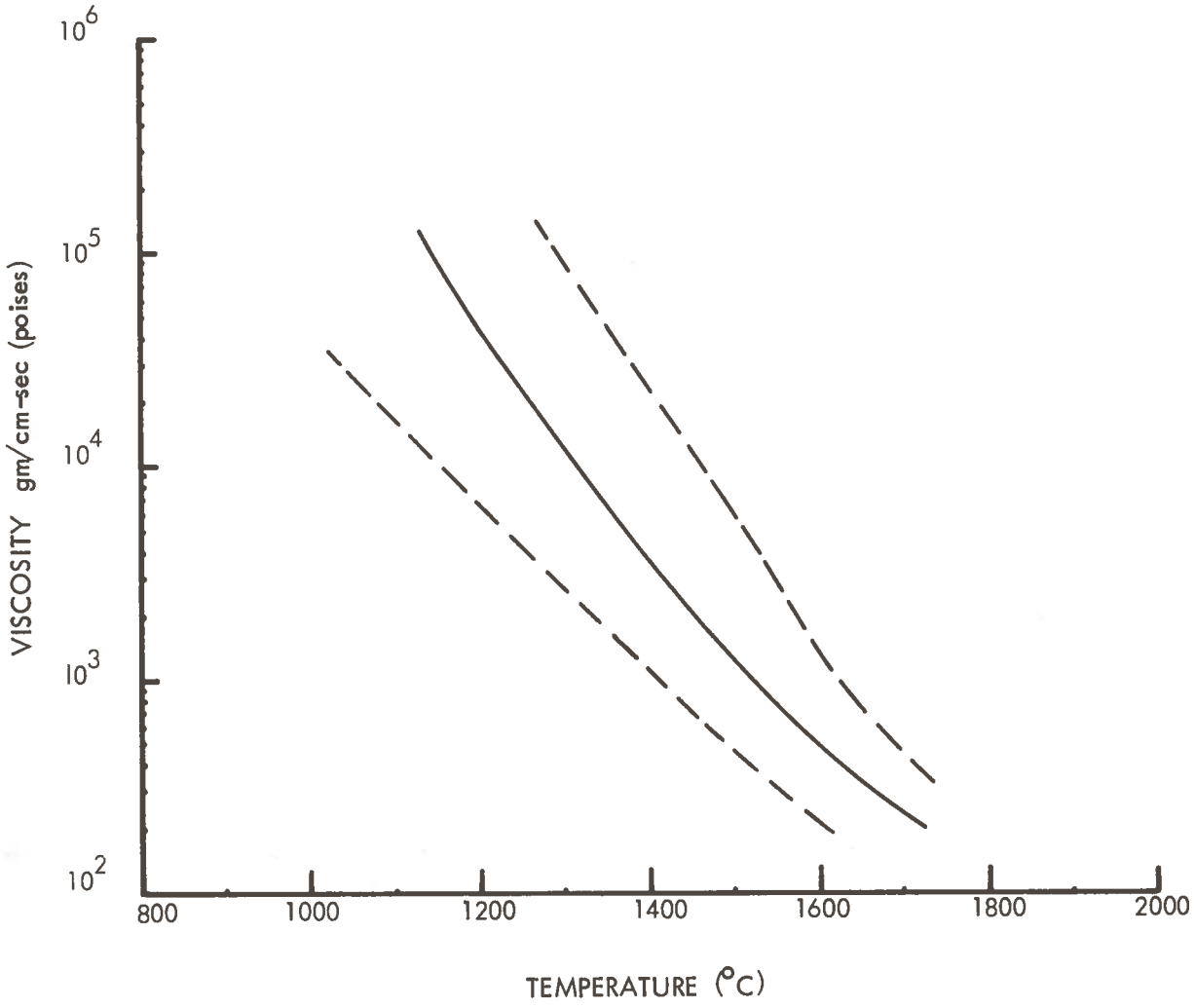

Figure 5-7c. Mean and Range Viscosity of UNCON

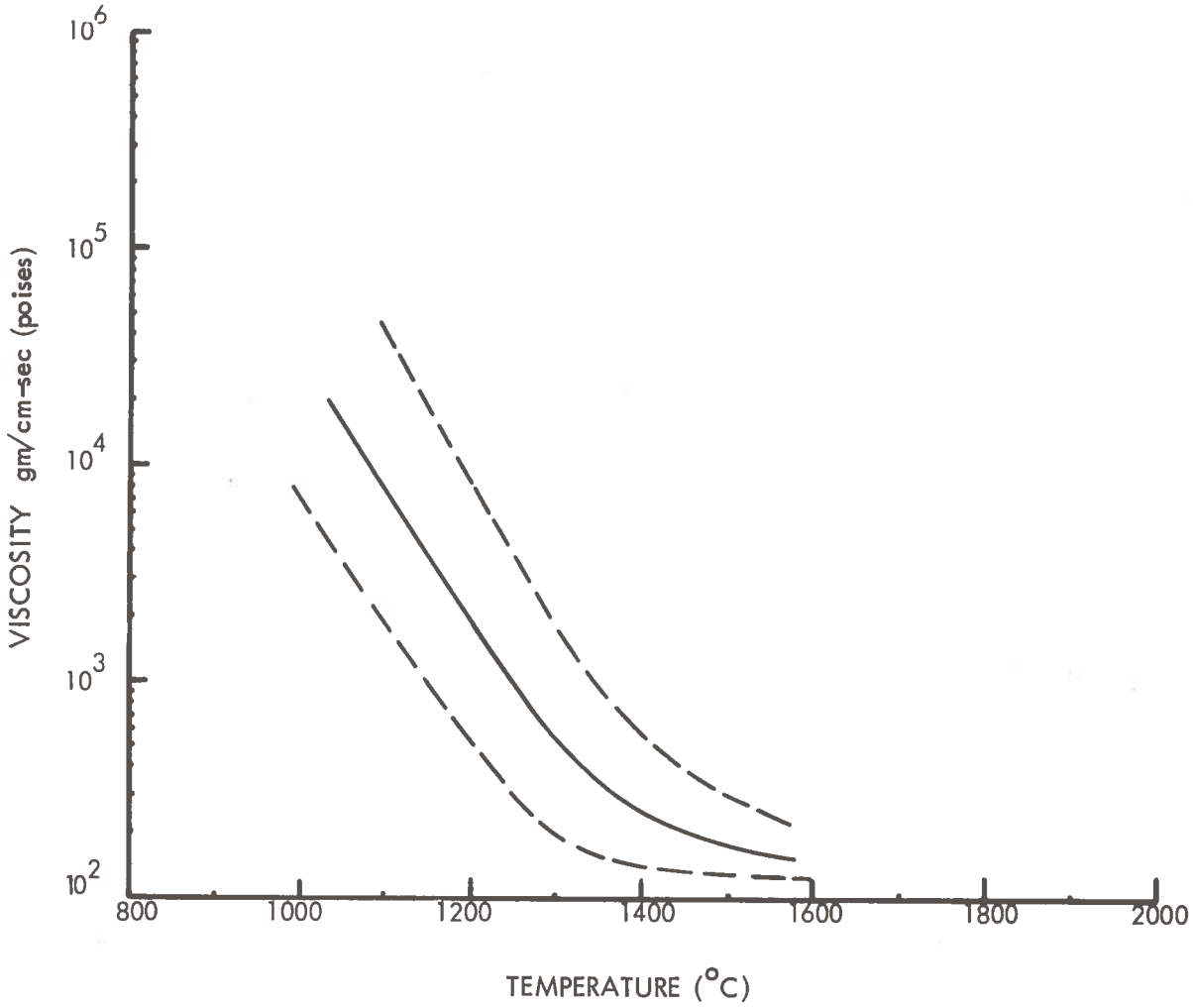

Figure 5-7d. Mean and Range Viscosity of SOSED

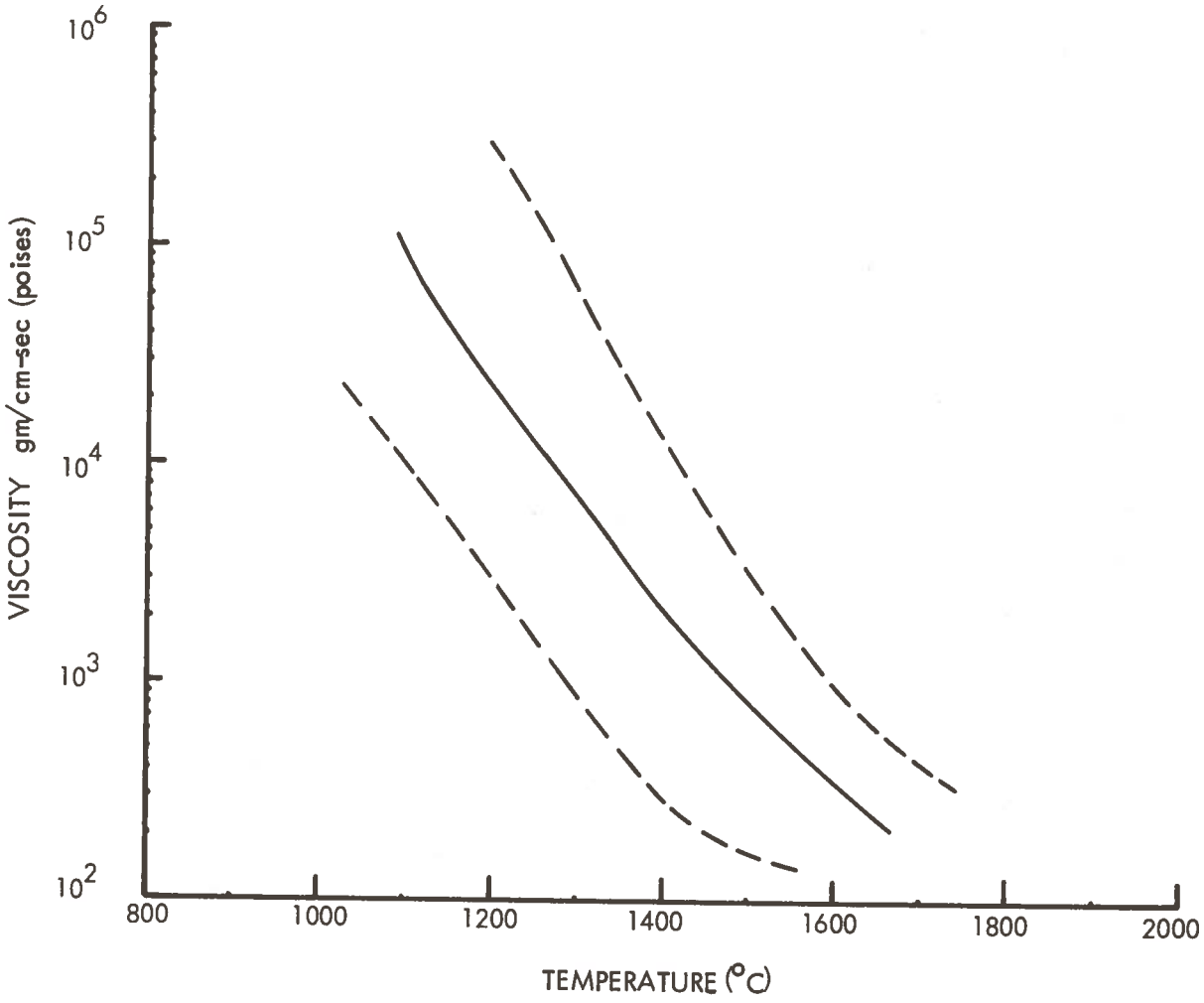

Figure 5-7e. Mean and Range Viscosity of MASIG

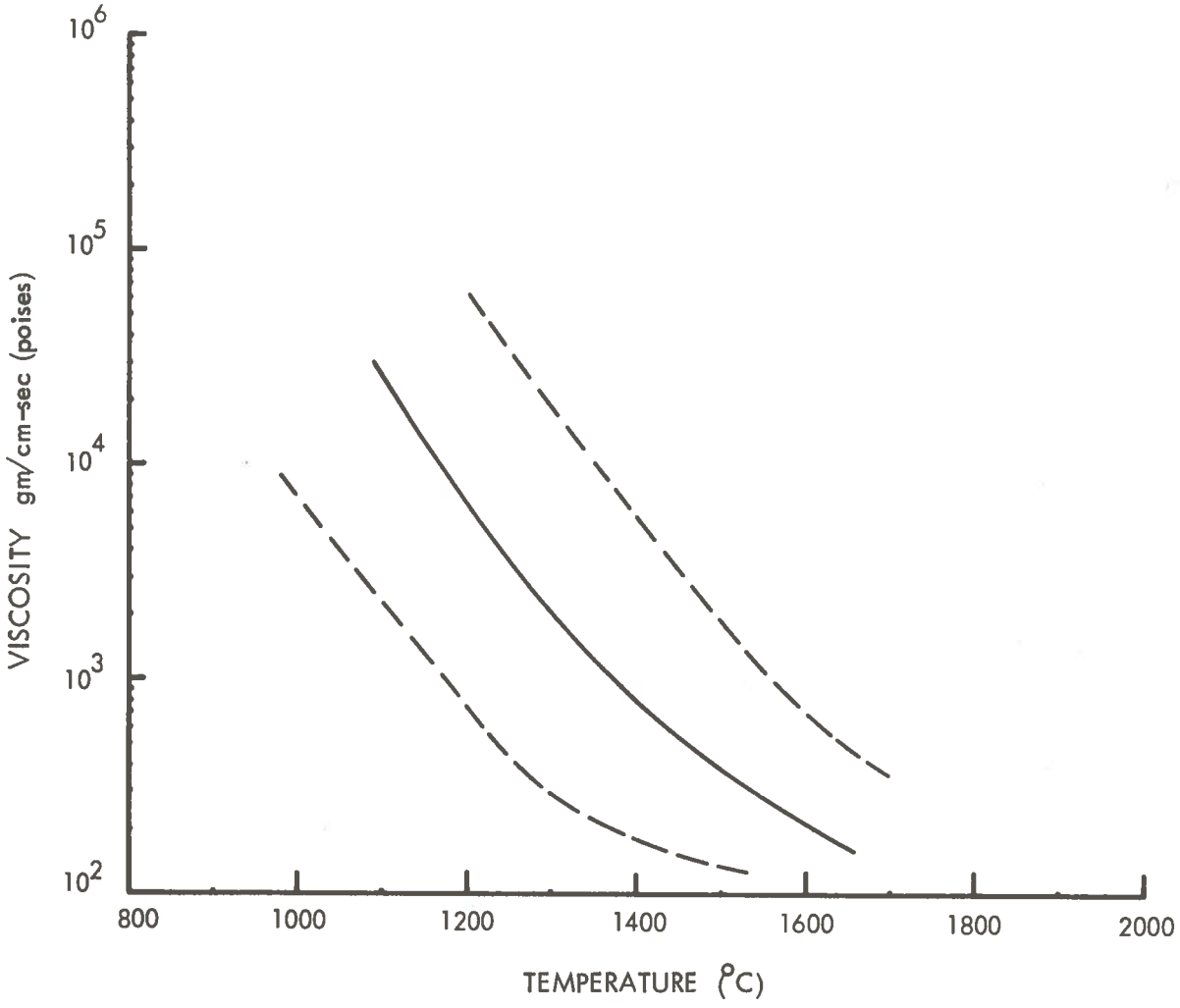

Figure 5-7f. Mean and Range Viscosity of FOLIA

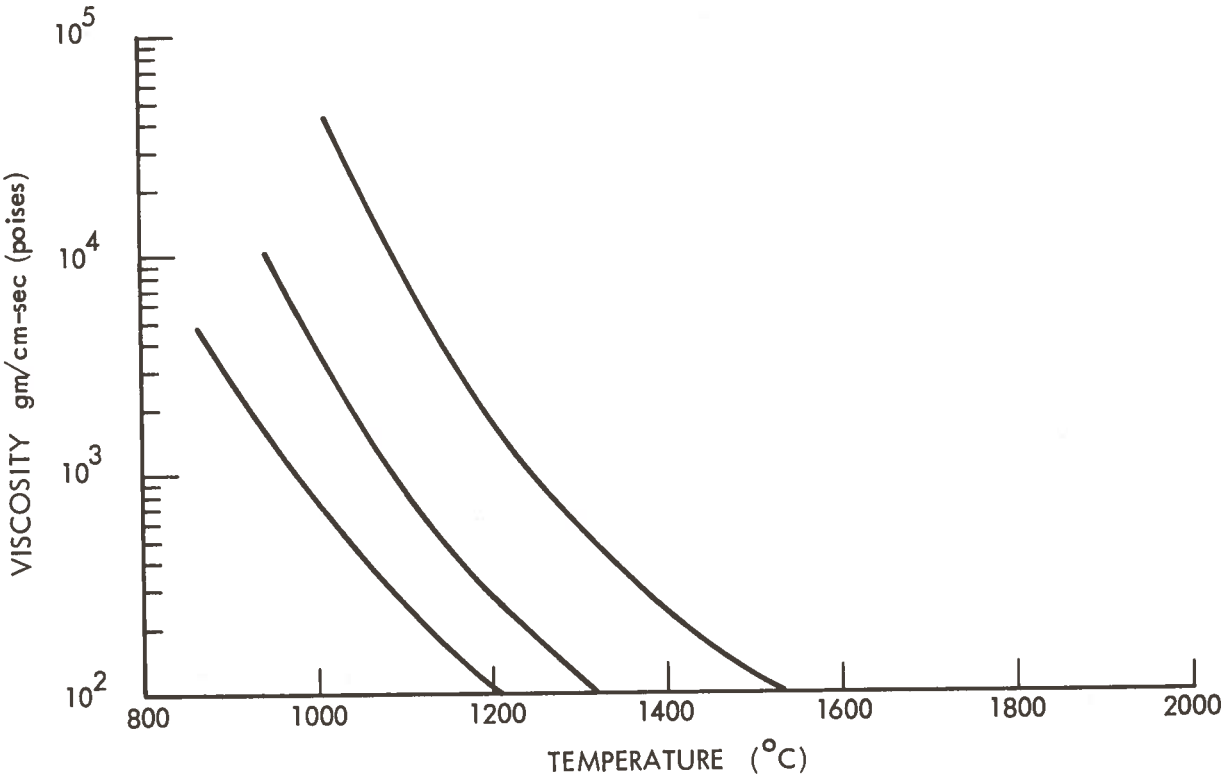

Figure 5-7g. Mean and Range Viscosity of CALCI

model, a dolomitic shaly limestone. The carbonate model CALCI is defined mineralogically as 50% calcite, 20% dolomite, 8% quartz, 7% feldspar, 5% mafic minerals (in this case calculated as biotite), and 10% clays (in this case calculated as kaolin). This corresponds to a chemical composition as follows:

SiO_2	18.9%
Al_2O_3	6.6%
CaO	34.2%
MgO	4.8%
CO_2	31.6%
K_2O	1.4%
Na_2O	0.12%
FeO	0.75%
H_2O	1.65%
	100.02%

The values are on a dry-weight basis. The H_2O is water of hydration (chemically bound water) present in the biotite and kaolin, not interstitial or free water. When the 5% pore water (including water in joints) is considered, the chemical composition is:

SiO_2	18.5%	
Al_2O_3	6.4%	
CaO	33.6%	
MgO	4.7%	
CO_2	31.0%	
K_2O	1.4%	
Na_2O	0.11%	
FeO	0.73%	
H_2O (chemically bound water)	1.62%	
H_2O (moisture)	1.9%	(all values by weight)
	99.96%	

As the temperature is raised, the loosely held water will mostly be volatilized at temperatures between 100°C and 200°C (373 and 473°K), and the lattice water in the micas and clays will be driven off below 800°C (1073°K). Below 900°C (1173°K) the CO_2 will be liberated from the calcite and dolomite. Most of the H_2O and CO_2 will be vented, but some small and variable portion will stay in the liquid phase. In this example, it is assumed that 10% of the CO_2 and bound water will remain in the system and be dissolved into the liquid phase. At 100% fusion, the resulting melt would therefore have the following composition:

SiO_2	27%
Al_2O_3	9%
CaO	49%
MgO	7%
CO_2	4%
K_2O	2%
Na_2O	0.2%
FeO	1%
H_2O	0.3%
	99.5%

The melting characteristics of this material can be approximated by comparison with Figure 5-8, from Roedder (5-30).

The CaO content of this ternary oxide model is about equal to the sum of CaO and MgO in the CALCI model. Roedder's model is more aluminous, and CALCI is more siliceous. The other constituents in the CALCI model are minor. Roedder's model shows that melting begins at 1335°C (1608°K), but fusion is only 13% complete at 1445°C (1718°K). Most of the melting occurs between 1445°C and 1470°C (1718 to 1743°K), and at 1470°C the

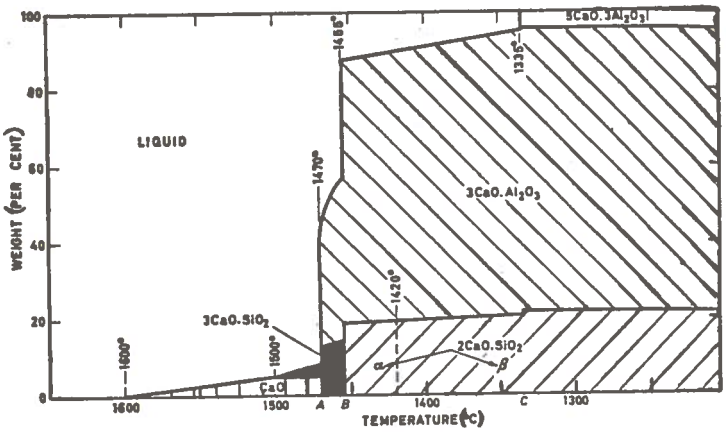

Figure 5-8. Diagram of Equilibrium Phases in a Mixture of Composition CaO 62.2%, Al_2O_3 30.2%, SiO_2 7.6%

melting is over 90% complete. The small amounts of solid-phase material remaining above 1470°C (CaO in Roedder's model) will ultimately be incorporated into the glass liner.

In any natural system approximating the CALCI model, other small amounts of solid-phase material will remain, such as MgO, CaO, and the minerals zircon, quartz, rutile, garnet, etc. These amounts will be small and will not greatly affect the melting characteristics. Their effect on the resulting glass liner may be significant, however. The melting range of the CALCI model (to 90% fusion) can be estimated as between 1400°C and 1500°C (1673 to 1773°K). More complete information for this and similar systems is given by Roedder, and by Schairer (5-31), and Levin, et al, (5-32, 5-33).

5.5.4 Thermal Expansion

In liquids and gases and in solids of the isometric crystal system thermal expansion is isotropic, the same in all directions. All other crystalline materials have either two or three principal directions of expansion, which must be measured to specify the linear expansion characteristics. In rocks there is a further complication arising from the unequal expansion of various mineral grains and the small amount of intergranular porosity that exists even in dense igneous rocks. On heating, the individual crystals expand by different amounts with the result that the porosity is slightly increased and, in the laboratory, a measured thermal expansion would not be a true one. Also, the measured data on cooling will be different from the heating data and subsequent runs will not be repeatable. In the field, further complexity is introduced by stratification, jointing and foliation. However, with these limitations in mind, estimates of total net thermal expansion can be made.

The thermal expansion, by volume, of most rocks is about 4-6% from ambient to melting temperature. Melting results in a further expansion of 6-8%, so the total volumetric expansion is 10-14% (Skinner 5-34). In rocks with more than 14% porosity, such as the UNCON and SOSED models, there will be a net consolidation resulting from heating, expulsion of interstitial water, and melting. In less porous rocks there will be a small net expansion, except when a large part of the rock is lost as a volatile component, such as in the CALCI

model. One gram molecular weight (mol) of $CaCO_3$ (100 gm) breaks down to 44 gm of CO_2 which leaves the system and 56 gm of CaO which stays behind. The volume of one mol of $CaCO_3$ (100 gm) is 36.9 cm^3 and that of CaO (56 gm) is 16.8 cm^3 (Robie, et al. 5-7). The total net thermal expansions from ambient temperature to 90% fusion are given in Table 5-1 as negative for three of the models, and small positive values on MASIG and FOLIA.

5.5.5 Ambient Temperature

The seasonal and diurnal changes in the temperature of near-surface earth materials are significant down to a depth which varies (approximately with latitude) from about 10 meters in the southern part of the United States to about 20 meters in the northern part. At this depth the annual temperature variation is less than $\pm 1^{\circ}C$, and the mean temperature is about 1 to $2^{\circ}C$ above the mean annual air temperature. This nearly constant temperature is about $24^{\circ}C$ ($75^{\circ}F$) along the southern edge of the U.S. and decreases to about $5^{\circ}C$ ($40^{\circ}F$) along the northern edge. Figure 5-9 from Todd (5-35), after Collins (5-36), shows the approximate variation of ambient temperatures at the depth of 10 to 20 meters in the United States.

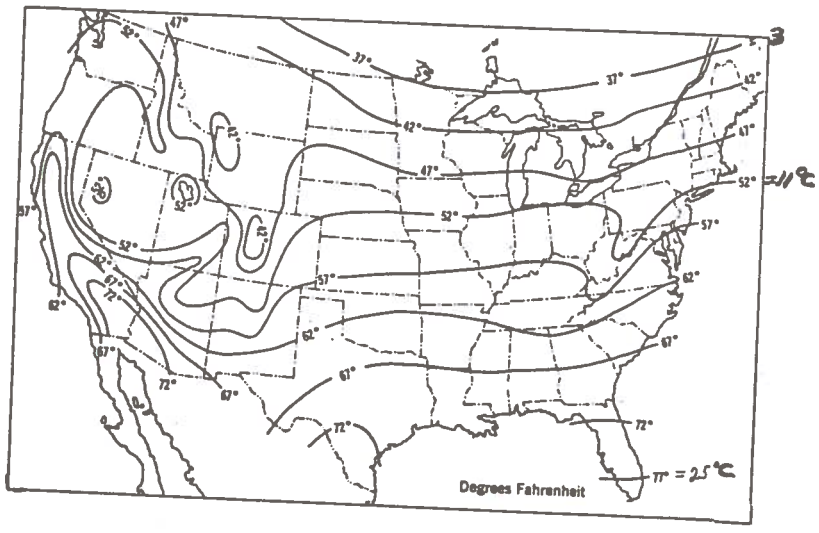

Figure 5-9. Approximate Temperature of Ground Water in the United States at Depths of 30 to 60 Feet

Below this depth, the annual range of temperature is very nearly zero, and the temperature increases with depth at $\sim 1^{\circ}C/30$ m. This geothermal gradient varies within a factor of 0.5 to 2.0 at most locations.

5.5.6 Solubility of Water in Silicate Melts

The solubility of water in silicate melts at 1000 - 1200°C and less than 300-500 bars pressure can be derived from figures given by Clark (5-37) as about 3% H_2O by weight. The composition of the aqueous phase in equilibrium with silicate melts at high temperature and pressure is given by Clark (5-37). For a silicate melt at 1000°C and 100 bars pressure, a good estimate appears to be about 98.5% H_2O, 1% SiO_2, and lesser amounts of Al, K, Na, Ca, and Mg. These solubilities have been taken into account in deriving the composition of the CALCI melt discussed in Section 5.5.3.

5.5.7 Rock Elastic Properties

The values of Poisson's ratio, Young's modulus, and compressive strength given in Table 5-1 (Section 5.4.2) are mainly taken from Birch (5-38, 5-39). Simpson and Fergus (5-13) and Haimson and Fairhurst (5-40). Most of the values were obtained on laboratory samples, so they do not take into account the effects of larger scale features such as stratification, jointing or shear zones. To account for these features, field measurements would have to be made in each individual case. Based on such measurements an effective modulus of deformation can be defined, which will be a more accurate indicator of the rock behavior. The Young's modulus values in Table 5-1 are given only to an order of magnitude. This is believed to be sufficient for the present purpose. Techniques for determining in situ modulus of deformation and for predicting the relationships between field and laboratory moduli using Rock Quality Index are given by Coon and Merritt (5-41) and Deere, et al., (5-42).

5.6 SUMMARY AND CONCLUSIONS

Five geologic models typical of near-surface continental crustal materials have been defined. The five models are representative of about 90-95% of the cases that will be encountered.

The models defined are (1) an unconsolidated sediment, (2) a stratified sediment, (3) a massive igneous rock of intermediate composition, (4) a foliated metamorphic rock, and (5) an impure carbonate sediment. The only rock types not covered by the models are the unusually pure quartz sandstones, quartzites, or carbonate rocks, and the less common rock types such as the ultrabasic rocks peridotite and amphibolite, some of the gabbros, evaporites such as rock salt or potash, coal, sulfide ores, and phosphate rock.

The changes that will occur in these rocks on heating have been described in terms of the principal crystallographic transitions; the dissociation reactions - dehydration, decarbonation, and desulfurization; and the anhydrous and hydrous melting reactions. The melting points of these complex materials are determined by the lowest melting constituents and the solubility of the remaining material in the early melts. In terms of the five models the temperatures of first melting are estimated at 1300-1600°K, and the temperatures of 90% fusion are estimated at 1400 - 1740°K. The highest values in each case are for the high calcium model CALCI, which has a melting range 200-300° higher than the other four models.

The total heat required from ambient temperature to 90% fusion (dry weight basis) varies from 2820 to 5200 joules/cm^3 for the first four models. The CALCI model requires 7580 joules/cm^3, the additional heat being needed mainly for liberation of CO_2 (1816 joules/gm of $CaCO_3$) and for the additional temperature rise to reach 90% fusion (1740°K).

When considered on a water saturated basis, the normal field condition, the total heat requirement increases considerably for the first two models (which are porous). The requirement for the three less porous models is not greatly affected. An estimate is made that the temperature

must be increased by 100°C (i.e., from 25°C to 125°C), and that all the interstitial water must be vaporized. With these estimates, the total heat requirement becomes:

	Total Heat Requirements (joules/cm^3)	
	Dry Weight Basis	Water Saturated Basis
UNCON	2820	3890
SOSED	4370	4820
MASIG	5200	5220
FOLIA	5050	5130
CALCI	7580	7710

These figures do not include heat losses to the surrounding rock.

The principal uncertainties in the estimates of geological conditions and their effects on subterrene performance are in three areas: thermal conductivity, viscosity, and the effect of interstitial water.

The thermal conductivity of rocks varies from about 8 to 40 W/cm $\cdot$°K x 10^{-3} (neglecting the air-saturated porous sediments, which are even lower). The dunites and peridotites (ultrabasic rock) and the quartzites are toward the high end of this range, but there seems to be no systematic way of predicting the values for most rocks. Most typical igneous rock values are of the order of 20 W/cm $\cdot$°K x 10^{-3}. For any given model the thermal conductivity can be estimated to an accuracy of $\pm$ 50%. These estimates could be improved by measuring the thermal conductivity of simulated models or in any area where a field test is anticipated.

The variation of effective viscosity with temperature through the melting range covers from three to five orders of magnitude. At the middle of the melting range, the least viscous rocks are about three orders of magnitude less viscous that the most viscous ones. For any given area where a rock melting device might be field tested, the effective viscosity near the middle of the melting range can be estimated to the nearest decade in magnitude.

The effect of water is important for two reasons; water pressure lowers the melting points of most rocks and in general aids the melting process, and the specific heat and the heat of vaporization of water are high enough to significantly increase the total heat requirement. The behavior of the interstitial water is difficult to estimate, but based on the assumptions that all the water in the path of the device must be raised in temperature by 100°C and converted to stea, and there will be negligible flow of water into the path of the device, the total heat requirements have been calculated. These assumptions, and the resulting heat requirements are believed to be reasonable, and accurate to ± 20%.

5.7 REFERENCES

5-1 Ronov, A. G. and A. A. Yaroshevsky, "Chemical Composition of the Earth's Crust," Amer. Geophys. Union Monograph 13, P. J. Hart, Editor, (1969).

5-2 Poldervaart, A., "Chemistry of the Earth's Crust," Geol. Soc. of Amer. Special Paper 62, A. Poldervaart, Editor, (1955).

5-3 Wyllie, P. J., The Dynamic Earth, John Wiley & Sons, (1971).

5-4 Clark, S. P. Jr., "High Pressure Phase Equilibria," Geol. Soc. of Amer. Memoir 97, S. P. Clark, Jr., Editor, (1966).

5-5 McLaughlin, R. J. W., "Thermal Techniques," Physical Methods in Determinative Mineralogy, J. Sussman, Editor, Academic Press, (1967).

5-6 Robie, R. A., "Thermodynamic Properties of Minerals," Geol. Soc. of Amer. Memoir 97, S. P. Clark, Jr., Editor, (1966).

5-7 Robie, R. A., P. M. Bethke, and K. M. Beardsley, Selected X-Ray Crystallographic Data, Molar Volumes, and Densities of Minerals and Related Substances, U. S. Geol. Survey Bulletin 1248, (1967).

5-8 Robie, R. A. and D. R. Waldbaum, Thermodynamic Properties of Minerals and Related Substances at 298.15°K (25.0° C) and One Atmosphere (1.013 Bars) Pressure and at Higher Temperatures, U. S. Geol. Survey Bulletin 1259, (1968).

5-9 Garrels, R. M. and C. L. Christ, Solutions, Minerals and Equilibria, Harper & Row, New York, (1965).

5-10 Harker, R. I. and O. F. Tuttle, "Studies in the System CaO-MgO-CO_2, Part 1, The Thermal Dissociation of Calcite, Dolomite and Magnesite," Amer. Jour. Sci., V253, p. 209, (1955).

5-11 Smyth, F. H. and L. H. Adams, "The System, Calcium Oxide - Carbon Dioxide," Jour. of the Amer. Chem. Society, V. 45, p. 1167, (1923).

5-12 Tuttle, O. F. and N. L. Bowen, "Origin of Granite in the Light of Experimental Studies in the System $NaAlSi_3O_8$ - $KAlSi_3O_8$-SiO_2-H_2O," Geol. Soc. of Amer. Memoir 74, (1958).

5-13 Simpson, B. R. and John H. Fergus, Jr., "The Effect of Water on the Compressive Strength of Diabase," Jour. of Geophysical Res., V. 73, No. 20, (1968).

5-14 George, W. O., "The Relation of the Physical Properties of Natural Glasses to their Chemical Composition," Jour. of Geology, V. 32, No. 5, (1924).

5-15 Manger, G. E., "Porosity and Bulk Density of Rocks," U. S. Geol. Survey Bulletin 1144-E, (1963).

5-16 Daly, R. A., G. E. Manger, and S. P. Clark, Jr., "Density of Rocks," Geol. Soc. of Amer. Memoir 97, S. P. Clark, Jr., Editor, (1966).

5-17 Davis, S. N. and R. J. M. DeWiest, Hydrogeology, John Wiley & Sons, (1966).

5-18 Krumbein, W. C. and L. L. Sloss, Stratigraphy and Sedimentation, W. H. Freeman & Co., (1963).

5-19 Lindroth, D. P., and W. G. Krawza, Heat Content and Specific Heat for Six Rock Types at Temperatures to 1000°C, U. S. Bur. of Mines, RI 7503, (1971).

5-20 Goranson, R. W., "Heat Capacity; Heat of Fusion," Geol. Soc. of Amer. Special Paper 36, F. Birch, J. F. Schairer, and H. C. Spicer, Editors, (1942).

5-21 Clark, S. P., Jr., "Thermal Conductivity," Geol. Soc. of Amer. Memoir 97, S. P. Clark, Jr., Editor, (1966).

5-22 Murase, T. and A. R. McBirnery, "Thermal Conductivity of Lunar and Terrestrial Igneous Rocks in Their Melting Range," Science, Vol. 170, (1970), pp 165-167.

5-23 Somerton, W. H., "Some Thermal Characteristics of Porous Rocks," Jour. of Petroleum Technology, V. 10, No. 5, (1958), p. 61.

5-24 Bean, R. J., "Relation of Gravity Anomalies to the Geology of Central Vermont and New Hampshire," Bull. Geol. Soc. of Amer, V. 64, (1953), pp. 509-538.

5-25 Clark, S. P. Jr., "Heat Flow in the Austrian Alps," Geophysical Journal of the Royal Astronomical Society, V. 6, No. 1, (1961), pp. 54-63.

5-26 Eaton, G. P. and J. L. Rosenfeld, "Gravimetric and Structural Investigations in Central Connecticut," Report of the Twenty-First Session, Norden - Part II, Geological Results of Applied Geochemistry and Geophysics. (International Geological Congress, Copenhagen), (1960).

5-27 Bacon, J. S., S. Russel and J. P. Carstens, "Determination of Rock Thermal Properties," Report of U. S. Bureau of Mines Contract No. H0220052, sponsored by Advanced Research Projects Agency, ARPA Order No. 1579, Amendment 3 (Program Code 62701 D), (1973).

5-28 Birch, F. and E. B. Dane, Jr., "Viscosity," Geol. Soc. of Amer. Special Paper 36, F. Birch, J. F. Schairer, and H. C. Spicer, Editors, (1942).

5-29 Clark, S. P. Jr., "Viscosity," Geol. Soc. of Amer. Memoir 97, S. P. Clark, Jr., Editor, (1966).

5-30 Roedder, Edwin, "Silicate Melt Systems," Physics and Chemistry of the Earth, V. 3, Pergamon Press, (1959).

5-31 Schairer, J. F., "The System CaO-FeO-Al_2O_2-SiO_2: I. Results of Quenching Experiments on Five Joints," J. Amer. Ceramic Soc., 25, (1942), pp. 241-274.

5-32 Levin, E. M., H. F. McMurdie, and F. P. Hall, "Phase Diagrams for Ceramists," Amer. Ceramic Soc., Columbus, Ohio, (1956).

5-33 Levin, E. M., and H. F. McMurdie, "Phase Diagrams for Ceramists - Part II," Amer. Ceramic Soc., Columbus, Ohio, (1959).

5-34 Skinner, B. J., "Thermal Expansion," Geol. Soc. Amer. Memoir 97, S. P. Clark, Jr., Editor, (1966).

5-35 Todd, D. K., Ground Water Hydrology, John Wiley & Sons, Inc., (1959).

5-36 Collins, W. D., "Temperature of Water Available for Industrial Use in the United States," U. S. Geological Survey Water-Supply Paper 520-F, (1925).

5-37 Clark, S. P., Jr., "Solubility," Geol. Soc. Amer. Memoir 97, S. P. Clark, Jr. Editor, (1966).

5-38 Birch, F., "Elasticity, Except Compressibility," Geol. Soc. of Amer. Special Paper 36, F. Birch, J. F. Schairer and H. C. Spicer, Editors, (1942).

5-39 Birch, F., "Compressibility, Elastic Constants," Geol. Soc. of Amer. Memoir 97, S. P. Clark, Jr., Editor, (1966).

5-40 Haimson, B. and C. Fairhurst, "In-Situ Stress Determination at Great Depth by Means of Hydraulic Fracturing," Rock Mechanics - Theory and Practice, Proc. Eleventh Symposium on Rock Mechanics held at the University of California, Berkeley, California, Society of Mining Engineers (1970).

5-41 Coon, R. F. and A. H. Merritt, "Predicting In Situ Modulus of Deformation of Rock," ASTM STP 477, American Society for Testing and Materials, (1970), pp. 154-173.

5-42 Deere, D. U., A. J. Hendron, Jr., F. D. Patton, and E. J. Cording, "Design of Surface and Near-Surface Construction in Rock," Failure and Breakage of Rock, Proc. Eighth Symposium on Rock Mechanics held at the University of Minnesota, C. Fairhurst, Editor, (1967).

6.0 THERMAL POWER

In the design of a subterrene tunneler, it is important to know the power requirements of the tunneling operation. It was recognized that the power requirement is a function of a large number of controlling variables that include subterrene geometry, size, rate of penetration and earth/rock physical properties. With this knowledge, an appropriate heat source can be selected and the economics of the design can then be evaluated. This section presents the derivations of the functional relations of controlling variables that permit the evaluation of the thermal power requirements. Verifications of the functional relations are shown through correlations with experimental and calculated data. Results of scoping analyses performed are presented and discussed.

Functional relations have been developed for the calculation of thermal power requirements for all five modes of tunneling. These relations have been verified through significant correlations with experimental and calculated data (overall mean deviation = -3.9%). Scoping calculations have delineated the limitations and capabilities of existing penetrator designs. To extend the capabilities of the basic concepts to higher rates of penetration and large tunnelers, a high performance design is proposed.

The total power required in a subterrene tunneling operatin, P_T, consists of a number of components. These include the total thermal power required (Q_T), power to overcome thrust loads (P_L), power to induce lithofracture (P_F), if lithofracture is desired, power to force molten earth/rock into the cracks formed by lithofracture (P_M), power required for excavation (P_E) and power required for life support (P_S):

$$P_T = Q_T + P_L + P_F + P_M + P_E + P_S \qquad (6\text{-}1)$$

Lithofracture may not be a desirable phenomenon for the formation of transportation tunnels because of the potential detrimental effect on the environment and because of the unpredictability of the phenomenon. The power required for excavation can be readily determined from conventional excavation practice, while the power required for life support is expected to be small and it can be readily estimated. For the above reasons, only the first two components of the various power requirements are treated here. The actual power required to overcome thrust loads is expected to be small and it is not nearly as important as the magnitude of the thrust load itself. However, it is included for the sake of completeness. Thrust loads are discussed separately in Section 7.0.

The total thermal power requirement, Q_T, can be separated into a number of components. These are the sensible heat (power to heat the earth/rock from the initial temperature up to the melting point) (q_s), the melt superheat (q_{su}), the fusion power (q_f), the heat losses to the ambient earth/rock (q_l), and the stem losses, axial conduction losses through the penetrator structure (q_a), i.e.,

$$Q_T = q_s + q_{su} + q_f + q_l + q_a \qquad (6\text{-}2)$$

Each one of these terms is a function of a number of variables that control the tunneling process. The approach used to develop functional relations of the controlling variables is discussed in the following sections.

6.1 DERIVATION OF THERMAL POWER FUNCTIONAL RELATIONS

6.1.1 Analytical Model Considerations

The motion of a rock melting subterrene tunneler through a mass of earth/rock is basically the classical problem of a moving heat source with the added complexity of phase change. Moving heat source problems have been solved for point and line sources in connection with applications to welding, extrusion, plane hardening, quenching and motion of a projectile through a gun barrel.[6-1, 6-2] These solutions, however are not applicable to the finite

sizes (up to ~ 9 meters or 30 feet in diameter) of the subterrene penetrators to be considered here. Nevertheless, the same basic approaches can be adopted.

The general partial differential equation describing the temperature field around a moving heat source can be used as a starting point. If one takes the viewpoint of an observer moving with the subterrene tunneler at a constant velocity, two potential models may be considered: One is the penetrator moving through the molten earth/rock, while the second considers the molten layer to be an integral part of the penetrator moving through unmolten earth/rock. The latter model has significant advantages. They are the following:

- The problem of non-uniform material properties between the melt and the earth/rock is eliminated.
- The problem of identifying various time-dependent thermal power components such as melt superheat, fusion power, and heat losses is eliminated, so that a steady state model results.
- The problem reduces simply to one of condution; (viscous flow effects can be ignored).

For these reasons, the latter model is adopted. It is evident that such a model can only permit the determination of the sensible heating of the earth/rock (q_s) and the heat loss to the ambient earth/rock (q_l). The other thermal power components, however, can be evaluated separately.

The general three-dimensional conduction equation is:

$$\frac{\partial T}{\partial t} = \alpha \left(\frac{\partial^2 T}{\partial x^2} + \frac{\partial^2 T}{\partial y^2} + \frac{\partial^2 T}{\partial z^2} \right) \qquad (6\text{-}3)$$

where α = the thermal diffusivity of the earth/rock

$$\alpha = \frac{k}{\rho_e C_p} \qquad (6\text{-}4)$$

where k is the earth/rock thermal conductivity, ρ_e is the density and C_p is the heat capacity. Following Jakob (6-4), a moving coordinate system can be adopted by setting:

$$\xi = x - U_\infty t \tag{6-5}$$

where U_∞ is the steady state rate of motion of the penetrator.

Equation (6-3) then transforms to the following equation:

$$-U_\infty \frac{\partial T}{\partial \xi} + \frac{\partial T}{\partial t} = \alpha \left(\frac{\partial^2 T}{\partial \xi^2} + \frac{\partial^2 T}{\partial y^2} + \frac{\partial^2 T}{\partial z^2} \right) \tag{6-6}$$

By taking the viewpoint of an observer moving with the subterrene tunneler at a steady state rate U_∞, the temperatures surrounding the tunneler will appear to reach steady-state, so that one may set $\partial T / \partial t = 0$. The result is an equation of the quasi-stationary state:

$$\left(\frac{\partial^2 T}{\partial \xi^2} + \frac{\partial^2 T}{\partial y^2} + \frac{\partial^2 T}{\partial z^2} \right) = - \frac{U_\infty}{\alpha} \frac{\partial T}{\partial \xi} \tag{6-7}$$

To solve this equation, three physical models were considered:

1. A hemispherical heat source moving along with a layer of molten material, moving through unmolten earth/rock.
2. A circular planer heat source moving along with the molten material through unmolten earth/rock.
3. A cylindrical heat source moving with a layer of molten material through unmolten earth/rock.

Physical model 1 was adopted to simulate a consolidating conical penetrator of the type tested at the Los Alamos Scientific Laboratory and designated as Mode 1. Models 2 and 3 were adopted to simulate extruders of various types used in Modes 2 to 5. In particular,

model 2 permits the calculation of sensible heat requirements in Modes 1 to 5, while model 3 allows the determination of heat losses to earth/rock through the cylindrical sides of penetrators in Modes 2 to 5. These models are summarized in Figure 6-1.

6.1.2 Moving Hemispherical Penetrators

Equation (6-7) can be written in terms of a temperature excess variable ψ such that

$$\psi = T - T_\infty \tag{6-8}$$

where T_∞ is the ambient, undisturbed earth/rock temperature. Equation (6-7) then becomes

$$\frac{\partial^2 \psi}{\partial \xi^2} + \frac{\partial^2 \psi}{\partial y^2} + \frac{\partial^2 \psi}{\partial z^2} = -\frac{U_\infty}{\alpha} \frac{\partial \psi}{\partial \xi} \tag{6-9}$$

In order to obtain a closed-form analytic solution, the thermal diffusivity is taken as a constant in space and time. This is reasonable for the physical models chosen because below the melting point of earth/rock, the effective thermal conductivity of some earth/rock materials and the density do not change appreciably with temperature.

Equation (6-7) has a solution of the form.

$$\psi = e^{-\left(\frac{U_\infty \xi}{2\alpha}\right)} \phi(\xi, y, z) \tag{6-10}$$

where $\phi(\xi, y, z)$ is an unknown function to be solved. Substituting this into Equation (6-8) yields the following partial differential equation:

$$\frac{\partial^2 \phi}{\partial \xi^2} + \frac{\partial^2 \phi}{\partial y^2} + \frac{\partial^2 \phi}{\partial z^2} - \left(\frac{U_\infty}{2\alpha}\right)^2 \phi = 0 \tag{6-11}$$

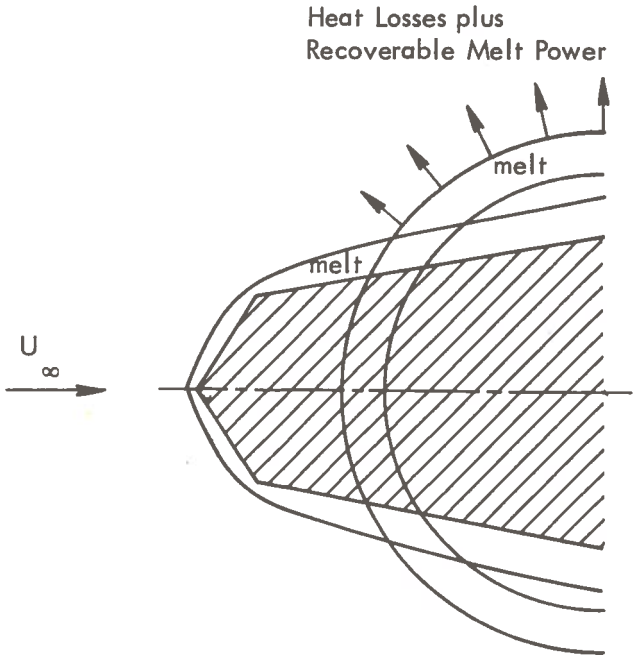

Moving hemispherical heat source, moving with the melt, to simulate conical penetrators in Mode 1 tunneling.

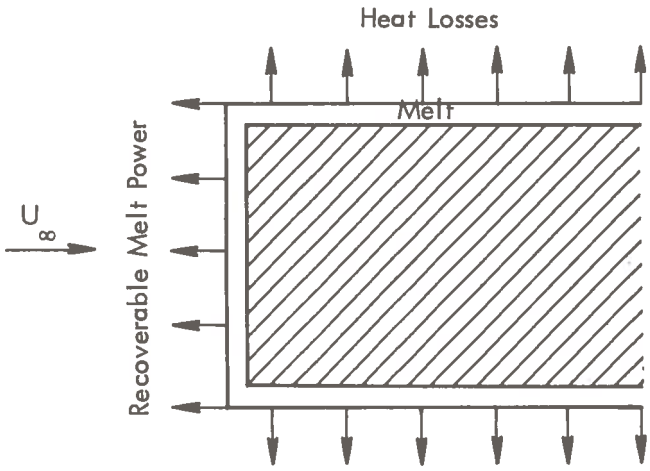

Moving cylindrical heat source, moving with the melt to simulate tunneling Modes 2, 3, 4, and 5.

Figure 6-1. Schematic Diagrams of Physical Models for Thermal Analyses of Various Modes of Tunneling

This auxiliary equation can be written in terms of the variable r, where

$$r = \sqrt{\xi^2 + y^2 + z^2} \tag{6-12}$$

so that Equation(6-11) transforms into the ordinary differential equation

$$\frac{d^2 \phi}{dr^2} + \frac{2}{r} \frac{d\phi}{dr} - \left(\frac{U_\infty}{2\alpha} \right)^2 \phi = 0 \tag{6-13}$$

In this model, the isothermal surfaces depend on r above. The boundary conditions are the following:

$$\psi = 0 \quad \text{when } r \longrightarrow \infty \tag{6-14}$$

$$\frac{\partial \psi}{\partial r} = \frac{q}{4 \pi k r^2} \quad \text{for } r = r_B \tag{6-15}$$

In addition, $T = T_m$ at $r = r_B$ (6-16)

where T_m is the melting point of the earth/rock, and r_B is the radius of the penetrator plus the melt thickness

$$r_B = r_p + \delta \tag{6-17}$$

and q is the rate of heat flow from the surface of the isotherm (at $r = r_B$) corresponding to the melting point T_m. Solution to Equation 6-11 with the boundary conditions 6-12 to (6-14) yields the following equation for the heat flow from the melt interface of a hemispherical penetrator.

$$q = \pi r_B^2 \rho_e C_p U_\infty (T_m - T_\infty) + 2 \pi k r_B (T_m - T_\infty) \tag{6-18}$$

This solution has two terms. The first is clearly the heat transferred to earth/rock to heat it from the initial temperature T_∞ up to the melting point; hence this is the sensible heat term, q_s. The second term is independent of the rate of penetration; it predicts that the heat loss to the earth/rock is a constant, independent of the rate of penetration, but directly proportional to the size of the penetrator ($r_B = r_p + \delta$) and the effective thermal conductivity of the earth/rock. Other heat transfer components such as melt superheat will be developed separately.

6.1.3 Moving Planar Heat Source

The basic partial differential Equation(6-9)given in the previous section can be used as a starting point. The planar heat source surface is the melt-earth/rock interface defined by $\xi = 0$.

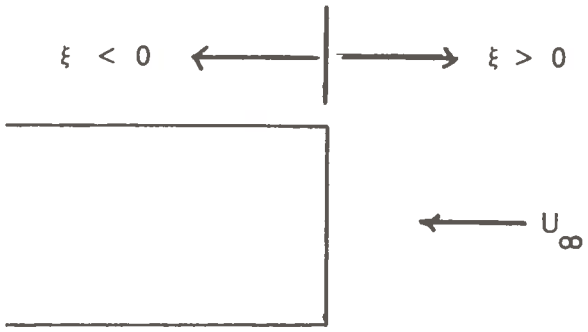

The heat is considered to flow in the ξ direction only; hence,

$$\frac{\partial \phi}{\partial y} = 0 \quad \text{and} \quad \frac{\partial \phi}{\partial z} = 0 \tag{6-19}$$

Equation 6-9 then reduces to

$$\frac{d^2 \phi}{d\xi^2} - \left(\frac{U_\infty}{2\alpha} \right)^2 \phi = 0 \tag{6-20}$$

The boundary conditions for this model are the following:

$$\psi = 0 \quad \text{or} \quad \frac{d\psi}{d\xi} = 0 \quad \text{for} \quad \xi = \pm\infty \tag{6-21}$$

$$-k \frac{d\psi}{d\xi} = q' \quad \text{for} \quad \xi = 0 \tag{6-22}$$

$$\text{or} \quad q' = \frac{q}{\pi r_B^2} = -k \frac{d\psi}{d\xi} \tag{6-23}$$

A solution to Equation 6-18 with the given boundary conditions yields the following equation for heat flow from the moving circular planar heat source:

$$q_s = \pi r_B^2 \rho_e C_p U_\infty (T_m - T_\infty) \tag{6-24}$$

It is apparent that, physically, Equation (6-24) represents the heat flow required for the sensible heating of the earth/rock for a penetrator-plus-liner radius r_B. Heat losses are not accounted for in this model. To estimate the heat losses, the following moving cylindrical heat source model is considered.

6.1.4 Moving Cylindrical Heat Source

For a cylindrical moving heat source with radial heat flow only, one can assume $\partial\psi/\partial z = 0$. Equation (6-1), written in cylindrical coordinates, becomes

$$\frac{\partial^2 \phi}{\partial r^2} + \frac{1}{r} \frac{\partial \phi}{\partial r} - \left(\frac{U_\infty}{2\alpha}\right)^2 \phi = 0 \tag{6-25}$$

The boundary conditions of the problem are the following:

$$\frac{\partial \psi}{\partial r} = 0 \quad \text{as} \quad r \longrightarrow \infty \tag{6-26}$$

$$-2 \pi kr \frac{\partial \psi}{\partial r} = q \quad \text{at} \quad r = r_B \tag{6-27}$$

$$\psi = 0 \quad \text{as} \quad r \longrightarrow \infty \tag{6-28}$$

The heat flow from the cylindrical surface of this model provides yet another boundary condition, i.e.,

$$\frac{\partial T}{\partial r} = - \frac{q}{2 \pi kr L_H} \quad \text{at} \quad r = r_B \tag{6-29}$$

where L_H is the length of the heated section. Solution of Equation (6-23) with the boundary conditions (6-24) to (6-27) yields the heat loss equation

$$q_l = \pi r_B U_\infty L_H \rho_e C_p (T_m - T_\infty)$$

$$+ \frac{2 \pi (r_p + \delta) L_H}{2 (r_p + \delta)} k_{eff} (T_m - T_\infty) \tag{6-30}$$

This equation suggests that heat loss from the cylindrical surface of a penetrator consists of two components: One is independent of the rate of penetrator advance, while the other is directly proportional to the rate of advance. This is reasonable because with zero rate of penetration, the mathematical model of a quasi-steady situation no longer holds true. With zero rate of penetration, there is a transient phenonenon where the earth/rock is

heated up continuously to ever higher temperatures and the heat source power output is mostly lost to the ambient earth/rock material. However, there does occure in time a situation where a thickness δ of the earth/rock surrounding the penetrator is molten. The thermal power required at this time is essentially that predicted by the second term in Equation (6-30).

Examination of the first term in Equation (6-30) suggests that it has physical meaning only if one considers L_H to be the depth to which the earth/rock is heated. Hence, for this term L_H is replaced by δ_e, where δ_e is now dependent on the earth/rock material, whereas, L_H should be independent of earth/rock materials. The first is expected to be a more realistic representation of the actual phenomenon. The second is simply the one dimensional conduction equation. It is interesting to note that for "static" heat loss, the model predicts that the effective conduction path length is effectively the diameter of the penetrator plus the liner.

For cylindrical penetrators, Equations (6-24)and (6-30) give the sensible heat and heat loss components, respectively. The fusion power and melt superheat terms are still to be determined.

6.1.5 Fusion Power

The fusion power is simply the rate at which the mass of earth/rock is melted times the latent heat of fusion (λ). This is simply given by the relation

$$q_f = \pi r_B^2 \rho_e U_\infty \lambda \qquad (6\text{-}31)$$

6.1.6 Melt Superheat

The melt superheat is the thermal power required to heat the melt from its melting point to the penetrator surface temperature. It is important to have a reasonably good estimate

of the melt superheat because, (1) it can contribute a significant fraction of the total melt power, and (2) the effective thermal conductivity of the melt increases sharply with temperature. To consider the factors that affect the melt superheat, reference is made to Figure 6-2, where the melt flow over a conical, consolidating penetrator is illustrated. It is noted in the figure that the total heat transfer rate from the surface of the penetrator consists of sensible heat (q_s) heat losses ($q_{l,d} + q_{l,s}$), melt superheat (q_{su}) and heat of fusion (q_f). However, the heat transfer across the melt-earth/rock interface consists of sensible heat and heat losses only. The heat of fusion is "consumed" at the melt interface while the superheat is "consumed" near the penetrator surface. Estimates showed that in general, the melt superheat is on the same order of magnitude as the fusion heat. Because of these facts, one can reasonably make the following important assumptions:

1. Only the sensible heat, heat of fusion, and heat losses establish the ΔT across the melt.
2. The heat flux is uniform from the heated penetrator surface.
3. The maximum penetrator surface temperature (and hence the maximum melt superheat) is associated with the fully developed glass liner thickness which occurs at the shoulder of the penetrator.
4. The mean melt superheat is a fraction of the maximum melt superheat, i.e. $\overline{T_s - T_m} = \gamma\,(T_{s,\max} - T_m)$ where γ is to be determined empirically.
5. The melt thermal conductivity is proportional to the temperature to the fourth power, i.e.

$$k_m = \beta\,(T/1000)^4 \qquad (6\text{-}32)$$

where β is an empirical constant.

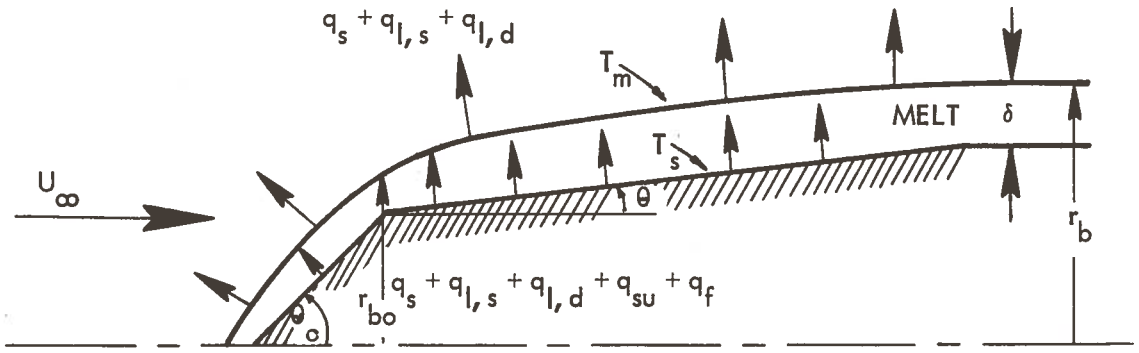

Figure 6-2. Model for Determination of Mean and Maximum Penetrator Surface Temperature - Mode 1 Tunneling

It is known that for the conical penetrator, the penetrator surface temperature is not uniform. This is due to varying melt thickness and stem losses which cause an appreciable axial temperature gradient in the penetrator.[6-5] Nevertheless, the heat flux can be unidorm across the penetrator surface. Because of stem losses, the maximum penetrator surface temperature is not expected near the shoulder of the penetrator, rather it is somewhat upstream of the shoulder. However, assumption 3 is a clos approximation. Assumption 4 is based on detailed thermal analyses reported in Reference (6-5), which may not apply under all conditions. Assumption 5 is reasonable in view of the significant contribution of thermal radiation to total heat transfer at temperatures above the melting point.

With the above assumptions, the melt superheat at any point along the surface of the penetrator is given by the simple one dimensional conduction equation

$$q = q_s + q_f + q_l = \frac{\overline{k}_m A_p}{L} (T_s - T_m) \qquad (6\text{-}33)$$

where L is the local melt thickness, $\overline{k}_m$ is the local mean melt effective thermal conductivity. At the shoulder of the penetrator, $L = \delta$ and $T_s = T_{s,max}$. The mean effective thermal conductivity can be defined by the equation

$$\overline{k}_m = \frac{\beta \int_{T_m}^{T_s} T^4 dt}{\int_{T_m}^{T_s} dT} \qquad (6\text{-}34)$$

Based on Equations (6-32) and (6-33), the maximum penetrator surface temperature is given by

$$T_{s,\,max} = \sqrt[5]{T_m^{\,5} + \frac{5\,\delta}{\beta}\left(\frac{q_s + q_f + q_l}{A_p}\right)} \qquad (6\text{-}35)$$

With this equation, the mean melt superheat, $\overline{T_s - T_m}$, can be evaluated, i.e.

$$\overline{T_s - T_m} = \gamma\,(T_{s,\,max} - T_m)$$

or

$$\overline{T_s - T_m} = \gamma\left[\sqrt[5]{T_m^{\,5} + \frac{5\,\delta}{\beta}\left(\frac{q_s + q_f + q_l}{A_p}\right)} - T_m\right] \qquad (6\text{-}36)$$

Equation (6-36) can therefore be used to estimate the melt superheat power, q_{su}, i.e.,

$$q_{su} = \pi\, r_B^{\,2}\, \rho_e\, U_\infty\, \overline{C_m}\, (\overline{T_s - T_m}) \qquad (6\text{-}37)$$

where $\overline{C_m}$ is the mean specific heat of the melt.

6.1.7 Summary of Equations

The total thermal power requirement, Q_T, can now be evaluated by summing the various contributing components. The complete equations for the two thermal models are summarized in Table 6-1.

TABLE 6-1

MATHEMATICAL MODELS OF THERMAL POWER
REQUIREMENTS FOR THERMAL TUNNELING

HEMISPHERICAL MODEL, MELT MOVING WITH PENETRATOR (APPLIES TO CONICAL PENETRATORS)

Total Thermal Power	=	"Static" Heat Loss	+	"Dynamic" Heat Loss	+	Sensible Heat	+	Superheat	+	Fusion Power	+	Stem Losses
Q_T		$q_{l,s}$	+	$q_{l,d}$	+	q_s		q_{su}		q_f	+	q_a
Q_T	=	$2\pi k_{eff}(r_p+\delta)(T_m-T_\infty)$			+	$\pi(r_p+\delta)^2 \rho_e U[C_p(T_m-T_\infty)$	+	$\overline{C}_m(\overline{T_s-T_m})$	+	$\lambda]$	+	q_a

CYLINDRICAL MODEL, MELT MOVING WITH PENETRATOR

$$Q_T = \pi k_{eff} L_H (T_m - T_\infty) + 2\pi(r_p+\delta)\delta_e \rho_e \overline{C}_p U (T_m - T_\infty) + \pi(r_p+\delta)^2 \rho_e U[C_p(T_m-T_\infty) + \overline{C}_m(\overline{T_s-T_m}) + \lambda] + q_a$$

k_{eff}, Effective Thermal Conductivity of Unmolten Earth/Rock Outside Melt Zone

6.2 VERIFICATION OF FUNCTIONAL RELATIONS

6.2.1 Available Data

In order to verify the functional relations developed, experimental data on the various thermal power components are needed in addition to the total power requirement. Unfortunately, carefully controlled experiments of the type needed do not exist; only one set of experimental data, obtained from a 50 mm penetrator in a single earth material (tuff), is available.[6-6] Moreover, only heat losses and melt power components were determined. The latter includes fusion power and melt superheat.

It was recognized that this would be inadequate for the verification of the functional relations developed and for extrapolation of the relations to other materials, other penetrator geometries and larger penetrator sizes. Consequently, data from detailed thermal analyses (using AYER code) carried out at the Los Alamos Scientific Laboratory* were also used extensively to check the validity of the functional relations. A description of the AYER code and the penetrator models used in the calculation is provided as follows:

Description of Ayer Code and Penetrator Models:

- Code provides implicit solutions of the general two-dimensional equation of heat conduction by finite element, numerical method.
- Code includes effects of time and velocity distributions.
- Model consists of penetrator moving with the melt through solid earth/rock.
- Model allows relatively arbitrary geometries within the constraint of axisymmetry.
- The following can be calculated:
  - Sensible heating of on-coming earth/rock
  - Heat losses to rock
- The following cannot be calculated:
  - Melt superheat and penetrator surface temperatures
  - Fusion power requirements

---

* Calculations were performed by G. E. Cort, Westinghouse Astronuclear Laboratory Staff Member on assignment at LASL.

While the AYER code is useful for detailed design calculations of specific penetrator geometries, penetrator sizes, tunneling through specific earth/rock materials at specified rates, it is relatively tedious, time consuming and costly to use. In addition, the code and model calculates only sensible heat requirements and heat losses; fusion power and sensible heat have to be calculated separately.

The functional relations derived in this study provide explicit calculations of total thermal power requirements in terms of key controlling parameters. They are useful for parametric design analyses and conceptual penetrator design calculations. The available experimental and AYER calculated thermal power data are summarized in Table 6-2. Together, they cover a wide range of conditions, conditions that may be encountered in transportation tunneling applications.

6.2.2 Correlation with Experimental Data

A single set of experimental data was obtained with a 50 mm conical consolidating penetrator melting through tuff, under both laboratory and field test conditions. The rate of penetration and the total thermal power were measured, while stem losses were obtained by static calibration. The melt power ($q_s + q_{su} + q_f$) was estimated so that the heat losses in turn can be estimated. The heat loss data are compared with those calculated by the two different models in Figure 6-3. The physical properties used for calculating the heat losses are those for tuff, given in Table 6-3. It is evident from the figure that there is considerable scatter in the heat loss "data" without a discernible trend. This is due to the approximations used in estimating the melt power, and the heat loss was rounded up to the nearest 100 watts.* It can be concluded that in the range of rates of penetration, both models appear to give gross levels of the data.

---

*See Reference (6-6), p. 9

TABLE 6-2

AVAILABLE DATA FOR VERIFICATION OF DERIVED FUNCTIONAL RELATIONS

Thermal Power

- Experimental 50 mm conical penetrators in tuff, heat losses and total melt power data.
- Experimental 75 mm conical penetrators in tuff, tatal thermal power only.
- AYER calculated data:
  - 50 mm conical penetrator in tuff and basalt, heat losses and rock sensible heat components only
  - 600 mm conical penetrator in tuff and basalt, heat losses and rock sensible neat components only
  - 10-foot and 30-foot conical penetrators in tuff and basalt, heat losses and rock sensible heat components only
  - 5.1 cm, 6.5 cm, 12 cm, 2 foot, and 30 foot cylindrical penetrators in tuff and basalt, heat losses and rock sensible heat components only

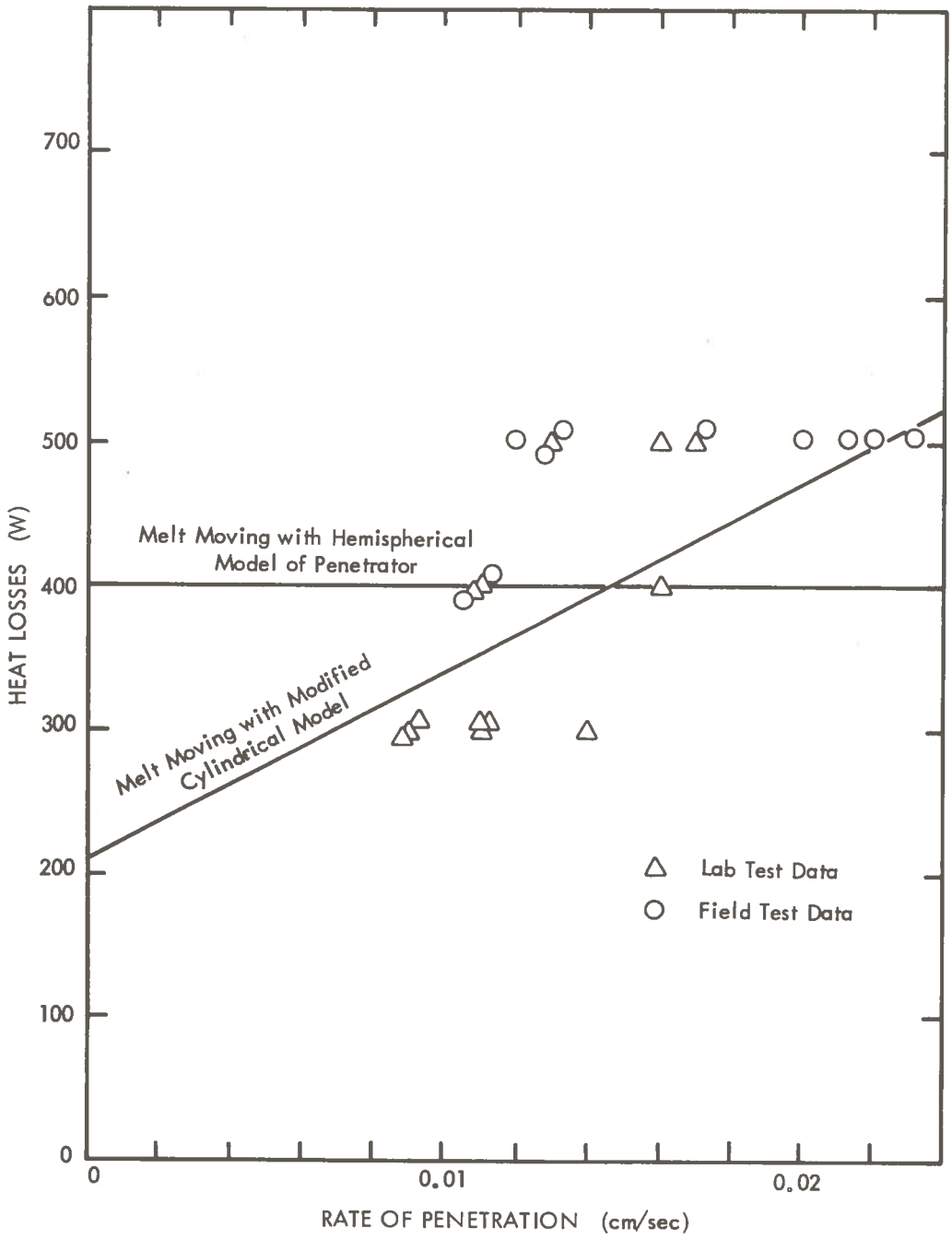

Figure 6-3. Comparison of Observed and Calculated Heat Losses for Different Penetrator Models 50 mm Conical Penetrator in Tuff Full Consolidation - Mode 1 Tunneling

TABLE 6-3

PHYSICAL PROPERTIES OF VARIOUS EARTH/ROCK MATERIALS USED IN THIS STUDY

Earth Model	T_m, °K	ρ_e, gm/cc	ρ_g, gm/cc	C_p, $\frac{W\text{-sec}}{gm\text{-}^oK}$	λ, $\frac{W\text{-sec}}{gm}$	k_m, W/cm · °K	μ_m, poises
Tuff (Bandilier)	1420*	1.4*	2.5*	1.01**	420**	4.6×10^{-3}**	4.3×10^{7}*
Basalt	1420+	2.8+	2.8**	1.01+	420+	1.1×10^{-2}**	5×10^{4}×
UNCON	1500	1.5	2.3	1.15	244	4×10^{-3}	10^{17}
SOSED	1400	2.3	2.3	1.14	307	1.1×10^{-2}	10^{7}
MASIG	1500	2.8	2.5	1.13	370	2.1×10^{-2}	10^{6}
FOLIA	1450	2.7	2.4	1.13	370	2.2×10^{-2}	10^{6}

* See Reference 6-6

\+ See Reference 6-10

× See Reference 6-11

** See Reference 6-7

Further verification of the functional relations will require predictions of the mean melt superheat $\overline{T_s - T_m}$ and the melt power. These can now be calculated by the techniques and equations developed in Section 6.1.6. The constant β in Equation 6-32 was determined to be 0.46×10^{-2} W/cm - °K at the tuff melting point. The calculated mean melt superheat is compared with one datum point obtained by a detailed thermal analysis in Reference (6-5). A comparison of the two yields a value of 0.8 for the coefficient γ. This is shown in Figure 6-4. With this coefficient, assumed to be constant under all conditions, the melt superheat and melt power can be estimated under all conditions. Results are presented in Figure 6-5 for the 50 mm consolidating penetrator. It can be seen from Figure 6-5 that the model and assumptions used to calculate melt superheat show that the maximum penetrator surface temperature and the maximum melt superheat increase with increasing rates of penetration. This is in qualitative agreement with experimental observations where it had been noted,[6-7] that for a given penetrator design, there is an upper limit on the rate of penetration above which the penetrator would fail as a result of penetrator deformation (due to melting and excessive stress). For the 2-inch (50 mm) molybdenum conical penetrator operating in tuff, the upper limit was estimated at 0.03 cm/sec[6-7]. A temperature of 1928°K, or 2/3 of the melting point of molybdenum is shown in Figure 6-5 as an approximate upper temperature limit and as a convenient reference point.

6.2.3 Melt Power Data

The total melt power (q_m) is the sum of earth/rock sensible heat, heat of fusion, and melt superheat. It can now be calculated from the equation

$$q_m = \pi (r_p + \delta)^2 \rho_e U_\infty \left[\overline{C_p} (T_m - T_\infty) + \overline{C_m} (T_s - T_m) + \lambda \right]$$

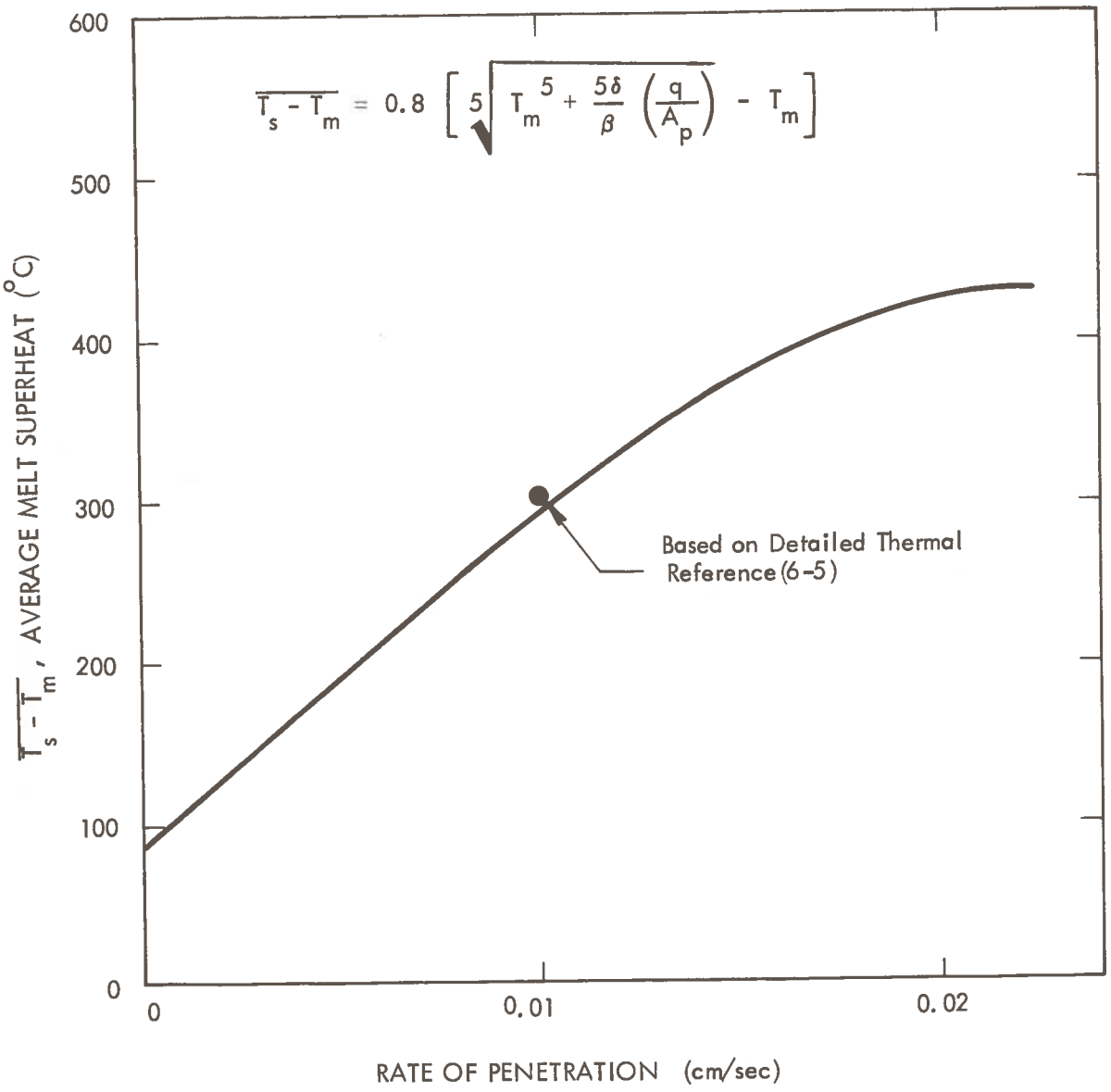

Figure 6-4. Effect of Rate of Penetration on Average Melt Superheat for 55 mm Conical Penetrator in Mode 1 Tunneling Through Tuff

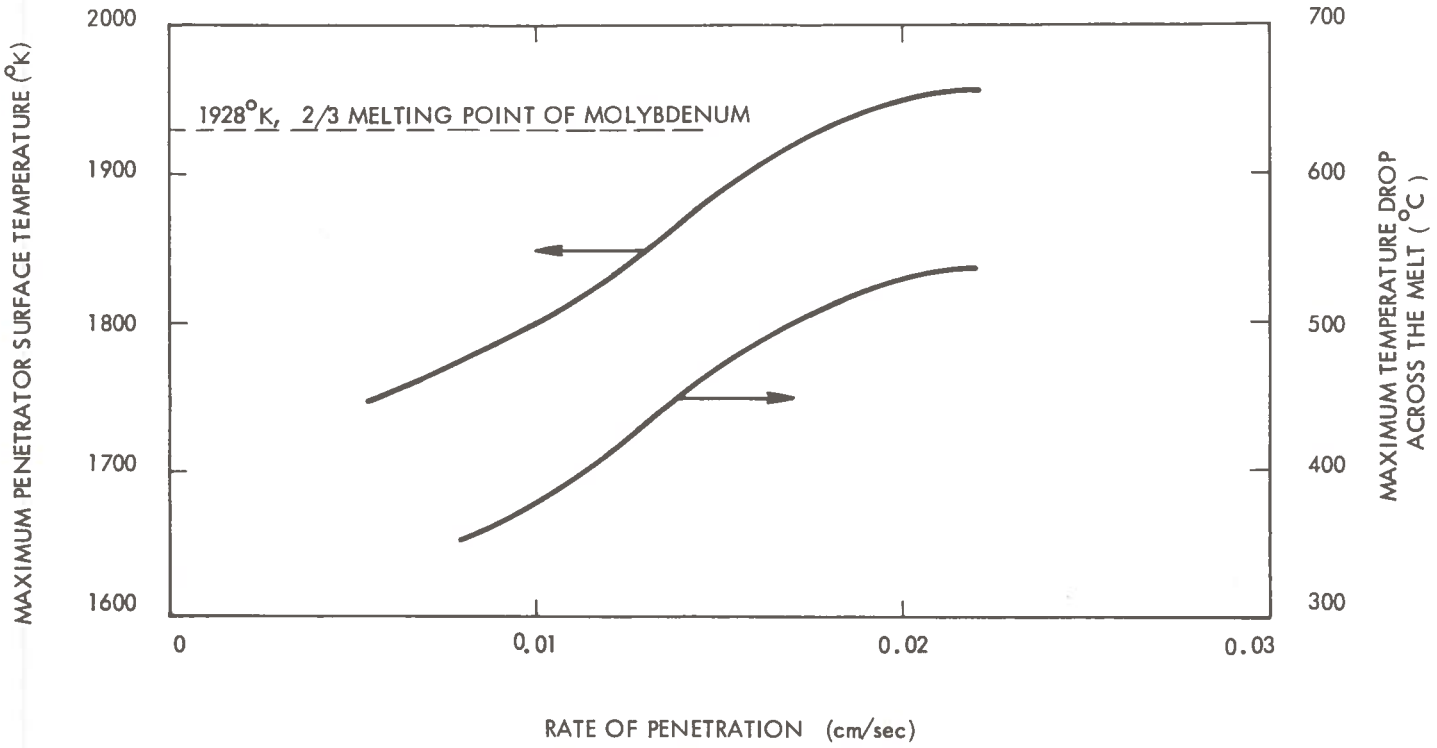

Figure 6-5. Effect of Rate of Penetration on Maximum Penetrator Surface Temperature and Temperature Drop Across the Melt for 50 mm Full Consolidation Conical Penetrators in Tuff

Note that this equation is identical for either the hemispherical or the cylindrical heat source model. The calculated melt power over a range of rates of penetration is compared in Figure 6-6. with the one set of laboratory and field test data. It is evident that there is a good correlation with the data. With the exception of one data point, the deviations are in general well within the errors expected as a result of the gross assumptions used in arriving at the melt power data. In particular, it should be noted that the analytical solutions predict slightly greater than a linear increase in total melt power with increasing rate of penetration. This is also in good agreement with the general trend of the data.

6.2.4. Total Thermal Power (Excluding Stem Losses)

It was evident that the hemispherical model is limited in its application. On the other hand, the cylindrical model cannot represent a conical penetrator. Consequently, a geometric factor was developed for the cylindrical model to permit its generalization to conical penetrators as well. It was obvious that penetrator geometry affects only the heat loss. By empirical correlation with experimental and AYER calculated heat loss data, the following geometric factor, ψ, was developed:

$$\psi = r_{Bo} \sin \theta_o + r_B \sin \theta \qquad (6\text{-}38)$$

where r_{Bo}, r_B and the angles refer to the specific conical penetrator design tested by LASL. These are identified in Figure 6-2. The generalized semi-empirical equation for thermal power is the following:

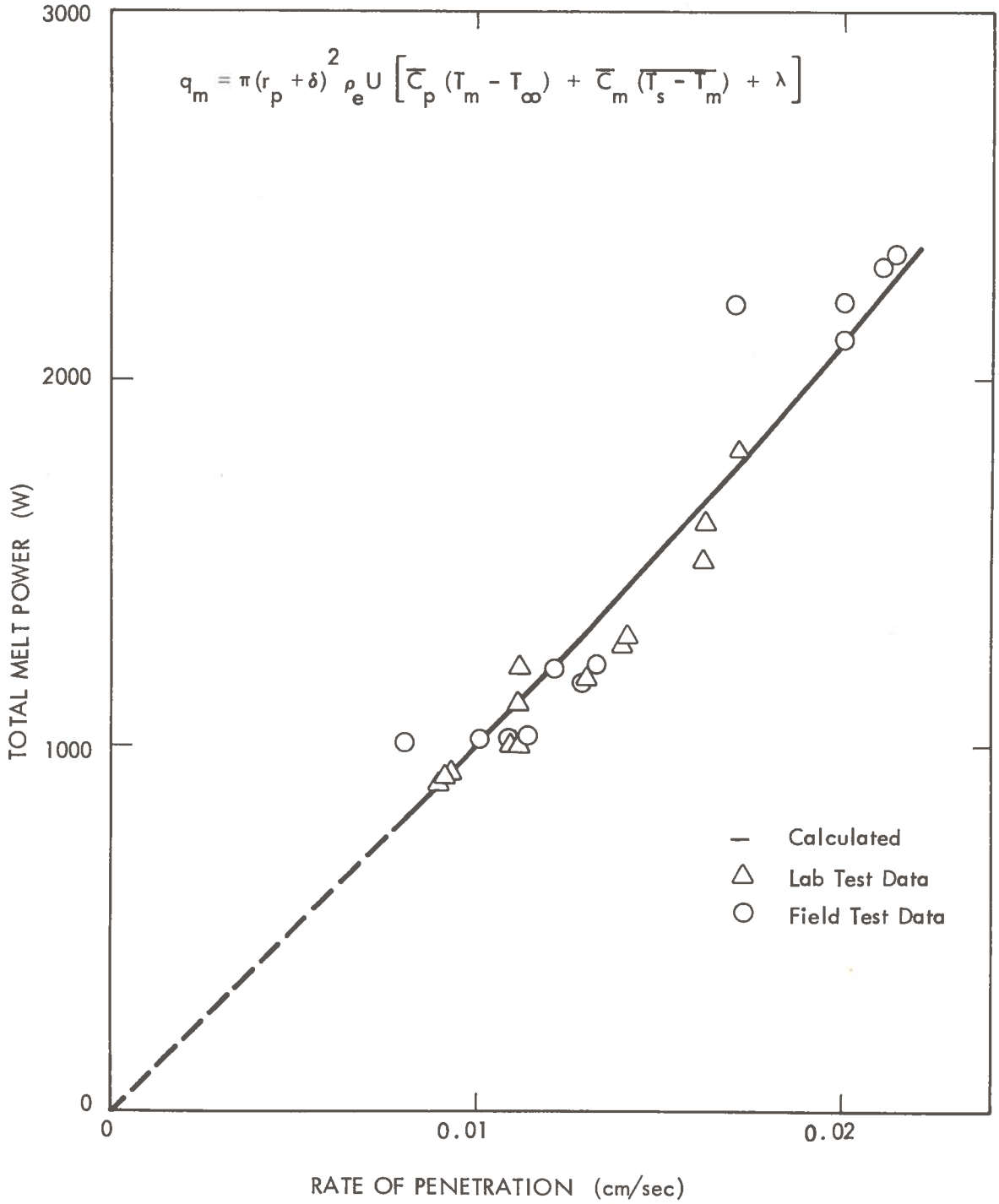

Figure 6-6. Comparison of Experimental and Calculated Melt Power for 50 mm Conical Penetrator in Tuff Full Consolidation - Mode 1 Tunneling

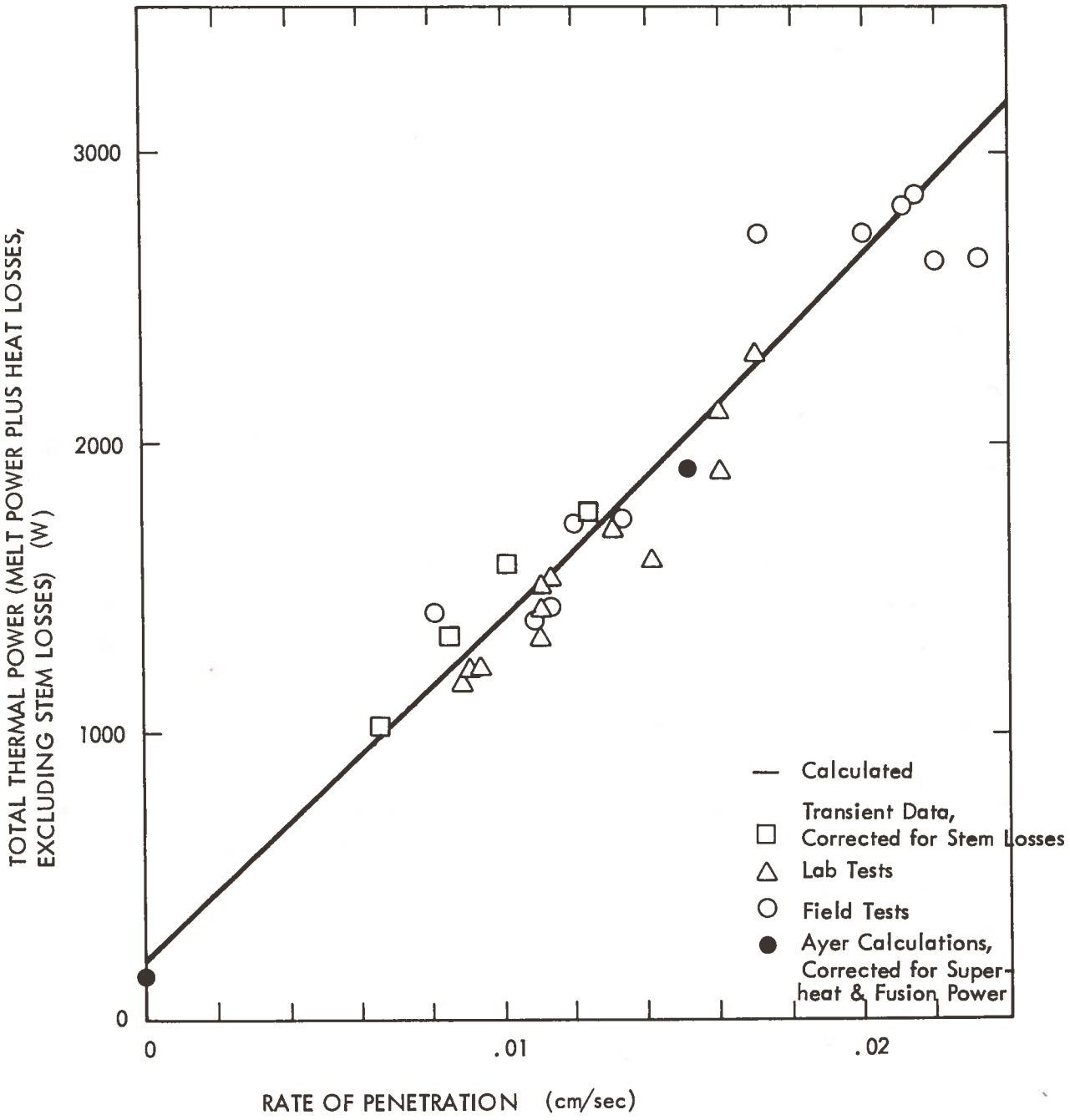

Figure 6-7. Comparison of Experimental and Calculated Total Thermal Power, Calculated by Modified Cylindrical Penetrator Model, Melt Moving with the Penetrator 55 mm Penetrator in Tuff, Full Consolidation - Mode 1 Tunneling

$$q_T = \pi k_{eff} L_H (T_m - T_\infty)$$
$$+ 2\pi \rho_e \delta_e C_p (T_m - T_\infty)(r_{Bo} \sin\theta_o + r_B \sin\theta) U_\infty$$
$$+ \pi (r_p + \delta)^2 \rho_e U_\infty \left[C_p (T_m - T_\infty) + \overline{C}_m \overline{(T_s - T_m)} + \lambda \right] \quad (6\text{-}39)$$

Correlation with data showed that k_{eff} should be evaluated at the melting point, and δ_e is a function of k_{eff}:

$$\delta_e = 1.087 \times 10^2 k_{eff} \quad (6\text{-}40)$$

The total thermal power calculated by Equation (6-37) (excluding stem losses) is compared with the experimental and AYER calculated data in Figure 6-7 for the 50 mm conical penetrator. It is significant to note that the analytical model is in excellent agreement with the AYER calculations including the heat loss to ambient earth/rock at zero rate of penetration. Further comparison of analytic and AYER calculated heat losses plus earth/rock sensible heat are shown in Figure 6-8. The deviations between results calculated by the two different methods are summarized in Table 6-4. Both sets of calculations use consistent physical properties, given in Table 6-3. It is noted that the functional relation developed satisfactorily predicts thermal power requirements for tuff and basalt over a wide range of penetrator diameters and rates of penetration. The modified cylindrical model is only slightly inferior to the hemispherical model when predicting power requirements for conical penetrators. However, since the modified cylindrical model is more general and can be used for all modes of penetration, it is recommended here for further use.

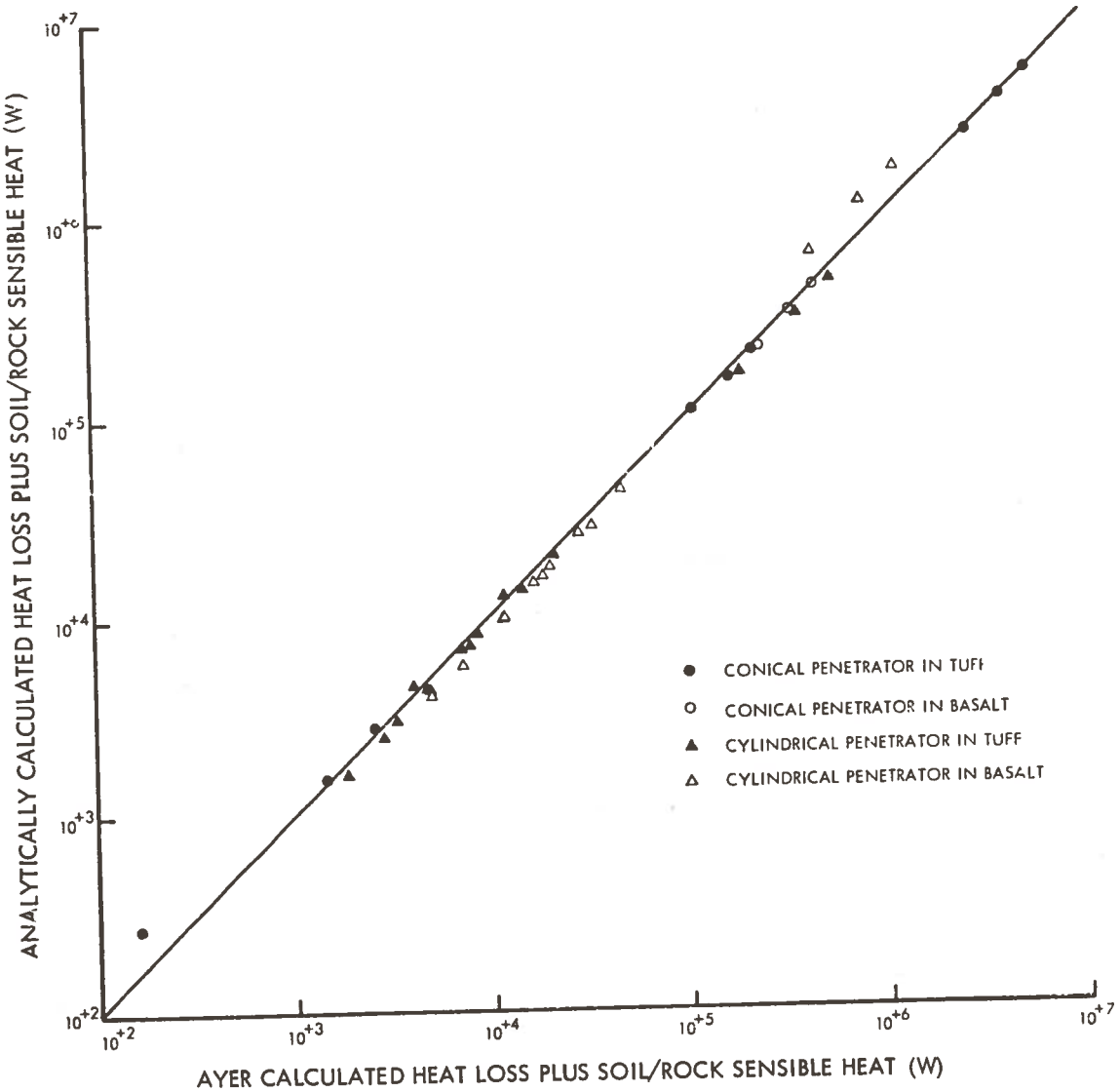

Figure 6-8. Comparison of Computer and Analytical Model Calculated Thermal Power for Mode 1 Tunneling

TABLE 6-4

COMPARISON OF ANALYTICAL SOLUTION WITH EXPERIMENTAL DATA AND AYER CALCULATED DATA

50 mm CONICAL PENETRATOR EXPERIMENTAL HEAT LOSS DATA IN TUFF

$$q_T = (q_{l,s} + q_{l,d}) + q_s + q_{su} + q_f$$

Deviation (%):	Avg. of Absolute Values	Mean
Lab test data, hemispherical model	17	+ 2.7
Lab test data, modified cylindrical model	17	+ 5.7
Field test data, hemispherical model	22	- 4.6
Field test data, modified cylindrical model	12	-10.8

AYER CALCULATED PENETRATORS IN TUFF AND BASALT, HEAT LOSS PLUS ROCK SENSIBLE HEAT

$$q_T = (q_{l,s} + q_{l,d}) + q_s + q_{su} + q_f$$

Deviation (%):		
50 mm (2-Inch) conical penetrators	11.4	+11.4
61 cm (2-foot) conical penetrators	3.0	- 3.0
3 m (10-foot) conical penetrators	1.1	- 1.1
9.1 m (30-foot) conical penetrators	3.3	+ 3.3
5.1 cm cylindrical penetrators	11.6	-11.6
6.5 cm cylindrical penetrators	12.1	- 7.8
9.0 cm cylindrical penetrators	11.4	- 7.5
12 cm cylindrical penetrators	8.4	- 8.4
61 cm cylindrical penetrators	11.8	-11.8
3 m cylindrical penetrators	3.3	+ 2.0
9.1 m cylindrical penetrators	3.2	+ 3.2
	7.0	- 3.9

6.2.5 Generalization to Other Geometries

Practical transportation tunnels are expected to be other than circular in shape. Consequently, it is desirable to generalize Equation (6-37) to any geometry. Examination of the terms and parameters in Equation (6-37) showed that the following general geometric parameters can be identified in the equation:

- C, effective mean circumference of heated portion of penetrator plus liner
- A_m, melt to earth/rock interfacial area
- S_m, cross-sectional area of region melted

Equation (6-37) expressed in terms of these parameters becomes

$$q_T = C \delta_e \rho_e C_p (T_m - T_\infty) U_\infty + \frac{k_{eff} A_m}{2 (r_p + \delta)} (T_m - T_\infty)$$

$$+ S_m \rho_e U_\infty \left[C_p (T_m - T_\infty) + \overline{C}_m \overline{(T_s - T_m)} + \lambda \right] \qquad (6\text{-}41)$$

The parameters C, A_m, and S_m for different tunnel geometries are summarized in Table 6-5. This general equation can be used for parametric analyses and conceptual design calculations.

6.3 GENERALIZATION TO DIFFERENT MODES OF TUNNELING

The five modes of tunneling essentially define five specific penetrator designs. Each has its unique geometric shape and operating parameters. The generalized thermal power equation (Equation 6-39) can be readily specialized to these models of tunneling. These are presented in this section.

6.3.1 Melt Thickness

One parameter that has a major effect on the thermal power requirement is the melt thickness. This thickness is highly dependent on the relative density of glass to earth/rock which

TABLE 6-5

GENERALIZED FUNCTIONAL RELATION FOR THERMAL POWER REQUIREMENTS IN THERMAL TUNNELING

$$q_t = C\,\delta_s \rho_e\,\overline{C}_p\,(T_m - T_\infty)\,U + \frac{k_{eff}\,A_m}{2(r_p+\delta)}\,(T_m - T_\infty) + S_m\,\rho_e\,U\left[\overline{C}_p\,(T_m - T_\infty) + \overline{C}_m\,\overline{(T_s - T_m)} + \lambda\right]$$

CONICAL PENETRATORS

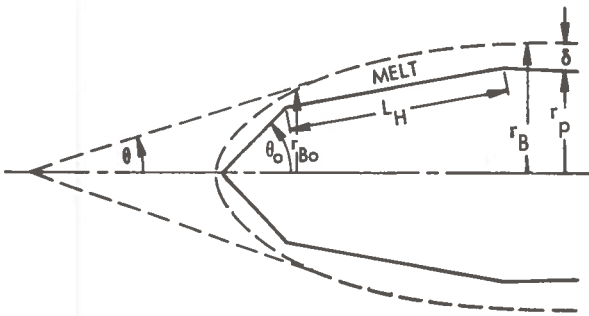

$$C = 2\pi\left[r_{Bo}\sin\theta_o + (r_p+\delta)\sin\theta\right]$$

$$r_{Bo} = \frac{r_{po}}{r_p}\,(r_p+\delta)$$

$$S_m = \pi\left[(r_p+\delta)^2\right]$$

$$A_m = 2\pi\,(r_p+\delta)\,L_H$$

CYLINDRICAL PENETRATORS

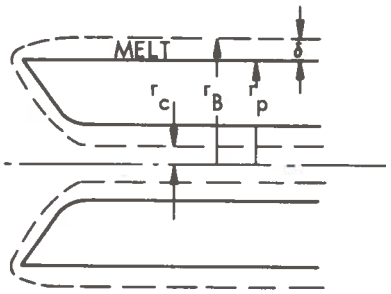

$$C = 2\pi\,(D_p + 2\delta)$$

$$S_m = \pi\left[(r_p+\delta)^2 - r_c^2\right]$$

$$A_m = \left[2\pi(r_p+\delta)\,L_H + (r_p^2 - r_c^2)\right]$$

HORSESHOE-SHAPED TUNNELS

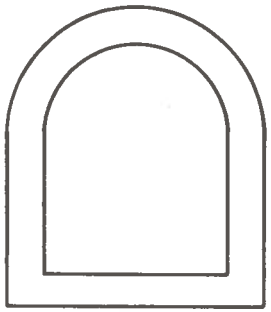

C = Effective mean circumference of melt-earth interface

S_m = Cross-sectional area of region melted

A_m = Area of melt to earth/rock interface

in turn determines the mode of tunneling that must be considered. The melt thickness is of importance for the following reasons:

- It determines the melt superheat and maximum penetrator surface temperature.
- It establishes the liner outside diameter (if a liner is created as in modes 1, 2, 4 and 5).
- It establishes the liner cooldown time and length of controlled cooldown section needed.
- It affects the frictional drag forces.

The required thickness of the glass liner must be established from considerations of glass liner strength requirements. This is discussed in Section 9.0. As another limit, the glass liner generated as a result of glass to earth/rock densities may be studied. For this limit, the glass liner generated can be determined from simple mass balances presented in Section 4.0.

6.3.2 Thermal Power Equations

Based on the different geometries and melt flow in the 5 modes of tunneling, the generalized thermal power Equation (6-39) can be specialized to each mode of tunneling. These are given below.

Mode 1

For Mode 1 tunneling, the generalized thermal power equation is directly applicable; hence

$$q_T = 2\pi \delta_e \rho_e U_\infty C_p (T_m - T_\infty)(r_{Bo} \sin\theta_o + r_B \sin\theta)$$
$$+ \pi k_{eff} L_H (T_m - T_\infty)$$
$$+ \pi (r_p + \delta)^2 \rho_e U_\infty [C_p (T_m - T_\infty) + \overline{C_m} \overline{(T_s - T_m)} + \lambda] \qquad (6\text{-}42)$$

Mode 2

Mode 2 tunneling can be regarded as a special case of Mode 4 with a zero core radius ($r_c = 0$). In this case, $\theta_o = 0$ and $\theta = 90^o$, which is the definition of a cylindrical penetrator. The generalized Equation (6-39) reduces to

$$q_T = 2\pi (r_p + \delta)\ \delta_e\ \rho_e\ U_\infty\ C_p\ (T_m - T_\infty)$$

$$+ k_{eff}\ \frac{[2\pi (r_p + \delta)\ L_H + \pi r_p^2]}{2(r_p + \delta)}\ (T_m - T_\infty)$$

$$+ \pi (r_p + \delta)^2\ \rho_e\ U_\infty\ [C_p\ (T_m - T_\infty) + \overline{C_m}\ (\overline{T_s - T_m}) + \lambda] \qquad (6\text{-}43)$$

Mode 3

In Mode 3, the external surface of the penetrator is not heated and a glass liner is not formed. Hence, $\delta = 0$, and $L_H = 0$, and Equation 6-45 reduces to

$$q_T = 2\pi r_p\ \delta_e\ \rho_e\ U_\infty\ C_p\ (T_m - T_\infty)$$

$$+ \frac{\pi k_{eff}\ r_p^2}{2(r_p + \delta)}\ (T_m - T_\infty)$$

$$+ \pi r_p^2\ \rho_e\ U_\infty\ [C_p\ (T_m - T_\infty) + \overline{C_m}\ (\overline{T_s - T_m}) + \lambda] \qquad (6\text{-}44)$$

Mode 4

For this mode of tunneling, where only an annular region is melted, the equation is

$$q_T = 2\pi (r_p + \delta)\, \delta_e\, \rho_e\, U_\infty\, C_p\, (T_m - T_\infty)$$

$$+ \frac{k_{eff}\, [2\pi (r_p + \delta)\, L_H + \pi (r_p^{\,2} - r_c^{\,2})]}{2 (r_p + \delta)}\, (T_m - T_\infty)$$

$$+ \pi [(r_p + \delta)^2 - r_c^{\,2}]\, \rho_e\, U_\infty [C_p\, (T_m - T_\infty) + \overline{C_m}\, \overline{(T_s - T_m)} + \lambda] \quad (6\text{-}45)$$

Mode 5

From the geometric configurations of this mode and the various parameters, shown in Figure 6-9, Equation 6-39 can be readily reduced to the following equation, applicable to Mode 5:

$$q_T = 2\pi (r_p + \delta)\, \delta_e\, \rho_e\, U_\infty\, C_p\, (T_m - T_\infty)$$

$$+ \frac{k_{eff}\, [2\pi (r_p + \delta)\, L_H + \pi (r_p^{\,2} - r_c^{\,2})]}{2 (r_p + \delta)}\, (T_m - T_\infty)$$

$$+ \pi [(r_p + \delta)^2 - r_c^{\,2}]\, \rho_e\, U_\infty [C_p\, (T_m - T_\infty) + \overline{C_m}\, \overline{(T_s - T_m)} + \lambda] \quad (6\text{-}46)$$

6.4 NUMERICAL EXAMPLES

Scoping calculations of various modes of tunneling were carried out to evaluate the capabilities of each and the extent of their operating limits.

6.4.1 Mode 1 Tunneling

Mode 1 tunneling, by definition, uses a full consolidation penetrator design. For this reason, this mode of tunneling is applicable to unconsolidated earth/rock materials such as alluvium, typified by the earth model UNCON, and porous materials such as tuff. Since this mode of tunneling is expected to be limited to relatively small penetrators, illustrative calculations were performed for tuff only. For this consolidating mode of penetration all of the molten material consolidates into a glass liner; consequently, the liner thickness increases with increasing penetrator diameter and the penetrator surface temperature also increases. In addition, the penetrator surface temperature increases with increasing rates of penetration, because greater amounts of heat are transferred across the melt. As a consequence, material temperature limitations are expected to restrict the size of tunnels and the rate of penetration that can be considered for this mode of tunneling. This is clearly illustrated in Figure 6-9, where the maximum penetrator surface temperature is plotted versus the tunnel diameter at constant rates of penetration. Potential penetrator materials of construction are molybdenum and tungsten. Two-thirds of the melting point of these materials are shown on the figure as reference points. These were selected arbitrarily as the upper limits on use temperature because experimental data on the yield strength of molybdenum and tungsten are not available at the higher temperatures of interest. Typical published data at lower temperatures are reproduced in Figure 6-10. An extrapolation of the tensile yield strength, which may be optimistic, suggests that at 2/3 of the melting point the tensile strength is on the order of 7×10^7 N/m^2 (10, 000 psi).

It is recognized that in the design of a penetrator for a given specified mission, the total applied thrust load and melt pressure must be taken into account to determine the upper operating limits. Meanwhile, there is experimental evidence[6-7] from the 50 mm full consolidation conical penetrator that the upper operating temperature for molybdenum is well above 2/3 of its melting point.

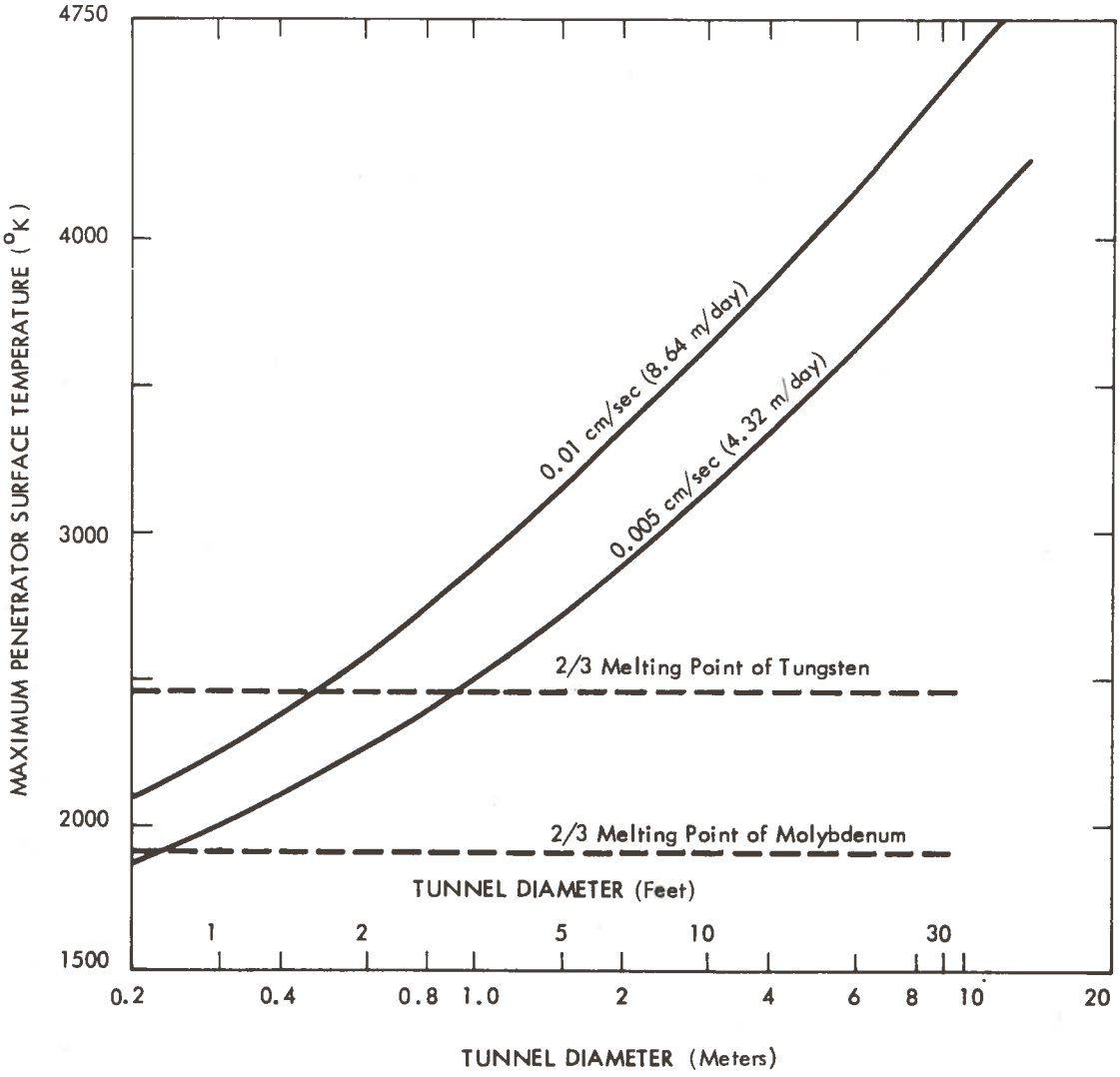

Figure 6-9. Effect of Tunnel Diameter on Maximum Penetrator Surface Temperature for Full Consolidation (Mode 1) Tunneling - Conical Penetrator in Tuff

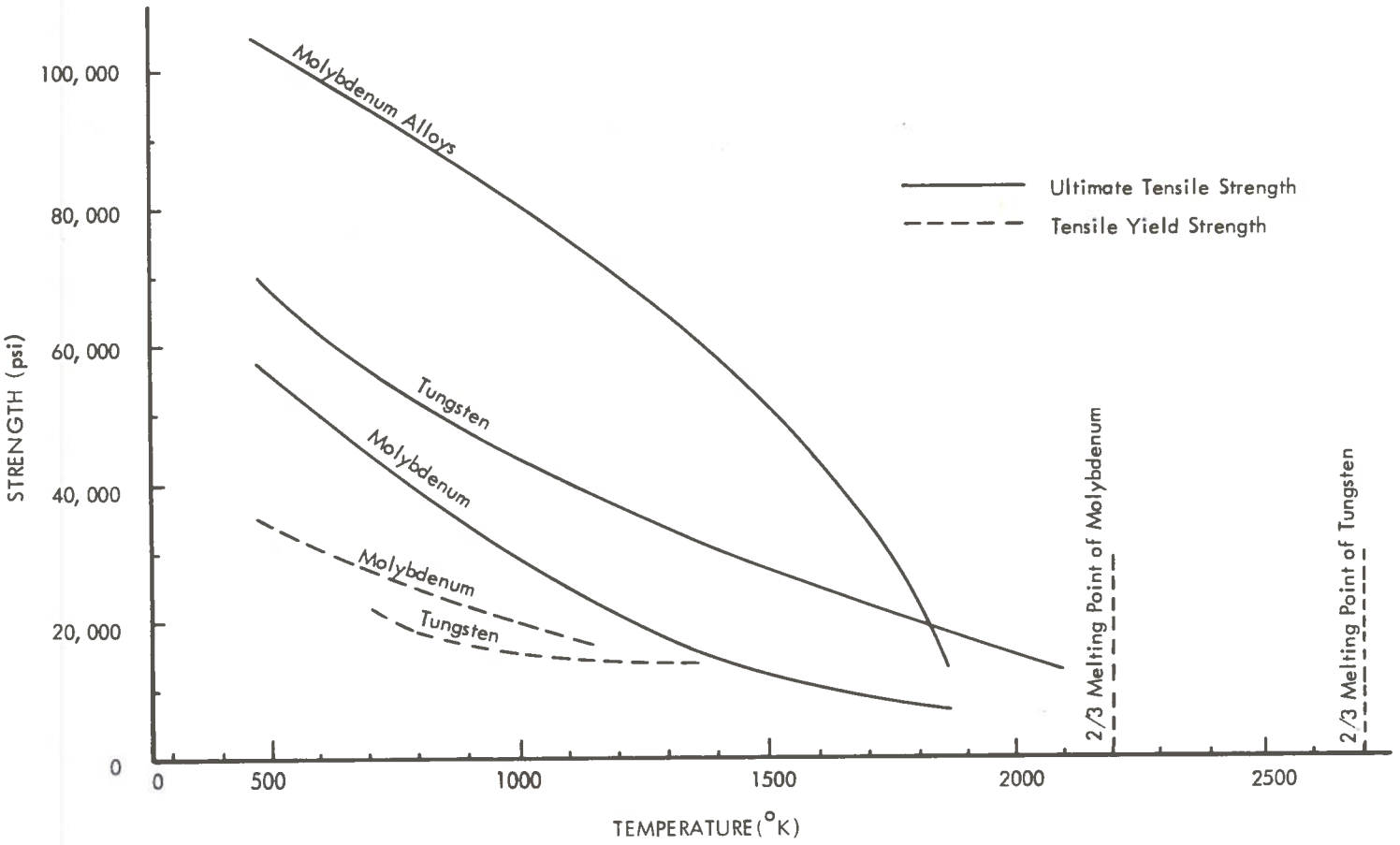

Figure 6-10. Some Strength Properties of High Temperature Refractory Metals
From Materials in Design Engineering, December 1965, pp. 126-129

It is apparent from Figure 6-9 that the upper use temperatures of tungsten and molybdenum severely limits the size of the tunnel and the rate of penetration that can be considered for Mode 1.

6.4.2 Mode 2 Tunneling

The upper operating limits observed in Mode 1 tunneling can be extended somewhat by back extruding a portion of the melt. This has the primary effect of reducing the melt thickness and thus reducing the penetrator surface temperature. For scoping calculations, it was assumed that the melt thickness at the throat of the extruder is equal to that of the glass liner. Under this constratint, maximum penetrator surface temperatures were calculated for various rates of penetration over a range of tunnel diameters. The results are compared with those calculated for Mode 1 tunneling in Figure 6-11. The extension of the operating limits by back extruding a portion of the melt is small in this mode of operation primarily because the surface temperature is still excessive due to the relatively thick melt layers.

6.4.3 Mode 3 Tunneling

For the same reasons given above, Mode 3 tunneling is not expected to yield any improvement over Mode 1. In fact, the operating limits are expected to be slightly lower thanthose for Mode 1 when tunneling through the same earth/rock material. The same amount of melt must now flow over reduced surface areas, thus causing greater heat flux and melt superheat. However, for certain types of earth/rock materials, where the glass formed has a lower density than that of the parent earth/rock material, Mode 3 is the only practical mode of tunneling of the first three.

In order to extend the rock melting technique to the excavation of tunnels large enough for transportation purposes, the total amount of material melted must be reduced in order to reduce the surface heat flux. A reduction of the heat flux in turn decreases the penetrator surface temperature. These two goals can be attained using tunneling Modes 4 and 5, where the penetrator melts an annular region of the earth/rock. The core is removed by conventional mucking

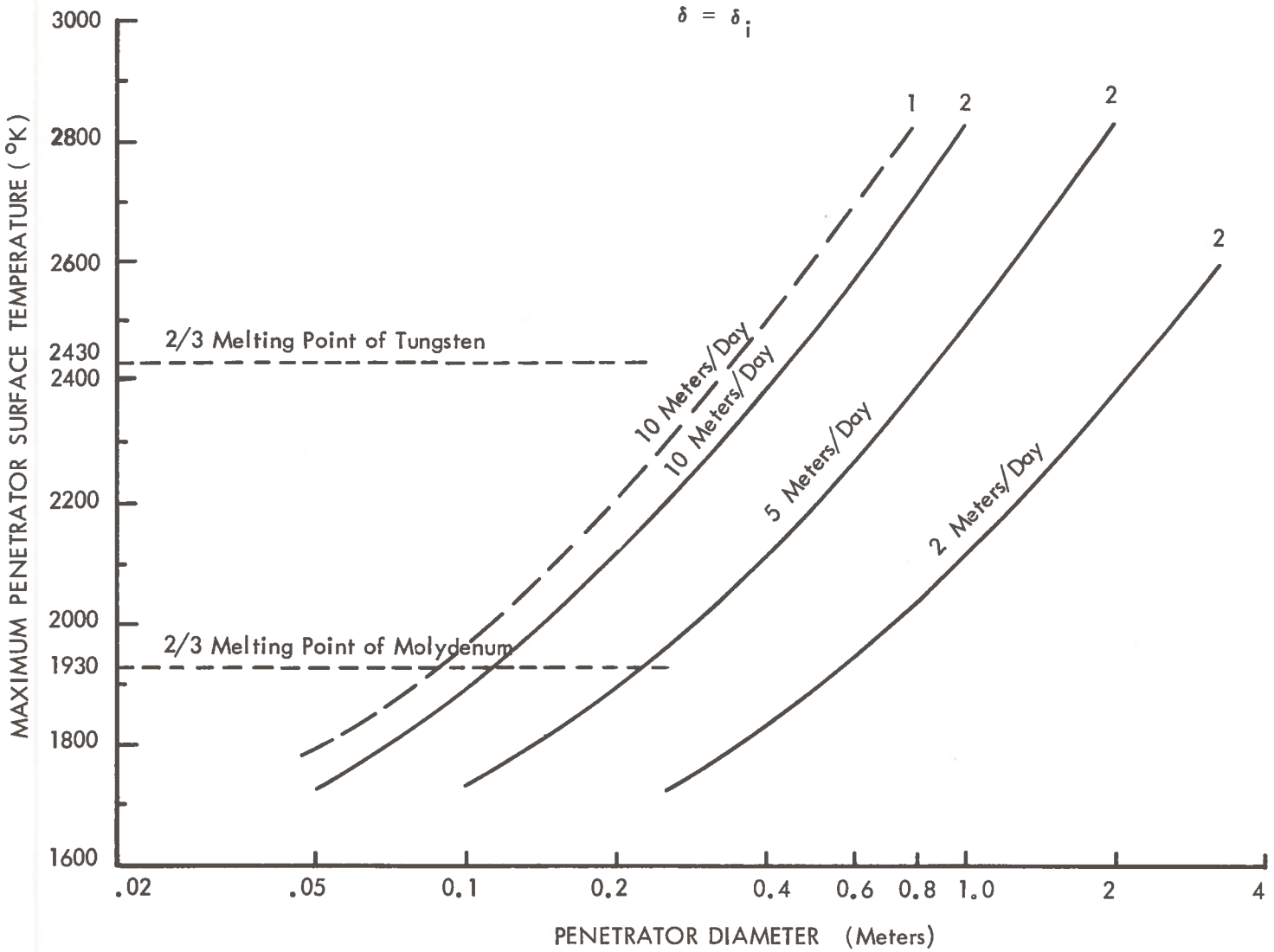

Figure 6-11. Comparing Effects of Tunnel Diameter on Maximum Penetrator Surface Temperature for Modes 1 and 2 Tunneling in Tuff

techniques. As in tunneling Modes 1, 2, and 3, these may or may not include back extrusion of the melt, depending on the type of earth/rock material. Tunneling Mode 4, discussed below, is basically a consolidator with the addition of coring, while Mode 5 includes back extrusion.

6.4.4 Mode 4 Tunneling

Mode 4 tunneling is basically the same as Mode 5 which includes Mode 4 as a special case. For this reason, numerical examples were not calculated separately for Mode 4 tunneling.

6.4.5 Mode 5 Tunneling

For large tunnel diameters, the glass liner thicknesses required would increase correspondingly, and the thermal power required can vary appreciably, depending on the core-to-penetrator diameter ratio. In order to perform scoping calculations, it was assumed that the melt thickness on the inside surface is equal to the glass liner thickness. This constraint provides a relatively uniform penetrator surface temperature if the heat flux is uniform. The inside melt thickness (δ_i) is given by the geometric relation

$$\delta_i = r_i - r_c$$

or

$$r_i = \delta_i + r_c$$

By substituting this into Equation (6-44) and by setting $\delta = \delta_i$, the core radius can be determined for any penetrator diameter, liner thickness, and any ratio of the rate of extrusion to the rate of penetration. For tunneling through UNCON, the maximum penetrator surface temperature was calculated for a wide range of tunnel diameters and rates of penetration up to 100 meters per day. Other specified conditions are the following:

$$U_e = U_\infty$$

$$L_H = D_p$$

$$\delta = 0.05\ D_p$$

The results for these conditions are presented in Figure 6-12. It becomes evident from this figure that operating limits are severely affected by penetrator surface temperature limits. This conventional penetrator is called a high heat flux design and is contrasted with a low heat flux design in the following section.

Under the assumed conditions and using tungsten as the materials of construction, it is seen that a 4 meter tunnel cannot advance more than 10 meters/day if 2/3 the melting point of tungsten is taken to be the upper limit on use temperature. At 100 meters/day, the maximum tunnel diameter that can be considered is less than one meter.

6.4.6 Extending Operating Limits

It is evident from these results that severe operating limits are encountered for all modes of tunneling. However, it must be pointed out that each one of the 5 modes of tunneling is associated with a specific penetrator design. These modes and penetrator designs were based on those proposed by LASL in early studies and early conceptual designs of small penetrators. Consequently, the operating capabilities observed are penetrator design limited. Evaluation of other penetrator shapes has shown that the operating limits can be extended significantly with modified penetrator designs. A relatively obvious modification is the use of extended heated surfaces or segmented heaters*. In practical tunneling applications, glass liner thicknesses are expected to be much greater than 10% of the tunnel radius (see Section 9.0). This is in general in conflict with the goal to minimize melt thickness. The problem has been solved by a unique segmented heater concept proposed in Reference 6-8. A schematic diagram of this concept is shown in Figure 6-13. A trimetric view of this concept as applied to a large scale tunneler is shown in Figure 6-14.

The proposed concept reduces the penetrator surface temperature by reducing the surface heat flux without adding heated length. This is accompanied by the formation of thick glass

---

* This concept was first advanced to solve the problem of tunneling through non-homogeneous materials to be discussed in Section 11.0. See Reference (6-8).

$$\delta = \delta_i = 0.05\, D_p,\ L_H = D_p,\ U_e = U_\infty$$

High Heat Flux Penetrator Design

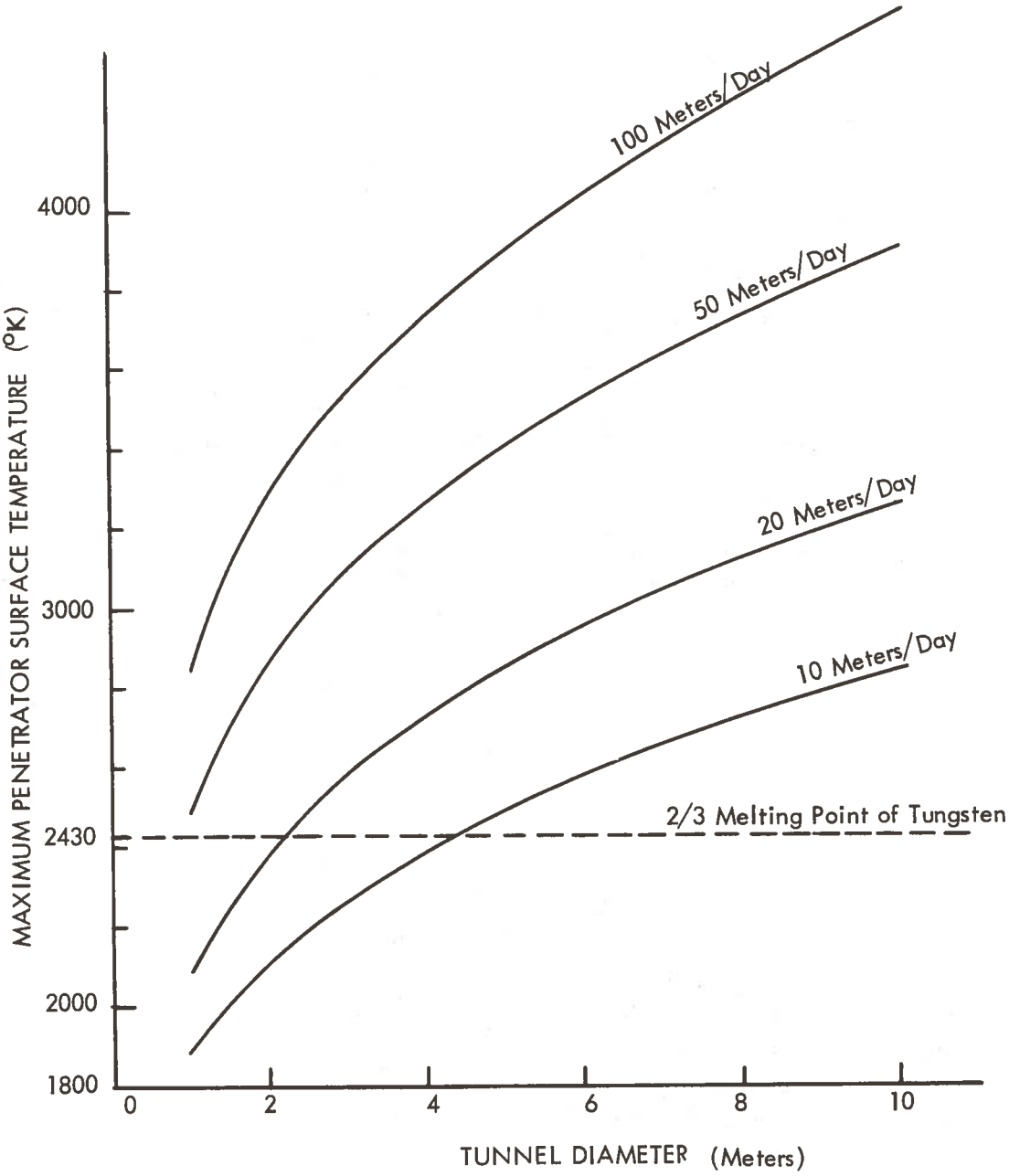

Figure 6-12. Effect of Tunnel Diameter at Constant Rates of Penetration on the Maximum Penetrator Surface Temperature in Mode 5 Tunneling Through UNCON

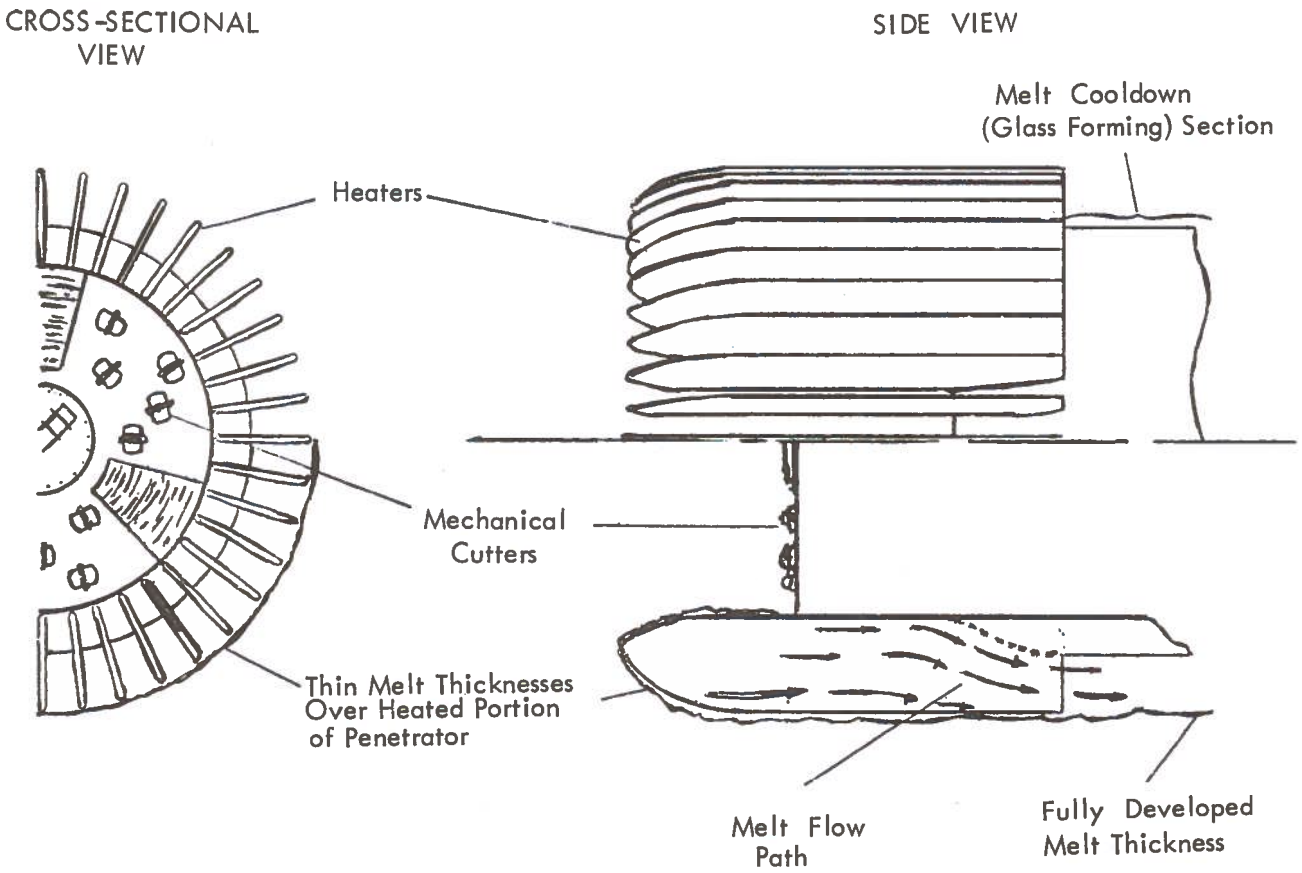

Figure 6-13. Schematic Diagram of Proposed High Performance Subterrene Thermal Tunneler

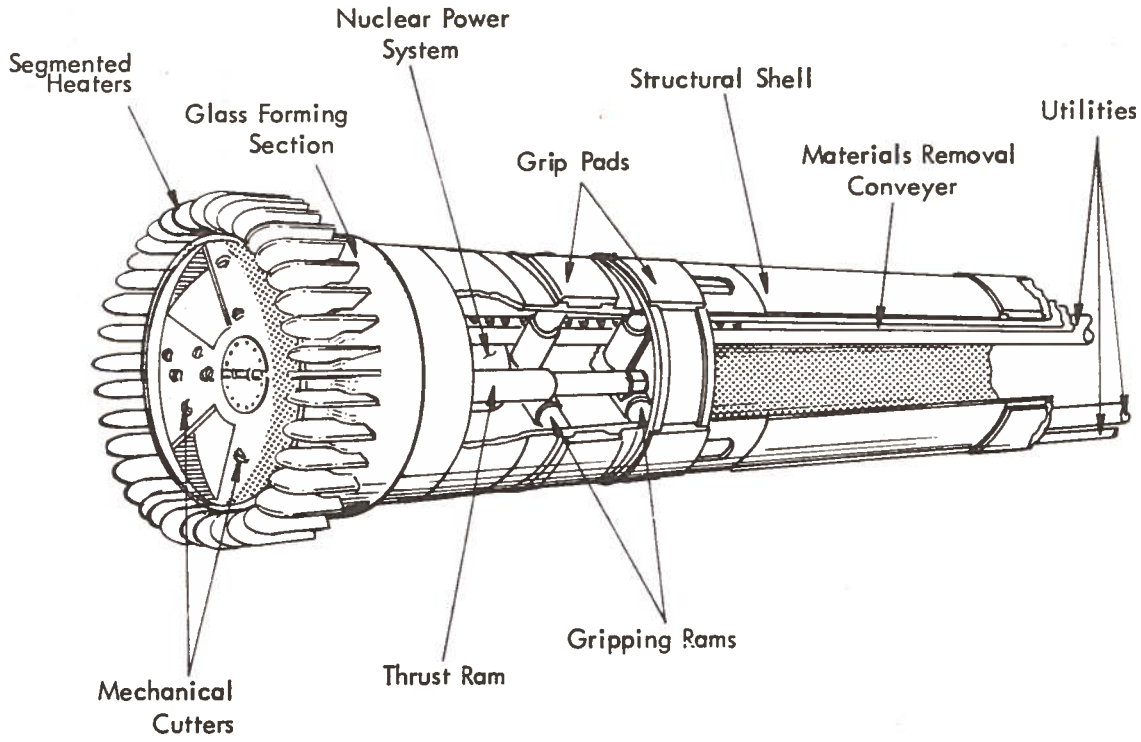

Figure 6-14. Trimetric View of Proposed Thermal Tunneler

liners. The concept incorporates finned and segmented heaters combined with either mechanical cutters (for coring through soft material, as shown in the figures) or other types of corers for coring relatively hard rock. The finned heater design reduces the surface heat flux as well as the maximum melt thickness over the heated portion of the tunneler. The melt, however, is consolidated (extruded) into a much thicker layer over the melt cooldown section just behind the heaters to form a thick glass liner.

By this concept, glass liners of any thickness can be formed without exceeding penetrator surface temperature limits. This is accomplished by maintaining relatively thin melt thicknesses over the heated portions of the penetrator. To illustrate the potential capabilities of this penetrator concept, the maximum penetrator surface temperature was calculated for the following conditions:

- Earth/rock material = UNCON
- Tunnel Diameter = 10 meters
- $L_H = D_p$ (same as before)
- Melt thickness over all heated portions = 1 cm
- Glass liner thickness = 0.05 meters (same as the previous calculation)
- $U_e = U_\infty$ (same as before)

The results of this calculation are presented in Figure 6-15, where the maximum penetrator surface temperature is given as a function of the rate of penetration. Significant improvements in performance capabilities can be obtained by using extended surface heater designs. Under the conditions selected, a 10 meter penetrator can advance at a rate up to 100 meters per day if tungsten is used as the material of construction. The rate of advance is reduced to 20 meters/day if molybdenum were used instead. For the same operating conditions, the total thermal power required (less stem losses) for tunneling through UNCON and MASIG were calculated. These results are presented in Figure 6-16. It can be seen that tunneling through

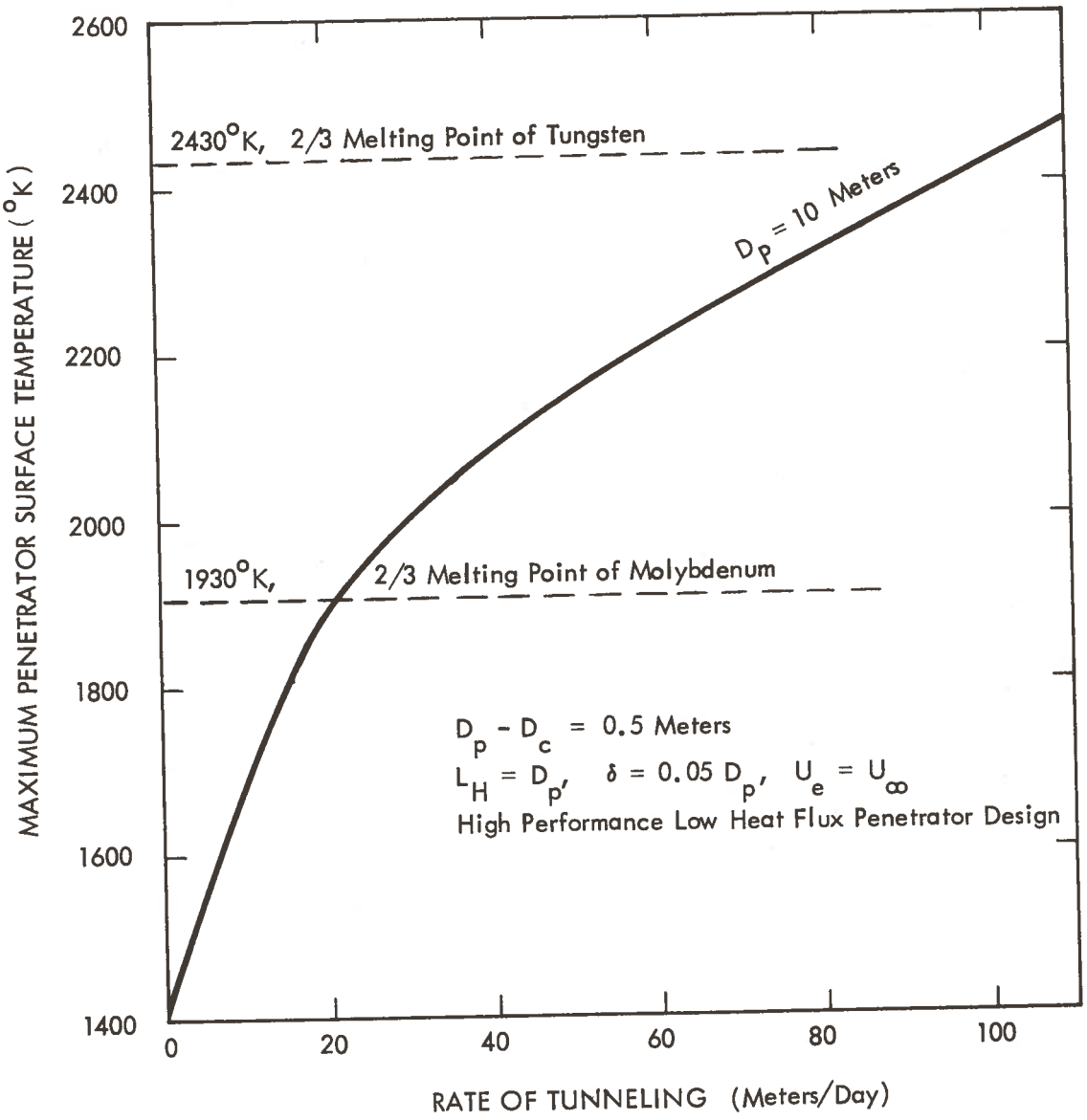

Figure 6-15. Effect of Rate of Tunneling on Maximum Penetrator Surface Temperature Mode 5 Tunneling Through UNCON

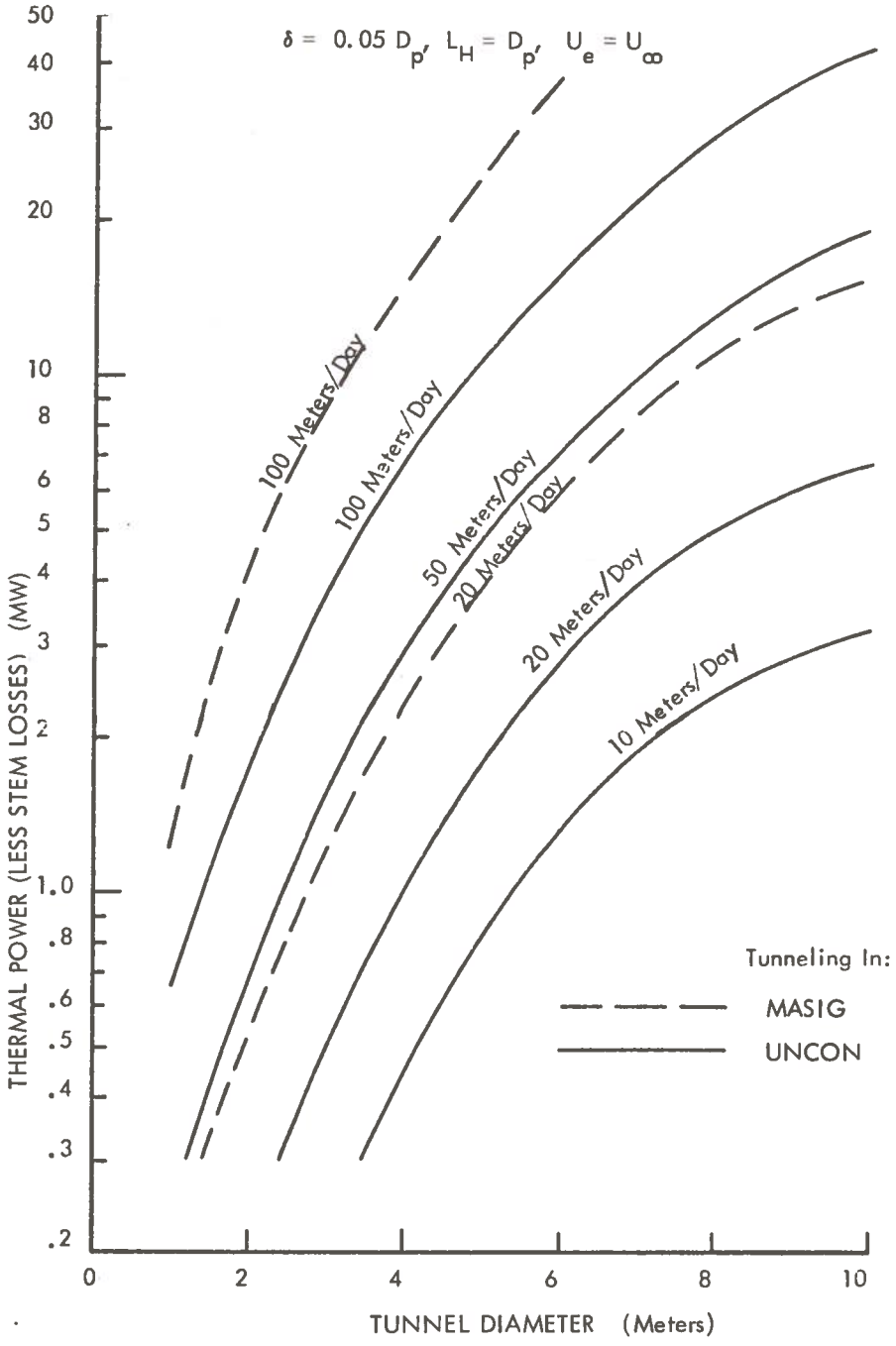

Figure 6-16. Effect of Tunnel Diameter on Total Thermal Power (Less Stem Losses) Required for Mode 5 Tunneling Low Heat Flux, Advanced Penetrator Concept

MASIG would require higher thermal power, primarily because of the higher density of MASIG when compared to that of UNCON. The power required for both types of earth/rock materials is seen to be fairly reasonable.

6.4.7 Conclusions and Recommendations

Based on the results of the above study, the following conclusions are made

1. All the penetrator designs considered in the study program are applicable to relatively small penetrators not suitable for transportation tunnel applications. These designs were selected based on early LASL concepts and experimental demonstrations.

2. For large scale tunneling, a penetrator concept incorporating a number of new features has been proposed. Scoping calculations suggest that this concept can meet the operating limits of interest to transportation tunnels, i.e., tunnel diameters up to 10 meters and tunneling rates up to 100 meters/day.

Two problems, however, have been recognized with the proposed concept. They are the following:

1. In the proposed concept, the penetrator diameter is greater than the tunnel. Therefore, retraction of the penetrator would be impossible unless the segmented heaters can be designed to be foldable, removable, or retractable into the core.

2. Leading edge heat flux is increased as a result of the reduced surface area. It is anticipated that an advanced heat transfer system such as heat pipes will have to be used to deliver the relatively high heat fluxes required.

   The use of heat pipes has advantages for transportation tunneling applications from another viewpoint. In order to tunnel through non-homogeneous materials without causing slowdowns and hot-spots, a new application of the

heat pipe has been proposed for use in large scale penetrator designs. (See Reference 6-9, "Isothermal Condenser, Variable Power Heat Pipes"). These problems are discussed further under Section 11.0.

Other than these engineering design problems, there appears to be little doubt as to the technical feasibility of the basic concept with regard to the amount of power needed and rate of advance attainable. However, as pointed out above, considerable design study and analysis are needed to explore the operating limits and capabilities of the concept. Such a study should be carried out with specified design goals and constraints.

6.5 REFERENCES

6-1 Rosenthal, D., "The Theory of Moving Sources of Heat and Its Application to Metal Treatments," Trans. ASME, 68,, (1946), p. 849.

6-2 Rosenthal, D. and R. H. Cameron, "Temperature Distribution in Cylinder Heated by Point Source Moving Along Its Axis," Trans. ASME, 69, (1947), p. 961.

6-3 Bird, R. B., et al., Transport Phenomena, John Wiley and Sons, Inc., (1960), p. 319.

6-4 Jakob, M. Heat Transfer, Vol. I, John Wiley and Sons, (1949), pp. 343-344.

6-5 Gido, R. G., "Internal Temperature Distribution of a Subterrene Rock-Melting Penetrator," LA-5135-MS, Jan., 1973.

6-6 Gido, R. G., "Subterrene Penetration Rate in Melting Power Relationship," LA-5204-MS, March, (1973), p. 10.

6-7 Private communications with G. E. Cort, WANL staff member on assignment at LASL.

6-8 Chi, J. W. H., "High Performance Subterrene Thermal Tunneler," Westinghouse Astronuclear Laboratory Invention Disclosure 73-11, July 17, 1973.

6-9 Chi, J. W. H., "Isothermal Condenser, Variable Power Heat Pipes," Westinghouse Astronuclear Laboratory Invention Disclosure 73-12, July 24, 1973.

6-10 Maurer, W. C., Novel Drilling Techniques, Pergaman Press, p. 8.

6-11 Neudecker, J. W., et al., "Design and Development of Prototype Universal Extruding Subterrene Penetrator," LA-5205-MS, March, 1973.